MEAN TEMPERATURE DIFFERENCE IN CROSS-FLOW HEAT EXCHANGE

applied to multipass air-cooled fin-tube units with a finite number of rows

by

FRANCIS JOHN LORRAINE NICOLE

Submitted in partial fulfilment of the requirements

for the degree of M.Sc. (Eng.)(Chem.)

in the Faculty of Engineering,

University of Pretoria,

PRETORIA

November, 1972

PRETORIA

F.J.L. NICOLE

MEAN TEMPERATURE DIFFERENCE IN CROSS-FLOW HEAT EXCHANGE

applied to multipass air-cooled fin-tube units with a finite number of rows

SYNOPSIS

The effective mean temperature difference (M.T.D.) in a heat exchanger depends on the terminal temperatures of the two streams, the distributions of flows over the transfer area with the associated local mixing effects and, most important, the relative *directions* of flow of the two streams. Air-cooled fin-tube exchangers, of the type considered here, are arranged for *cross-flow*.

Measurements for several *counter-cross-flow* row-and-pass arrangements, on a test rig using commercially available fin-tubes, have shown that models (presented in the literature or derived here) which assume that the air stream contacts the tube rows sequentially, adequately predicted the *overall* performance (effective M.T.D.) of such exchangers. For predicting *local* temperature changes from row to row, however, a more sophisticated model allowing for partial air bypassing of alternate rows, as well as local partial transverse mixing of air at different temperatures, appears necessary, particularly for wide fin-tip clearances. The fin-tube geometry effectively prevents significant longitudinal (tube length direction) mixing, and models assuming complete longitudinal mixing of the air at any cross-section predict over-conservative (low) M.T.D.'s.

MEAN TEMPERATURE DIFFERENCE IN CROSS-FLOW HEAT EXCHANGE

applied to multipass air-cooled fin-tube units with a finite number of rows

FRANCIS JOHN LORRAINE NICOLE

Leier : PROFESSOR D.J. SCHOEMAN

DEPARTEMENT CHEMIESE INGENIEURSWESE

M.Sc. (ING.)(CHEM.)

SINOPSIS

Die effektiewe gemiddelde temperatuurverskil (G.T.V.) in 'n hitteruiler is afhanklik van die eindpunttemperature van die twee strome, die verspreiding van die vloei oor die oordragoppervlak inagnemend die mate van plaaslike menging en, die belangrikste, die relatiewe vloeirigtings van die twee strome. Dwarsvloei is van toepassing by die lugverkoelde vinbuisruilers, hier onder bespreking.

Verskeie dwarsvloeirangskikkings, waar die effektiewe vloei van die twee strome in teenoorgestelde rigtings is, is eksperimenteel ondersoek. Dit is gevind dat die algehele warmteoordragvermoë (effektiewe G.T.V.) van sodanige ruilers effektief voorspel kan word deur modelle, of afgelei of uit die literatuur verkry, wat gebaseer is op die aanname dat die lugstroom opeenvolgend in kontak kom met die rye buise. 'n Meer komplekse model, waarin toegelaat word vir 'n gedeeltelike omloop van lug oor alternatiewe rye en vir gedeeltelike dwarsmenging van lug by verskillende temperature, is blykbaar nodig, veral by hitteruilers waar die vinrandspasiëring groot is, om plaaslike temperatuurveranderings van ry tot ry te voorspel. Weens die geometrie van die vinbuisopstelling vind daar bykans geen menging plaas in 'n longitudinale rigting (dws rigting van buislengte) nie. Modelle gebaseer op die aanname van algehele menging in *hierdie* rigting sal te klein waardes vir die G.T.V. voorspel.

CONTENTS

1 INTRODUCTION

In the design of heat transfer equipment, whether done manually or using an efficient computer program for cost optimisation[1] of the many variables involved, the heat transfer calculation usually becomes prohibitively time consuming if a numerical stepwise integration must be performed. Thus suitable methods for approximating the mean heat transfer coefficient[2;3], overall pressure drop[4] and mean temperature difference (M.T.D.) are required.

The main aim of the project[5], part of which is reported here, is to develop simple, yet adequate, approximation formulae for estimating the effective M.T.D. obtained in the different tube row and pass arrangements of extended surface (fin-tube) air-cooled heat exchangers as used in the process industries[6;7]. These cross-flow exchangers, normally have from 3 to 6 horizontal fin-tube rows at right angles to the air flow.

A literature survey revealed that although much theoretical work has been published on M.T.D.'s in cross-flow heat exchange, no experimental confirmation of the proposed theoretical models has been published. Further, as these models were generally developed for the compact type of heat exchanger[8] as used in aircraft and nuclear reactor coolers (box with rectangular channels), it was necessary at first to investigate their applicability to process air-cooled heat exchangers and where required to introduce modifications.

To this end an air-cooled heat exchanger test rig was built, which was designed to be as flexible as possible with respect to row and pass arrangements. An experimental programme was carried out in which local temperature differences in individual rows of the exchanger in addition to overall flow rates and temperatures were measured. Eight different arrangements of rows and passes were considered. For the multipass arrangements these were arranged in a counter-cross-flow pattern.

In this report the results of the experimental work are given and compared with the theoretically calculated temperatures.

1.1 ACKNOWLEDGEMENTS

The author wishes to express his gratitude to Professor D.J. Schoeman of the University of Pretoria for invaluable discussions and to Dr. D.L. Peters of the Chemical Engineering Group, CSIR for his continuous interest and guidance during the course of this work.

Thanks are due to the CEG workshop staff for erecting the test tig, to Mr. J. Seegers for his contribution to a major instrumentation task and to Mr. J. Stander for his extensive assistance in the experiments.

The gift of the original fin-tube bundle to the CEG by E. Green & Son (S.A.) (Pty) Limited is gratefully acknowledged.

2 LITERATURE SURVEY

Several papers[9-22] have appeared in the literature over the past 60 years in which the *theoretical* analysis of the mean temperature difference (M.T.D.) in cross-flow heat exchange has been reported. The contents of these references are briefly summarised in Appendix 8.1. Reviews co-ordinating the results of various investigators have appeared; particularly noteworthy is the one by Bowman *et al.*[13] The work was extended by Stevens *et al.*[20] to cover those cases of one, two and three passes with overall counter-current and co-current flow which had not previously been solved mathematically.

To review this work again in detail would be repetition. It is, however, necessary to consider which of the flow conditions, for which solutions are available, are likely to be applicable to air-cooled fin-tube exchangers.

2.1 TERMS AND CONCEPTS

2.1.1 Mixing

Complete mixing, as used in this context with no dispersion in the direction of flow, implies that all the fluid in any given plane normal to the flow has the same temperature although this temperature does change in the direction of flow. Unmixed flow implies on the other hand that temperature differences within the fluid in at least one direciton normal to the flow can exist but that no heat flux due to these differences occurs.

The three possible flow combinations for a single pass cross-flow exchanger[11,45], if it is assumed that either fluid is completely mixed or unmixed, are shown here schematically. It is assumed that there is no variation of temperature in the 3rd dimension.

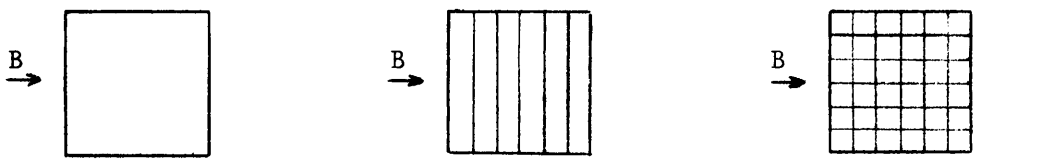

BOTH FLUIDS MIXED

FLUID A UNMIXED
FLUID B MIXED

BOTH FLUIDS UNMIXED

When the fluid is unmixed, the terminal temperature of either stream is defined as that which would result after complete mixing.

Bowman *et al.*[13] noted that a method for calculating the M.T.D. when either or both fluids are only *partially* mixed does not exist; this is still the case. They also noted that the M.T.D. is lower when either fluid is mixed than when both are unmixed.

2.1.2 Pass arrangement

In multipass arrangements in cross-flow, the overall direction of flow of the one fluid relative to the other is either counter-current or co-current. True counter-current flow yields the maximum attainable temperature difference whereas true co-current flow yields the smallest temperature difference for the same terminal temperatures. Hence multipass air-coolers are almost invariably of the *counter-cross-flow* type except in unusual cases, e.g. where low pour points or a high viscosity index of the process fluid may dictate the use of co-cross-flow. Only the counter-cross-flow type where the process fluid flows in alternate directions in alternate passes will be considered in this work. Stevens *et al.*[20] noted that the multipass arrangement where the flow is in the same direction in each pass yields a slightly higher M.T.D. for the same terminal temperatures. For obvious practical reasons such arrangements are seldom used in the process industry.

2.1.3 Temperature cross

In any cross-flow arrangement (even when both streams are completely mixed)[11] the temperatures of the two streams may cross. The greater the number of passes in a counter-cross-flow arrangement, the larger will be the attainable temperature cross.

2.2 MODELS FOR AIR-COOLED FIN-TUBE EXCHANGERS

2.2.1 Realistic flow model

The structure of a fin-tube bundle is such that the most realistic model is probably that in which the air is unmixed in the longitudinal direction even between tube rows, whilst the process fluid is mixed within any one tube at a given cross-section but

unmixed within any one pass, and then mixed in the headers (box- or D-type rather than U-bend) between passes. Partial longitudinal mixing of air in the space between tube rows will only be considered if found to be significant from the experimental results. It is normally assumed that the air mixes completely in the "transverse" direction (i.e., the direction normal to the flow and parallel to the fins) and contacts each tube row sequentially. In view of the tubeside flow pattern, the M.T.D. is dependent on the number of tube rows[22] as well as the number of passes and any model must take cognisance of this.

2.2.2 Alternative flow model

Work by Dunn and Bonilla[23] indicated that mixing of the air in the transverse direction may be poor. Consequently, an alternative model in which this is taken into account, especially when the fin-tip clearance is appreciable compared with the tube pitch, should also be considered.

2.2.3 Use of published models

Cook[24], indicating methods for the design of air-cooled exchangers, suggested that the solutions for the M.T.D. for one and two process passes as given by D.M. Smith[11] generally be used where the process fluid is unmixed but where the air is *mixed*. He further indicated that the solution for two passes would adequately cover more passes as well. E.C. Smith[25], on the other hand, proposed that those solutions for models where both fluids are unmixed be used, if there is a temperature cross; otherwise no correction for cross-flow was proposed.

FLOW MODELS USED BY COOK[24]:

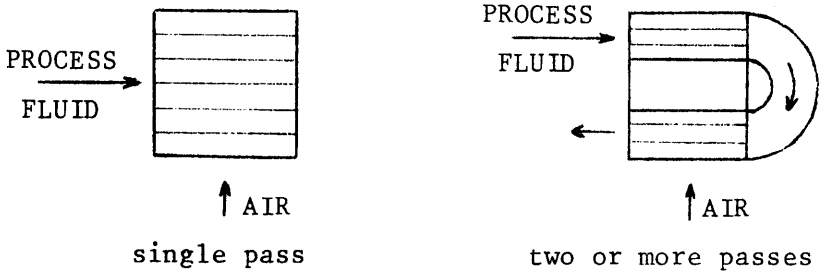

FLOW MODELS USED BY E.C. SMITH[25]:

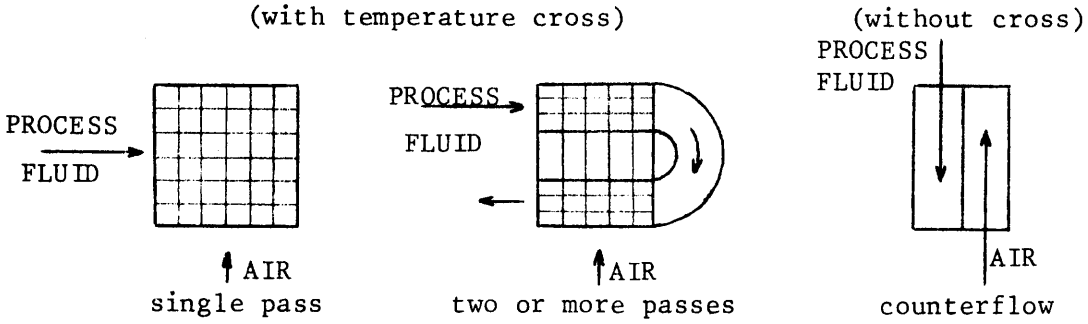

Neither of these approaches comply with the requirements for a realistic model and should, therefore, not be used.

Cases which have been solved previously and which comply with the requirements for a realistic model are shown schematically:

EXISTING MODELS FOR A SINGLE TUBE ROW PER PASS

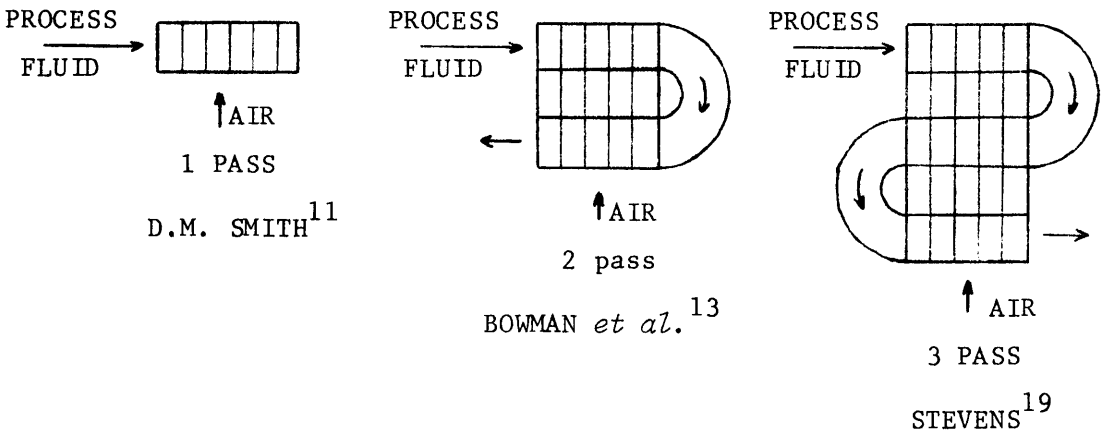

These models may be applicable only if there is a single tube row per pass. Bowman *et al.*[13] stated that the solutions for the M.T.D.

were derived by Drew for more than three such passes, but these solutions were not published.

When there is more than one row per pass published solutions exist only for a single process pass. Schedwill[21] derived an exact formula for any number or rows. Roetzel[22] presented an approximation formula for the M.T.D. for any arbitrary number of rows which is easier to use than the exact formulae which can be derived from Schedwill's work. This approximation formula generally estimates the M.T.D. sufficiently accurately for terminal temperatures normally encountered in practice. However, owing to the simple form of the approximation formula, it cannot be expected to cover the entire range of independent variables; inaccuracies were, in fact, found by checking the results from the approximation formula with those obtained from Schedwill's exact formulae.

Solutions have not been published for any of the row and pass arrangements for the alternative air flow model with incomplete mixing in the transverse direction.

2.3 SUMMARY

Provided the assumptions made for a realistic flow model with complete mixing in the transverse direction apply to air-cooled exchangers, then published solutions for the M.T.D. exist for the following cases:

(i) Any finite number of tube rows in a single pass[21];

(ii) multipass with a single row per pass for 2 passes[13] and 3 passes[20].

Solutions for more than 3 passes with a single row per pass and for any of the multipass cases with more than one row per pass are not available.

The effects of partial mixing in the longitudinal direction and of incomplete transverse mixing of the air stream, between tube rows, have not been considered for any of the row and pass arrangements of practical interest.

3 THEORY

The amount of heat transferred to or from a medium per unit of time is calculated from the flow rate, specific heat capacity and terminal temperatures:

$$Q = WC(T_1 - T_2) = wc(t_2 - t_1) \qquad (1)$$

The rate of heat transfer, Q, is dependent on the heat transfer area, A, the resistances to transfer which in turn are dependent on the fluid properties, flow rates and temperatures, and the driving force which is a function of the temperature differences throughout the exchanger. To avoid integration along the flow paths, the resistances are usually expressed as an overall heat transfer coefficient, U, and the driving force as a mean temperature difference, ΔT_m. Thus the heat transferred

$$Q = UA\ \Delta T_m \qquad (2)$$

For *counter-current* flow of the two media the driving force (derived by integration) is the logarithmic mean temperature difference:

$$\Delta T_{l.m.} = \frac{(T_1 - t_2) - (T_2 - t_1)}{\ell n\left(\frac{T_1 - t_2}{T_2 - t_1}\right)} \qquad (3)$$

In *cross-flow* the logarithmic mean temperature difference may be multiplied by a correction factor, F_T, to account for the arrangement deviating from true counterflow[13]:

$$\Delta T_m = F_T\ \Delta T_{l.m.} \qquad (4)$$

To avoid the use of absolute temperature magnitudes, to facilitate comparison of different flow arrangements and for algebraic convenience, a number of *dimensionless* variables are derived[13;20]. In many cases the names given to these variables have little physical meaning.

3.1 DERIVED VARIABLES

The stream *effectivenesses*

$$p = \frac{T_1 - T_2}{T_1 - t_1} \quad \text{and} \quad q = \frac{t_2 - t_1}{T_1 - t_1} \tag{5}$$

The *counter-flow factor*

$$r_{count} = \frac{\Delta T_{l.m.}}{T_1 - t_1} = \frac{p - q}{\ell n\left[\frac{1 - q}{1 - p}\right]} \tag{6}$$

The *cross-flow factor*

$$r_{(cross)} = \frac{\Delta T_m}{T_1 - t_1} \tag{7}$$

For convenience this subscript will be dropped and the cross-flow factor merely referred to as r.

The correction factor F_T (Equation (4)) may then be expressed in terms of r and r_{count} :

$$F_T = \frac{r}{r_{count}} \tag{8}$$

The *thermal capacity ratio*,

$$R = \frac{wc}{WC} = \frac{T_1 - T_2}{t_2 - t_1} = \frac{p}{q} \tag{9}$$

The overall *number of transfer units*, on the process side

$$NTU_p = \frac{UA}{WC} = \frac{T_1 - T_2}{\Delta T_m} = \frac{p}{r} \quad ; \tag{10}$$

on the air side on a *total* heat transfer area basis

$$NTU_a = \frac{UA}{wc} = \frac{t_2 - t_1}{\Delta T_m} = \frac{q}{r} \quad ; \tag{11}$$

or as used here, on the air side on a *per row* basis

$$NTU_{an} = \frac{UA}{nwc} = \frac{q}{nr} \tag{12}$$

3.2 HEAT EXCHANGE WITH TEMPERATURE CHANGES OF BOTH FLUIDS

The following assumptions are commonly made[13;20] in deriving mean temperature differences (M.T.D.'s) in cross-flow for non-isothermal airside and tubeside conditions:

(i) The overall heat transfer coefficient, U, is constant throughout the exchanger;

(ii) each pass has the same heat transfer area, i.e. un-symmetrical pass arrangements are not considered;

(iii) neither stream undergoes a change of phase;

(iv) the specific heat capacity of each stream is constant and independent of temperature;

(v) the flow rates of both streams are steady;

(vi) the flow of both fluids is evenly distributed over both the local and the total transfer area, (this assumption is not always stated explicitly);

(vii) heat losses from the system are negligible.

Theoretical equations were either taken from the literature where available (see Section 2.3), or were derived here for the cross-flow factor, r, and for the dimensionless local tubeside temperature drops across each row. Two alternative air flow patterns through the fin-tube bundle, both assuming *no longitudinal mixing*, were considered:

(i) the *no-bypass* model (*sequential air flow* model) where the air is assumed to be completely mixed in the *transverse* direction and to contact each row sequentially;

(ii) the *bypass* model where a fraction of the air is assumed to bypass alternate tube rows *without* mixing (in the transverse direction) with that fraction of the air which has contacted the fin-tubes.

3.2.1 Sequential air flow model

As previously noted, if the following further assumptions are made, equations appearing in the literature for certain idealised flow arrangements may be applicable to air-cooled exchangers with interpass headers:

(i) The process fluid is completely mixed at a given cross-section within any one tube but is unmixed within any one pass;

(ii) complete mixing of the process fluid takes place in the headers between passes;

(iii) the air is unmixed, even between tube rows, in the *longitudinal* direction;

(iv) there is no dispersion in the direction of air flow;

(v) the air is completely mixed in the direction normal to the flow and parallel to the fins (transverse direction);

(vi) the rows are contacted sequentially by the air stream.

Based on these combined sets of assumptions, a heat balance can be formulated over infinitesimal elements of airside fluid traversing a fin-tube, and then of tubeside fluid within that tube. By integration (first in the direction of air flow and then in the direction of tubeside flow) the equations for the cross-flow factor, r, and local dimensionless tubeside temperature drops per row can be derived. This development is given for the 1 row 1 pass arrangement, as an example, in Appendix 8.2. The equations for r, for a finite number of rows in a single pass, were taken from Schedwill's[21] general formula, while those for 2 row, 2 pass[13] and 3 row, 3 pass[20] arrangements were also taken from the literature. However, the detailed derivations for the above arrangements were nonetheless repeated as these references do not give the local dimensionless tubeside temperature drops for each row.

Four additional cases not previously reported in the literature were derived in full, namely the arrangements having 4 rows with either 2 or 4 passes and the 5 and 6 row arrangements with a single row per pass. The final equations are given in Appendix 8.3. Equations for the local tubeside temperature drops for the 5 and 6 row arrangements are however not included, as these were not required for comparison with the experimental data. The development of the theoretical equations for all these arrangements is analogous to that for the 1 row 1 pass arrangement, except that where in the latter case the inlet air temperature to the row was constant, for all other arrangements the inlet air temperature to the second and subsequent rows is a function of the tube length, being the exit air temperature from the previous row. For this reason, the equations for the local tubeside temperature drops, for the longitudinal air temperature profiles and for the cross-flow factor become increasingly complex and the derivations are filed elsewhere[26].

Preliminary comparison of the predicted local tubeside temperature drops with those measured showed poor agreement in some cases (Section 5). Therefore an alternative model for the air flow pattern through the fin-tube bundle was considered.

3.2.2 Bypass air flow model

As a gap normally exists (for fabricational reasons) between the fin tips of adjacent fin-tubes a portion of the total air flow can bypass alternate rows without affecting any significant heat transfer in the bypassed rows. Brauer[27] and Neal and Hitchcock[28], in visual studies of the detailed flow pattern through a staggered fin-tube bundle, found that, even when the fins were touching, certain areas (primarily wake regions behind the tubes) were relatively inactive in transferring heat. Their results have not however been applied here in detail. Instead a rather simplified model, considering mainly bypassing through the gap for wide fin-tip clearances, is used. Alternatively, a more detailed approximation of the air flow pattern, taking the wake regions behind the tubes into account can be considered[29].

As a simplifying approximation, for staggered fin-tube layouts where the tube pitch is not too great, the air flowing across the tubes was assumed to be divided, in the transverse direction, in to two discrete streams : that stream bypassing alternate rows being the fraction $f_B/2$ of the total air flow, and that stream contacting every row being the fraction $1 - f_B$, as shown in Figure 1. The possibility of an *overall* bypass stream due to excessive tube pitch and wall flow was not considered here. On the basis of equal flow velocities at the plane of minimum flow cross-section in the bundle the bypass fraction for any tube row was calculated (for an equilateral triangular pitch) from

$$\frac{f_B}{2} = \frac{S_t - d_f}{S_t - d_f + (d_f - d_r) \times (1 - n_f t_f)} \qquad (13)$$

When $d_f >> d_r$ the fractional fin-tube area contacted by the $f_B/2$ counterpart of this air stream may be approximated by

$$g_1 = \frac{2}{\pi} \{y\sqrt{1 - y^2} + \arcsin y\} \qquad (14a)$$

where

$$y = \frac{f_B}{2 - f_B} \qquad (14b)$$

The fraction of the air flow which contacts all the fin-tubes (viz. $1 - f_B$) then contacts the fractional fin-tube area, $g_2 = 1 - g_1$. Equations (14a) and (14b) do not account for the "passive" wake region behind the tube which becomes important when d_f is *not* $>> d_r$. Although this latter condition applied to the fin-tube bundle geometry used in this work, this simplified model gave values of g_1 and g_2 which were reasonably close to those given by the more detailed model[29].

As a further limiting and simplifying approximation, any *transverse mixing* between these two streams was *ignored*, both when flowing in the channels between fins and in the open gaps between tubes and rows, although complete mixing was assumed (parallel to the fins) within either stream. Thus three different and discrete air temperatures were assumed to exist at any horizontal cross-section drawn transversely through the bundle.

The entire fin surface at any cross-section was assumed to be at the same temperature as that of the fluid within the tube. The effect of fin, bond and tube wall resistances was accounted for in the overall heat transfer coefficient (Appendix 8.8).

The more realistic assumption of partial transverse mixing between streams leads to complex thermal relationships, even in the case of isothermal tubeside flow, and was not pursued here. In the opposite limiting case of *complete* transverse mixing between fin-tube rows, flat temperature profiles entering subsequent rows would be obtained, so that the previously considered model for sequential flow (Section 3.2.1) would then be valid provided the effective airside film coefficient was correctly defined.

The differential equations for the simplified bypass model without transverse mixing were formulated and integrated for the single pass cases having up to 4 rows, and for the two and three pass arrangements with a single row per pass. The resulting equations, both for the cross-flow factor and the local tubeside temperature drops per row, are given in Appendix 8.3. The development of these equations is analogous to that for the sequential air flow model, except that the differential equations have to be formulated and integrated for the air temperature of the three discrete air streams (see Figure 1). This, therefore, leads to more complex relationships than those for the sequential air flow model. The derivations of these equations are on file[26].

3.3 ISOTHERMAL TUBESIDE CONDITIONS

For the special case of isothermal tubeside flow, a correction to $\Delta T_{l.m.}$ is not necessary if the air stream contacts the rows sequentially. However, a correction has to be applied if the bypass air flow model is assumed, to account for the differences in air stream temperatures leaving the various rows. Such a correction, which is dependent on the number of rows, has been derived[29] for the limiting case of *no* transverse mixing, and is given in Appendix 8.4.

4 EXPERIMENTAL

4.1 EQUIPMENT

An overall view of the air-cooled test rig is shown in Figure 2.

4.1.1 Airside duct

Most of the experimental work to determine airside heat transfer and pressure drop characteristics across fin-tubes has been performed on relatively small (0,5 m × 0,5 m) bundles situated within the test section of a wind tunnel. The advantage was that an essentially uniform air velocity profile existed upstream of the bundle but boundary effects may have been important. In order to obtain an appreciable tubeside temperature difference across any one row, a longer tube length had to be used for the tests reported here, and as a wind tunnel with a sufficiently large test section was not available it was necessary to erect a suitable duct for the air flow.

Normally on industrial air-cooled units the fans are located not more than one fan diameter from the bundle. This leads to irregular air flow patterns approaching the bundle[30] especially when the unit is of the forced draught type. In induced draught industrial units especially without a long inlet plenum section and on test units with the bundle located reasonably close to a "bell-mouth" inlet, it has been shown[31] that lower heat transfer takes place in the first few rows of the bundle. This effect, referred to as a *row factor*, is apparently caused by lower turbulence as the air flows across these rows. Such a row factor was also found[32] when the bundle was located in a test rig with long straight sections on either side. No apparent advantage therefore appeared to exist for either forced or induced draught. Consequently, mainly for practical convenience, a forced draught arrangement was chosen for this test rig.

The two axial flow fans, each capable of delivering 33 m^3/s of air at standard temperature and pressure (21,1^{o}C; 1 atm.) against a static pressure of 380 N/m^2, were located within a sound proofing box (Figure 3) to reduce the noise level within the building.

Each fan, driven by a 5,6 kW motor rotating at 2 900 revolutions per minute has 7 manually adjustable blades on a rotor 0,482 m in diameter. Air at ambient temperature and pressure was drawn from within the building and the hot air after passing through the fin-tube bundle was discharged outside the building.

As it was desired to provide a relatively uniform velocity profile without yaw or swirl at the entrance to the fin-tube bundle, thus approaching an ideal wind tunnel configuration, the ductwork, made of sheet metal, was designed adhering as far as possible to recommendations in the literature[33;34]:

(i) A circular/square transition section followed by a honeycomb section with individual cell dimensions 54 × 54 × 150 mm;

(ii) four square/rectangular sections transforming each duct to the dimensions of half the fin-tube bundle;

(iii) a straight rectangular section 1,25 m long with a 50 × 20 mm diamond mesh screen at a distance 0,8 m upstream of the bundle; provision was also made for the installation of a second honeycomb should this be necessary;

(iv) a sharp 90^{o} turn in the duct within which four curved vanes with trailing edges to guide the flow were located;

(v) an adjustable louvre, at the end of each vane, to balance the flow across the bundle if this should be necessary due to varying length of air flow path, or because of outside wind conditions;

(vi) access points both below and above the bundle for the insertion of measuring equipment.

4.1.2 Fin-tube bundle

The fin-tube bundle was assembled using commercially available fin-tubing. To allow for complete flexibility, each tube row containing 10 tubes was supported by individual metal frames (Figure 4). The frame dimensions used in this experimental work were such that the tubes were spaced on a 68,5 mm equilateral triangular pitch. The overall bundle width was 0,725 m and the tube length 2,135 m. The tube pitch, which was wider than that normally used on industrial exchangers having fins of the same dimensions as used in this test rig (60,5 mm), was dictated by the cast-on (zinc) supports used for supporting the tubes at intervals along their length. This pitch also allowed access lanes for thermocouple probes, etc. in the diagonal and horizontal directions through the bundle.

A section of the fin-tube bundle is shown in Figure 5, which also shows the solid wooden strips which were located for alternate tube rows on each of the duct side-walls to minimise air by-passing along the bundle boundaries. The dimensions of these wooden strips were calculated so as to allow, at the plane of minimum cross-section, only 50% of the free flow area existing between adjacent fin-tubes. This was found necessary so as to allow for the greater friction factor for flow across fin-tubes as opposed to that across a smooth surface (flat wall or the wooden forms).

A cross-section of a fin-tube used in this work is shown in Figure 6. Each tube had 433 aluminium L-type fins (15,9 mm high) per metre, spirally wound under tension on to the 25,4 mm o.d. mild steel tube. The fin thickness at the base was 0,444 mm and tapered to 0,292 mm at the tip, the mean value being 0,368 mm.

4.1.3 Headers

Pass arrangements were attained using individual external pass headers, with an available flow area 2,5 times the total flow area of the tubes in any one header, in an attempt to achieve good flow distribution. Figure 7 shows a typical assembly of two such headers for a 4 row, 2 pass arrangement. Figure 4 shows how the fin-tubes were connected to these headers by means of flexible rubber hoses.

Pass partition plates (Figure 7) fabricated from insulating materials to minimise heat transfer from pass to pass within the headers were used. These were either inserted for the multipass arrangements, or omitted for the single pass arrangements between individual headers as required. The headers, after assembly, were covered by temporary insulation (not shown) to minimise heat losses to the ambient air.

The top blind flange of each header assembly was provided with a vent for bleeding trapped air from the system.

4.2 EXPERIMENTAL PROGRAMME

4.2.1 Air flow distribution

To test the performance of the fans and to investigate the air velocity profile both upstream and downstream of the bundle, the air velocity was measured at a number of points. These measurements were taken under isothermal conditions.

4.2.2 Preliminary calibration runs: airside film coefficient

Published data[35] of the airside heat transfer coefficient, when compared with available correlations[36;37], exhibit a scatter of roughly ± 50%. Consequently, it was necessary to determine experimentally a correlation valid for the specific fin-tube geometry used in this work.

A limited number of heat transfer tests were carried out in which saturated steam was condensed in selected tubes within the fin-tube bundle. These tests were, however, for various reasons inadequate for establishing a reliable correlation.

Therefore a more extensive series of tests was performed in which water, at a relatively high flow rate, was cooled through small temperature ranges using different air flow rates. For these tests a 6 row bundle was assembled in a single pass. Initially water flowed only through the top, middle and bottom two rows. These tests established the existence of a row factor with respect to the bottom rows. Consequently, tests for determining the airside heat transfer correlation were carried out using the top 4 rows only.

4.2.3 Main series of runs: performance of different tubeside arrangements

The main series of runs involved the study of local tube-side temperature differences attained in eight arrangements of rows and passes as shown in Figure 8. These were from one to four rows of tubes arranged in a single pass as well as the multi-pass counter-cross-flow cases consisting of 2 rows 2 passes, 3 rows 3 passes and 4 rows with 2 and 4 passes. A six row bundle was also used for these tests.

The main parameters varied for each run were the tubeside flow rate and water inlet temperature. The flow rates were chosen with the aim of attaining an outlet temperature cross with the multipass arrangements, and also such that tubeside velocities (and hence film coefficients) were approximately the same for all the different arrangements. Likewise the fan blades were set at a fixed pitch so as to maintain an essentially constant air flow rate and consequently a constant airside heat transfer coefficient. This flow rate was such that the face velocity approximated that used in industrial exchangers.

4.3 MEASUREMENTS

Only those experimental measurements which were taken during the tests to determine a correlation for the airside heat transfer coefficient, and those for the main series of runs are discussed in this section.

4.3.1 Air side

Measurements on the air side included ambient barometric pressure and relative humidity, point velocities and local temperatures, the latter before and after the fin tube bundle. The measurement of point velocities and the analysis of these results to obtain overall air flow rates is discussed in Appendix 8.5.

Air temperatures were measured using calibrated iron/constantan thermocouples connected to a Honeywell Electronik 15 recorder. One thermocouple was located, at the centre of each half of the duct, on the diamond mesh screen upstream of the bundle, for determining the mean inlet air temperature. Eight thermocouples were located at the

centres of equal areas as well as one thermocouple at a reference point in the centre of the duct, 200 mm downstream of the bundle, for measuring air temperatures leaving the bundle. The mean exit air temperature was found from a profile fitted through these measured and subsequently normalised values. As a check on the mixed air exit temperature one thermocouple was placed in the middle of the horizontal portion of duct before the air discharge point.

4.3.2 Tube side

Overall water flow rates and inlet and outlet temperatures to and from the bundle were measured. In the main series of runs local temperature differences across all the tubes in the arrangement were also measured.

The flow rate was measured indirectly via the pressure differential (mercury manometer) across a calibrated orifice plate situated in the vertical section of inlet water pipe (Figure 2). Three orifice plates of varying diameter were used to cover the range of water flow rates desired, so that in all cases pressure differentials of reasonable magnitude (10 - 100 cm Hg) could be measured.

Absolute water temperatures were measured, using iron/constantan thermocouples inserted in stainless steel thermowells containing oil, immediately prior to entering the inlet header and after leaving the exit header and also in a limited number of individual tubes (Figure 4). These thermocouples were connected to the Honeywell Electronik 15 recorder.

Local temperature differences across individual tubes were measured using screened copper/constantan thermocouples. The thermal voltages from these couples were recorded on a Hewlett Packard 2010 data acquisition system. Difficulty was experienced in finding a suitable technique for measuring these local temperature differences sufficiently accurately. The various techniques which were tried are discussed in Appendix 8.6. The copper/constantan thermocouples, inserted through the header/tube hose connections, and placed in direct contact with the water (Figure 4) were found to give the most reliable, and at the same time most consistent results.

5 RESULTS AND DISCUSSION

5.1 TEST DATA

The overall test data from the heat transfer runs are divided into two sections:

(i) preliminary calibration runs to determine the airside film coefficient (Table 1);

(ii) the main series of runs for studying the performance of different tubeside pass arrangements (Table 2.1).

5.1.1 Air side

Isothermal runs made initially to test the performance of the fans and to determine air velocity profiles both up- and downstream of the bundle showed that, over the relevant range of air flow rates, velocity profiles immediately upstream of the bundle were reasonably flat. The results of these runs are discussed in greater detail in Appendix 8.5. The complete results are filed[26].

In the preliminary calibration runs and in the main series of heat transfer tests, air flow rates were determined as described in Appendix 8.5, and inlet and mean exit air temperatures measured as described in Section 4.3.1. The mean exit air temperatures, after normalisation according to the reference point reading which usually led to negligible corrections, were in close agreement with the "approximately mixed" temperatures as measured by a single thermocouple prior to exit from the duct. The specific heat capacity of the ambient air was calculated taking humidity into account.

5.1.2 Tube side

In the main series of runs, the local tubeside temperature drops across each row were taken as the mean of the differentially measured temperature drops for all 10 tubes within that row. These mean values, along with the calculated 95% confidence limits are given, for each such row, in Table 2.2. Although these temperatures have been tabulated to a precision of 0,01°C, the actual experimental precision was ca. 1/40°C (see Appendix 8.6).

Generally, the overall temperature changes as determined from absolute measurements (Table 2.1) agreed closely with those calculated either from averaging (single pass; multirow, assuming uniform distribution) and/or from summing (multipass; 1 or 2 rows per pass) the means of the temperature drops across individual rows.

The ratios of the overall absolute to the summed differential temperature changes are shown in Table 2.1. The usually very small discrepancies appear random and do not indicate any systematic error. Absolute measurements in selected tubes of individual rows for the multipass arrangements showed that the mean outlet temperatures from one pass were almost always identical to the inlet temperatures to the next pass, thus indicating negligible heat losses from the only partially insulated headers.

In runs (i) and (j) of the 3 row, 3 pass and 4 row, 4 pass arrangements, overall temperature drops on the tubeside did not agree with the summed averages for individual rows. The local temperature drops moreover varied widely among tubes in a given row. At the low Reynolds numbers (Re_t <4 000) laminar/transitional flow with rather unpredictable (see Section 5.3) local film coefficients would be expected. Any possible air accumulation in the system may have biased the absolute temperature measurements as well. Thus, the results of these runs are suspect.

As the difference between overall inlet and outlet temperatures (measured absolutely) was considered to be more accurate than the summed *and* averaged local temperature drops across individual rows, although measured to a greater precision, the reported tubeside heat duties were determined from the measured water flow rate, the specific heat capacity at the mean water temperature, and the terminal temperatures as measured absolutely. This procedure was, moreover, consistent with that used in the preliminary calibration runs, at which stage the local inherently more accurate differential thermocouples had not yet been installed.

5.1.3 Heat balance

From Table 1 the heat balances (ratios of the heat apparently gained by the air to that apparently lost by the water) are in general far better (error random and less than ± 10%) if the heat gained by the air is calculated from air velocity measurements *upstream* of the bundle. When the airside duties were calculated from measurements *downstream* of the bundle, discrepancies of up to +30% were found (largely systematic with $Q_{air} > Q_{water}$). These discrepancies are discussed in more detail in connection with the measurement of air flow rates (Appendix 8.5).

As the flow rates and terminal temperature measurements on the tube side, combined with the measured air side temperatures (only) were considered to be the most accurately measured of the overall parameters, air flow rates, both in the preliminary calibration runs and in the main series of runs, were determined from the integrated velocity profiles upstream of the bundle, *corrected by a heat balance* assuming the tubeside heat duties and measured air temperature rises to be correct.

5.2 PRELIMINARY CALIBRATION RUNS: AIRSIDE FILM COEFFICIENT

The results of the preliminary calibration runs, with 2 rows and 4 rows in a single pass, and with relatively high tubeside flow rates, to establish an airside heat transfer correlation are discussed in detail in Appendix 8.7.

The 2 row runs showed that the local airside coefficient varied from row to row in the first two rows of the assembled 6 row bundle. Consequently, only the top 4 rows of the bundle were used for the main series of heat transfer tests. For this particular fin-tube arrangement correlations for the airside heat transfer coefficient in the top 4 rows were determined and are given in Appendix 8.7. These correlations taking both no air bypass as well as an air bypass stream into account, are only valid over a limited range of air velocities.

5.3 MAIN SERIES OF RUNS: PERFORMANCE OF DIFFERENT TUBESIDE ARRANGEMENTS

The results of the main series of runs were analysed for the assumptions of (i) sequential contacting of all tube rows by the air, and (ii) a given fraction of the air bypassing alternate tube rows. For the latter assumption, only the extreme limiting case of no transverse mixing of the air streams at different temperatures was considered. As discussed in Section 8.7.2.1, this bypass fraction was assumed to be $\frac{1}{3}$ of the total air stream. This was based on the simplified assumption of equal air velocities over the minimum cross-sectional flow area of the fin-tube bundle - Equation (13). In the following discussion the former assumption, (i), will be referred to as "no-bypass" and the latter, (ii), as "$\frac{1}{3}$ bypass". Where "$\frac{1}{3}$ bypass" has been assumed, symbols used in equations have a "prime", and parameters calculated from the experimental data given in Tables 1 and 2, are in *italics*.

The M.T.D.'s were calculated from the experimental measurements for both assumptions and were compared with those predicted by the theoretical equations (Appendix 8.3) based on the effectivenesses of each stream, p and q, as calculated from the measured terminal temperatures. The measured local tubeside temperature drops for each row were also compared with those predicted theoretically for the two assumptions (Appendix 8.3).

5.3.1 Overall heat transfer performance

The mean overall heat transfer coefficients, U, were calculated from the following equation:

$$\frac{1}{U} = \frac{1}{h_{io}} + \frac{1}{h_m} + F_i + \frac{1}{h_o} \qquad (15)$$

where

$$h_{io} = \frac{h_i \, d_i}{d_o} \qquad (16)$$

$$\frac{1}{h_m} = R_m + \frac{1}{h_w} \qquad (17)$$

$$\frac{1}{h_w} = \frac{(d_o - d_i)}{2k_w} \qquad (18)$$

The fin metal resistance, R_m, was calculated as described in Appendix 8.8.

The tubeside film coefficients, h_i, were estimated using the Engineering Sciences Data Unit correlation[38] for turbulent flow of liquids inside tubes for Reynolds numbers in the range $4\,000 < Re_t < 10\,000$, viz.

$$St = \exp[-3{,}796 - 0{,}205 \ln Re_t - 0{,}505 \ln Pr_t - 0{,}0225(\ln Pr_t)^2] \quad (19)$$

The Dittus-Boeltar equation has been found[38] to underestimate the coefficient by up to 50% in this low Reynolds number range and was therefore not used in the analysis of the main series of runs as much of the data was taken in this range. The Dittus-Boeltar equation was however used for analysis of the preliminary calibration runs where Re_t was greater than 20 000. Corrections for free convection[39;40] at low Reynolds numbers were also considered, but were found to be negligible for flow inside *horizontal* tubes.

The airside film coefficients, h_o for no bypass or h_o' for $\frac{1}{3}$ bypass, were calculated using the experimentally determined correlations for this bundle (Appendix 8.7).

The mean values of the experimentally derived mean temperature differences, $(\Delta T_m)_{exp}$, and the corresponding correction factors, $(F_T)_{exp}$, were then calculated from

$$(\Delta T_m)_{exp} = \frac{Q_{water}}{UA} \quad (20)$$

and

$$(F_T)_{exp} = \frac{(\Delta T_m)_{exp}}{\Delta T_{l.m.}} \quad (21)$$

The mean values of U and $(F_T)_{exp}$ for no bypass and those of U' and $(F_T)'_{exp}$ for $\frac{1}{3}$ bypass are given along with $\Delta T_{l.m.}$ in Table 2.1.

As both h_o and h_o' were determined experimentally, predicted values are accurate only within upper and lower confidence limits. The corresponding confidence limits on U and U' in the main series of runs were calculated, which in turn yielded corresponding confidence limits for $(\Delta T_m)_{exp}$, $(\Delta T_m)'_{exp}$, $(F_T)_{exp}$ and $(F_T)'_{exp}$.

The limits for the former two parameters are given in Table 2.2 and are plotted in Figures 9 to 16 as $(F_T)_{exp}$ and $(F_T)'_{exp}$. The best estimate of $(F_T)_{exp}$ and $(F_T)'_{exp}$ lies mid-way between the respective upper and lower limits.

For many runs the upper limit and even in a few cases the lower limit for $(\Delta T_m)_{exp}$ or $(\Delta T_m)'_{exp}$ was greater than $\Delta T_{l.m.}$ which is theoretically the maximum attainable M.T.D. for pure counterflow. This fact, therefore, indicated error or bias in the relevant experimental data points.

Values of the dimensionless parameters p and q (Equation (5)), and K, K_1 and K_2 defined in Appendix 8.3 are given in Table 2.2. The mean values of U and U' were used in the calculation of K, K_1 and K_2.

Theoretical predictions of the M.T.D.'s and local tubeside temperature drops across individual rows for the 4 row, 2 pass and 4 row, 4 pass arrangements for the case of $\frac{1}{3}$ bypass have not been shown as the theoretical equations for these arrangements had not been derived.

5.3.2 Mean temperature differences

The M.T.D.'s as predicted by the available theoretical equations for each different arrangement (Appendix 8.3.1), for no-bypass and $\frac{1}{3}$ bypass, as well as by the following approximating function ($\frac{1}{3}$ bypass only) are given in Table 2.2

$$(\Delta T_m)_{comp} \simeq \Delta T_{l.m.} (F_T)_{comp} \qquad (22)$$

where

$$(F_T)_{comp} = F_T \, F''_T \qquad (23)$$

F_T is the correction factor for the appropriate arrangement assuming no air bypassing to occur, while F''_T is that for the bypass air flow model with corresponding isothermal tubeside conditions for an even or odd number of rows, as appropriate (Appendix 8.4). Corresponding isothermal tubeside conditions are such that p = 0 but with the same airside effectiveness q as for the non-isothermal tubeside data.

For those arrangements with only a single pass, the value predicted by the no-bypass model for a large number (approaching ∞) of rows in a single pass[21] are also given in Table 2.2, but these are not plotted.

The predicted values are plotted in Figures 9 to 16, in the form of correction factors, viz. F_T, F_T' and $(F_T)_{comp}$, versus the mean tubeside Reynolds number which is dependent on the water flow rate and water inlet temperature. As the correction factors depend not only on the tubeside Reynolds number but also on airside parameters which determine the effectivenesses p and q, lines are not drawn through the predicted values.

Owing to the relatively large uncertainty in the "measured" experimental F_T 's (primarily due to uncertainty in the air film coefficient), it is not obvious, for most arrangements, which theoretical model predicts the experimental data better. However, for the 3 row, 3 pass and 3 row, 1 pass arrangements the no-bypass model was distinctly better.

The mean temperature differences predicted using the approximating function, Equation (22), are for most arrangements only slightly different from those predicted using the $\frac{1}{3}$ bypass model. Thus the approximating function may well be reasonably valid for these arrangements and may therefore be used if air bypassing occurs, instead of the more rigorous, complex equations for non-isothermal tubeside conditions with air bypass. The approximating function has been shown[29] to be *exact* for any arrangement with complete transverse mixing between rows, including specifically the 1 row, 1 pass arrangement. Only in the case of the 2 row, 2 pass arrangement did the approximation appear to fail, $(F_T)_{comp}$ being closer to F_T than to F_T'.

5.3.3 Local tubeside temperature drops

The predicted local tubeside temperature drops across each row for the cases of no bypass and $\frac{1}{3}$ bypass (Appendix 8.3.2) are compared with the measured values in Table 2.2. The ratios of the predicted to measured temperature drops are plotted against mean tubeside

Reynolds number in Figures 17 to 24 along with the upper and lower experimental confidence limits centred about unity. The individual rows are numbered in *ascending* order from the *air inlet*, e.g. row 1 is the first heated row contacted by cold air; the location (LOC), from the bottom of the 6 row bundle, of the rows used for heat transfer is given.

For all arrangements (excluding 1 row 1 pass which is discussed later in this section) the analysis which assumes no bypass almost invariably over-predicted the local temperature drop in the first effective row but under-predicted the difference in the second row, thus indicating that a fraction of the air was probably bypassing the first row and contacting the second row at an effective temperature close to the cold inlet air temperature t_1. If $\frac{1}{3}$ of the air was assumed to bypass alternate rows, the predicted temperature drops for both the first and second rows were usually much closer to, if not within, the 95% confidence limits of the measured drops. On the other hand, in the 4 row, 4 pass arrangement, the local temperature drops in both the first and second rows for the *no-bypass* model were within the measured limits.

Moreover, in any arrangement with more than two rows, the predicted local temperature drops with no bypass were always closer to the experimental values for the *third* and *fourth* rows. Possible explanations are:

(i) Any significant bypass occurred *only* across the first and second heated rows which is an unlikely model, in view of physical considerations.

(ii) Appreciable transverse mixing occurred between rows and tended to flatten the local airside transverse temperature profile. This effect would result in a closer approach to the no-bypass model in the subsequent heated rows.

(iii) The heat transfer coefficient varied appreciably from row-to-row in the heated rows. This could possibly be caused by *free convection* effects at the relatively low air velocities, or could possibly be due to actual *bias* in the *air flow resistance/transfer characteristics* of the different fin-tube rows.

Any possible row-to-row variation of the transfer coefficient was further investigated, based on the experimental data from the 1 row, 1 pass arrangement in *each* of the top four rows of the 6 row bundle. Although data for rows 5 and 6 were sparse and thus inconclusive, the $\frac{1}{3}$ *bypass model* fitted the data for *row 3* better, whereas the *no-bypass model* was more in agreement with the data for *row 4* (Figure 17). Since rows 3 and 4 were supposedly identical, and as free convection effects should have been the same in the two cases, the overall transfer coefficient apparently *did* differ between these two rows, presumably due to a variation of the controlling airside coefficient.

5.4 SUMMARY OF FINDINGS

Owing largely to apparent row-to-row variation of the local airside transfer coefficients within the experimental bundle, neither of the two proposed models for airside flow pattern could be conclusively distinguished within the limits of *local* temperature measurement error. As the *no-bypass* model generally better predicted the *overall* performance of the various arrangements, an intermediate model allowing for bypass *with* considerable local *transverse mixing* of air streams at different temperatures within the bundle appears most acceptable from physical considerations. This intermediate model reduces to the no-bypass model in the limiting case of complete transverse mixing. However, the theory for such a model has not yet been developed: its development is probably only warranted for unusual wide pitch fin-tube bundle configurations.

Since the experimental data yielded apparent values of the cross-flow correction factor greater than unity in many of the runs

indicating an underestimation of U, longitudinal mixing of the air cannot be significant regarding overall performance. Airside mixing in this direction would always tend to lower the effective mean temperature difference[13].

The range of tubeside and airside effectivenesses (p and q) which could be examined was limited by various test rig constraints for any given row and pass arrangement.

(i) For a given bundle size and air flow rate, p rises (with q decreasing but more slowly) with decreasing *water flow rate*, but the flow at rates lower than those tested, would have become largely laminar. Under these conditions the tubeside coefficients would have become controlling, variable along the length, and probably not completely predictable because of entrance/exit effects.

(ii) For a given bundle width, airside *velocity* and water flow rate, p also rises (again with q decreasing but usually more slowly) with increasing *tube length*. However longer tube lengths could not be accommodated owing to space limitations as well as the more complex ducting (re number of fans, straightening vanes, honeycombs etc.) that would have been required to ensure an even air distribution over a long, narrow cross section.

(iii) For a given physical exchanger, somewhat greater tubeside effectivenesses, p, could have been attained (for a given q) by using *alternative tubeside fluids* (e.g., chlorinated hydrocarbons) in place of water, but the existing heating system would then have had to be revised and serious safety hazards (re toxicity or flammability) would have arisen.

(iv) For a given bundle size, and water flow rate, q rises (with p decreasing but more slowly) with decreasing *air rate*, but the test rig fans were in any case being

operated at minimum blade pitch and, at lower air rates, the uncertain relative contribution of airside free convection would have increased.

(v) For a given number of tubes of fixed length, water flow rate, and *airside velocity (at minimum cross-section within the bundle)*, q also rises (again with p decreasing but more slowly) with decreasing *fin-tip clearance*. Such narrower bundle width configurations should perhaps be investigated in future work.

As a result of these constraints, no attempt was made to compare different tubeside arrangements for the same values of p and q, and temperature crosses for the 4 row, 4 pass arrangement (p + q>1) were achieved only at water velocities so low (see item (i)) that the resulting data were discounted.

Commercial fin-tubes may always exhibit some bias from tube to tube and also from row to row due to small variations in bond resistance and in tube pitch caused by non-uniform fin-tube supports. Such bias limited the application of the idealised theory to the experimental results.

Fin-tube exchangers in the process industry generally have smaller fin-tip clearances than that used in the test rig. Thus the simpler model for the air flow pattern with *no-bypass* and negligible longitudinal mixing will generally predict the *overall* true M.T.D. satisfactorily for such industrial units. However the bypass model with appreciable transverse mixing between rows appears to be necessary for exchangers with *wide* fin-tip clearances for low outside pressure drops, e.g., in high temperature waste heat rejection units ("economisers"), mine stope coolers, and some air-conditioning applications. The effect of row and pass arrangement, however, must be taken into account.

For the no-bypass model, theoretical equations are available in the literature for all the single pass cases, and for the multipass cases with a single row per pass up to 3 passes. The

preceding analysis has been extended in this work to include the latter type of counter-cross-flow multipass cases with up to 6 rows and 6 passes as well as the 4 row, 2 pass arrangement. M.T.D.'s for the 4, 5 and 6 row arrangements with a single row per pass, at values of p and q normally encountered in industrial units (at most, a moderate temperature cross) are all very close to those for counter-flow and, as an approximation, may be so considered ($F_T \simeq 1{,}0$). Theoretically (even for infinite area), no counter-cross-flow arrangement with only a finite number of rows, permits all combinations of high p and high q to be achieved. Appreciably larger temperature crosses are however theoretically attainable, the greater the number of passes.

For the no-bypass model, the cross-flow factors, r, are plotted against p, with q as a parameter (Figures 25 to 32) for all the arrangements up to 4 rows with 4 passes. These plots may be used for manual calculation. For computer design the implicit theoretical equations (Appendix 8.3) alternatively may be solved by iteration. Simpler *explicit* equations approximating the theoretical cross-flow factors for the different arrangements should be developed.

For the arrangements with 6 rows and either 2 or 3 passes (for which theoretical equations have not yet been derived), M.T.D.'s will be conservatively estimated from the equations for 2 row, 2 pass or 3 row, 3 pass respectively. Alternatively the following two approximation formulae, derived by interpolation, might be used:

for 6 row, 2 pass, $$r_{6;2} = \frac{4}{3}(r_{4;2} - r_{2;2}) + r_{2;2} \qquad (24)$$

for 6 row, 3 pass, $$r_{6;3} = r_{count} - \frac{(r_{count} - r_{3;3})(r_{count} - r_{4;2})}{(r_{count} - r_{2;2})} \qquad (25)$$

6 CONCLUSIONS

A complete range of tubeside and airside effectivenesses (p and q) could not be examined, owing to test rig limitations. These included tubeside flow rates required to maintain turbulent flow of water, tube length, tubeside fluid, fan characteristics and tube pitch. Thus the performance of different tubeside arrangements (rows and passes) could not be compared for the same p and q. A temperature cross ($p + q > 1$) was only achieved at transitional or laminar tubeside flow rates; these data are therefore suspect.

(i) As the cross-flow correction factors, F_T, were in most cases close to unity, the various theoretical models for the airside flow pattern could not be conclusively distinguished. In some cases, measurements of *local* tubeside temperature drops across individual tubes allowed comparison between the different models. These results were, however, somewhat biased by (a) *row-to-row* variation of the airside transfer coefficient, and (b) apparent variation of transfer coefficients or tubeside flow resistances among tubes of a *given row*.

(ii) Within the limitations set out above, and based on physical considerations as well, the following model was arrived at: for wide fin-tip clearances part of the air flow bypasses alternate tube rows, but appreciable transverse mixing of air streams at different temperatures occurs, primarily between the tube rows. This reduces the effects of "bypass" on transfer rates in subsequent rows. Longitudinal mixing apparently occurs only to a limited extent, if at all; theoretical models based on complete longitudinal mixing would grossly underestimate the measured transfer performance.

(iii) In most industrial air-cooled fin-tube exchangers fin-tip clearances are small so that the effects of bypass and transverse mixing may be neglected especially with respect to *overall* performance. In such cases the simpler flow models, assuming sequential contacting of the tube rows by the air stream, are acceptable.

(iv) By including models for arrangements with up to 6 rows and 6 passes, equations for the mean temperature difference are now available for most of the air-cooled fin-tube configurations normally used by the process industries.

7 REFERENCES

1 PETERS, D.L. and NICOLE, F.J.L. *Efficient programming for cost-optimised heat exchanger design*, The Chem. Engr. No.259, 98-111 (March, 1972).

2 ROETZEL, W. *Berücksichtigung veränderlicher Wärmeübergangskoeffizienten und Wärmekapazitäten bei der Bemessung von Wärmeaustauschern*, Wärme- u Stoffübertr. 2, 163-170 (1969).

3 PETERS, D.L. *Heat exchanger design with transfer coefficients varying with temperature or length of flow path*, Wärme- und Stoffübertr. 3, 220-226 (1970).

4 ROETZEL, W. *Calculation of single phase pressure drop in heat exchangers considering the change of fluid properties along the flow path*, accepted for publication in Wärme- und Stoffübertr. 1972.

5 NICOLE, F.J.L. *Cross-flow characteristics of an extended surface heat exchanger; progress report*, CSIR-CEG MEMO 70/29 (Oct. 1970).

6 KRZYMUSKI, J.I. *The application of air coolers in industry*, The Industrial Chemist, 35, 63-69 (Feb. 1959).

7 MATHEWS, R.T. *Economic applications of air cooling to process industries*, Brit. Chem. Engng. 13 (10), 1425-32 (497-504) (Oct. 1968).

8 KAYS, W.M. and LONDON, A.L. *Compact heat exchangers*, McGraw-Hill, New York, 1958.

9 NUSSELT, W. *Der Wärmeübergang im Kreuzstrom*, Zeitschrift des Vereines deutscher Ingenieur, 55, 2021-4 (1911).

10 NUSSELT, W. *Eine neue Formel für den Wärmedurchgang im Kreuzstrom*, Techn. Mechan. u. Thermodynamik, 1 (12), 417-422 (1930).

11 SMITH, D.M. *Mean temperature difference in cross-flow*, Engineering (Nov.), 479-81 and 606-7 (1934).

12 BINNIE, A.M. and Poole, E.G.C. *The theory of the single-pass cross-flow heat interchanger*, Cambridge Philosophical Soc. Proc. 33, 403-411 (1937).

13 BOWMAN, R.A., MUELLER, A.C. and NAGLE, W.M. *Mean temperature difference in design*, Trans. A.S.M.E. 62, 283-294 (May, 1940).

14 TAKAHASHI, Y. *Mean temperature difference in multi-pass cross-flow heat exchangers*, Trans. The Japan Soc. of Mech. Engrs. 8 (30/II), 1-9 (1942).

15 TAKAHASHI, Y. *Mean temperature difference in two-pass cross-flow heat exchangers*, Trans. The Japan Soc. of Mech. Engrs. 9 (36), 85-89 (1943).

16 KORST, H.H. *Mean temperature difference in multi-pass cross-flow heat exchangers*, Proceedings of the 1st U.S. National Congress of Applied Mechanics, A.S.M.E., 949-955 (1952).

17 MASON, J.L. *Heat transfer in cross-flow*, Proceedings of the 2nd U.S. National Congress of Applied Mechanics, A.S.M.E., 801-803 (1955).

18 FERNANDEZ, J. *Mean temperature difference in co-cross-flow heat exchangers*, MS-thesis, Southern Methodist University, Dallas, Texas (1956).

19 STEVENS, R.A. *Mean temperature difference in counter-cross-flow heat exchangers*, MS-thesis, Southern Methodist University, Dallas, Texas (1956).

20 STEVENS, R.A., FERNANDEZ, J. and WOOLF, J.R. *Mean temperature difference in one, two, and three-pass cross-flow heat exchangers*, Trans. A.S.M.E. 79, 287-297 (Feb. 1957).

21 SCHEDWILL, H. *Thermische Auslegung von Kreuzstromwärme-austauschern,* Fortschr.- Ber. VDI-Z. Reihe 6, Nr.19 (1968).

22 ROETZEL, W. *Mittlere Temperaturdifferenz bei Kreuzstrom in einem Rohrbündel-Wärmetauscher,* Brennstof-Wärme-Kraft (BWK), 21 (5), 246-250 (1969).

23 DUNN, W.E. and BONILLA, C.F. *Heat transfer with extended surface - No mixing parallel to the extended surface,* Ind. & Engng Chem. 40 (6), 1101-04 (June, 1948).

24 COOK, E.M. *Rating methods for selection of air-cooled heat exchangers,* Chem. Engng. 71 (16) (3 Aug), 97-104 (1964).

25 SMITH, E.C. *Air-cooled heat exchangers,* Chem. Engng 65(23), (17 Nov.), 145-50 (1958).

26 CSIR-CEG File No.66/51/4530.

27 BRAUER, H. *Wärmeübergang und Strömungswiderstand bei fluchtend und versetzt angeordneten Rippenrohren,* DECHEMA Monograph 40, 41-76 (1962).

28 NEAL, S.B.H.C. and HITCHCOCK, J.A. *A study of the heat transfer processes in banks of finned tubes in cross-flow, using a large scale model technique,* Proc. 3rd Int. Heat Transfer Conf., I. Mech. E., 290-298 (1966).

29 PETERS, D.L. *Mean temperature difference in cross-flow for isothermal tubeside conditions,* Unpublished work.

30 LAMBERT, P.C., COWAN, G.H. and BOTT, T.R. *Flow characteristics in a box-shaped plenum chamber associated with an air-cooled heat exchanger,* Chem. Eng. Division, A.E.R.E., Harwell, Berkshire, AERE-R7130 (June, 1972).

31 WARD, D.J. and YOUNG, E.H. *Heat transfer and pressure drop of air in forced convection across triangular pitch banks of finned tubes*, Chem. Eng. Prog. Symposium Series 55 (29), 37-44 (1959).

32 LAPIN, A. and SCHURIG, W.F. *Heat transfer coefficients for finned exchangers*, Ind. & Eng. Chem. 51 (8), 941-44 (Aug., 1959).

33 PANKHURST, R.C. and HOLDER, D.W. *Wind tunnel technique*, Sir Isaac Pitman & Sons Ltd, London, 1952.

34 STOKER, R.L. *Methods of producing uniform velocity distribution*, Ind. & Eng. Chem. 38 (6), 622-4 (June, 1946).

35 COWAN, G.H. *Heat exchangers with extended surfaces*, Heat Transfer and Fluid Flow Service, D.R.3, AERE R6186, January, 1970 (CONFIDENTIAL).

36 BRIGGS, D.E. and YOUNG, E.H. *Convection heat transfer and pressure drop of air flowing across tiangular pitch banks of finned tubes*, Chem. Eng. Prog. Symposium Series 59 (41), 1-10 (1963).

37 SCHMIDT, E. *Heat transfer at finned tubes and computations of tube bank heat exchangers*, Kältetechnik 15 (4), 98 (1963) and 15 (12), 370 (1963).

38 *Forced convection heat transfer in circular tubes Part I: Correlations for fully developed turbulent flow - their scope and limitations*, Engineering Sciences Data Unit, London, Item No.67016 (April, 1967).

39 *Forced convection heat transfer in circular tubes Part II: Data for laminar and transitional flows including free convection effects*, Engineering Sciences Data Unit, London, Item No.68006 (Feb., 1968).

40 KERN, D.Q. and OTHMER, D.F. *Effect of free convection on viscous heat transfer in horizontal tubes*, Trans. A.I.Ch.E. 39, 517-555 (1943).

41 KERN, D.Q. *Process heat transfer*, Tokyo, McGraw-Hill/ Kōgakusha, 1950.

42 TODD, J.F. *Field tests needed for air coolers*, Petroleum Refiner, 38 (4), 115-118 (April, 1959); see also C.E.P. 55 (6), 74-5 (June, 1959).

43 PETERS, D.L. *Air velocity and heat transfer in an air-cooled condenser*, CSIR Special Report CHEM 90 (Feb., 1969) (CONFIDENTIAL).

44 FRANCIS, J.C. *The testing of air-cooled heat exchangers*, Jnl. of Inst. of Fuel 34, 24-30 (Jan., 1965).

45 NICOLE, F.J.L. and PETERS, D.L. *Measured and calculated heat transfer in an air-cooled condenser*, CSIR Special Report CHEM 205 (May, 1972) (RESTRICTED).

46 COWAN, G.H., DELL, F.R. and STINCHCOMBE, R.A. *Airflow measurement on the air-cooled heat exchanger of the H.T.F.S. industrial test loop*, Chem. Eng. Division, A.E.R.E., Harwell, Berkshire, AERE - R7107 (June, 1972) (CONFIDENTIAL).

47 COWAN, G.H., DELL, F.R. and STINCHCOMBE, R.A. *An experimental investigation of the use of vane type anemometers to determine air mass-flow rates through finned tube bundles*, Chem. Eng. Division, A.E.R.E., Harwell, Berkshire, AERE - R6720 (Jan., 1971) (CONFIDENTIAL).

48 STRUCKMEIER, H. *Air velocity measurements with thermistors*, Staub 28 (5), 28-31 (May, 1968).

49 OWER, E. *The measurement of air flow*, Chapman & Hall, London, 1949.

50 EVANS, G.V., SPACKMAN, R., ASTON, M.A.J. and CLAYTON, C.G. *Measurement of gas flow by radiotracer methods*, Int. Conf. on Modern developments in flow measurement, Harwell, Berkshire (1971), to be published.

51 MANDERSLOOT, W.G.B., HICKS, R.E. and LANGEJAN, J.J.D. *Flow rates from multipoint measurements with velocity probes (Pitot tubes)*, The Chem. Engr. No.232, CE 370-80 (Oct., 1969).

52 PAULSEN, J.P. and HICKS, R.E. *Computation of gas and dust flow rates from point measurements in a duct, using surface fitting. User's guide to the* FORTRAN *programme* EMIT, CSIR Special Report CHEM 149 (April, 1971).

53 HICKS, R.E. *Measurement technique and systematic errors in sampling dust laden gas streams*, CSIR Special Report CHEM 188 (Nov., 1971).

54 *Survey of resistance temperature detectors*, Instruments and Control Systems, 44, 97-110 (June, 1971).

55 BECKER, J.A., GREEN, C.B. and PEARSON, G.L. *Properties and uses of thermistors - thermally sensitive resistors*, Trans. A.I.E.E., 65, 711-725 (Nov., 1946).

56 *Thermistor survey*, Instruments and Control Systems, 42, 95-100 (Oct., 1969).

57 VERSTER, T.C. *The silicon transistor as a temperature sensor*, 5th Symposium on Temperature, Washington D.C. (June, 1971).

58 VERSTER, T.C. Private communication.

59 MARQUARDT, D.W. *Least squares estimation of non-linear parameters*, Engineering Dept., E.I. Du Pont de Nemours & Co.,Inc., Wilmington, Delaware (Aug., 1966).

60 KAYS, W.M. and LO, R.K. Tech. Rept. NR-035-104, Dept. of Mech. Eng., Stanford University, Calif. (Aug., 1952).

61 NICOLE, F.J.L. and PETERS, D.L. *Cost-optimised design of air-cooled heat exchangers including isothermal condensers. User's guide to the heuristic* FORTRAN *programmes* AEROCOOL *and* AEROCOND, *each with either budget- or detailed costing,* CSIR Special Report CHEM 161 (Jan., 1971) (RESTRICTED).

62 DUSINBERRE, G.M. *Fin efficiency,* Mech. Eng. 78 (6), 570 (1956).

8.1 LITERATURE SURVEY - SUMMARY OF REFERENCES ON MEAN TEMPERATURE DIFFERENCE IN CROSS-FLOW

Ref.	Author	Pass		Rows	Mixed (M) or Unmixed (U)			r or ΔT_m presentation					Analysis			Remarks
		Single	Multi		tube side	air side	between passes	Series	Implicit	Explicit	Tabular	Graphical	Analytical	Numerical	Graphical	
9	Nusselt	Y		∞	U	U		Y	Y				Y			Presented equation for mean outlet temperature of either fluid; slowly converging infinite series in form of Bessel functions
10	Nusselt	Y		∞	U	U		Y	Y		Y		Y			Presented a more rapidly converging infinite series; introduced concept of dimensionless temperature differences; presented tables of r and F_T as functions of p and q
11	Smith,D.M.	Y	Y	∞	MU	MU	U	Y	Y	Y		Y	Y			For Nusselt case, presented implicit doubly infinite series for r i.t.o. p and q. First to present all three cases of single pass cross-flow; also two of the 2 pass cases.
12	Binnie & Poole	Y		∞	U	U		Y	Y				Y			Implicit series for ΔT_m; slightly different form to that of Nusselt
13	Bowman, Mueller & Nagle	Y	Y	∞ finite	MU	MU	MU	Y	Y	Y		Y				Review of all previous work; included unpublished equations for trombone coolers; presentation in the form of F_T's
14	Takahashi		Y	∞	U	U	U					Y			Y	Graphical trial and error method for obtaining ΔT_m for multipass arrangements based on single pass case
15	Takahashi		Y	∞	U	U	U					Y			Y	As for previous ref. (14) but specifically for two-pass exchangers
16	Korst		Y	∞	U	U	MU					Y	Y	Y		First to propose cyclical reiteration process of numerical integration for counter-cross-flow arrangements
17	Mason	Y		∞	U	U		Y	Y				Y			Solved differential equations using Laplace transforms, yielding explicit relation for p i.t.o. NTU, but implicit for r; series converges more rapidly than those of Nusselt (10) or Binnie and Poole (12).
18	Fernandez	Y	Y	∞ finite	MU	MU	MU		Y		Y	Y	Y	Y		Review of solutions for co-cross-flow; presented solutions for previously unsolved cases up to 3 passes; graphs of effectiveness correction factor versus NTU
19	Stevens	Y	Y	∞ finite	MU	MU	MU		Y		Y	Y	Y	Y		Review of solutions for counter-cross-flow; used Korst's method (16) for solving unsolved cases up to 3 passes; same presentation as Fernandez (18)
20	Stevens Fernandez & Woolf	Y	Y	∞ finite	MU	MU	MU		Y			Y	Y	Y		Paper based on the work of Stevens (19) and Fernandez (18)
21	Schedwill	Y		finite	U	U		Y	Y			Y	Y			Derived general implicit equation for r for any finite number of rows in a single pass; presented graphs for up to 3 rows
22	Roetzel	Y		finite	U	U				Y			Y			Proposed approximation formula for r for any finite number of rows in a single pass based on power law interpolation between r for 1 row and Nusselt's (9; 10) case for ∞ rows

8.2 DEVELOPMENT OF THE THEORETICAL EQUATIONS FOR THE 1 ROW, 1 PASS ARRANGEMENT

To illustrate the general method of derivation, equations for the cross-flow factor, r, and for the dimensionless tubeside temperature drop are developed in detail here for the *sequential* air flow model only. The mathematical solution for this case is well known in the published literature[11;41].

Consider the differential element of area contacted by the two streams in cross-flow, as shown :

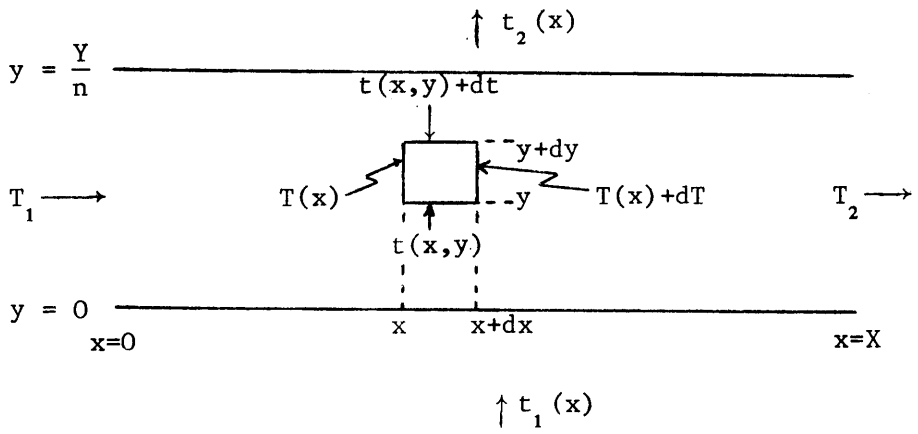

Here n=1 and XY is the total heat transfer area, A.

An amount of air = $wc(\frac{dx}{X})$ flows past the strip dx exchanging heat with the mixed tubeside fluid at temperature T(x).

Thus $wc(\frac{dx}{X})dt = U\ dx\ dy(T-t)$ (26a)

or $$\frac{dt}{dy} = \frac{XU}{wc}(T-t) \tag{26b}$$

Integration followed by substitution of the boundary conditions,

at y=0, $t=t_1$

and at $y = \frac{Y}{n}$, $t=t_2$, with XY = A, gives

$$\frac{T - t_1}{T - t_2} = \exp\left\{\frac{UA}{nwc}\right\} = e^{q/nr} \tag{27}$$

since $$\frac{UA}{nwc} = \frac{q}{nr} \tag{12}$$

Thus $$t_2 - t_1 = (T - t_1)K \tag{28}$$

with $$K = 1 - \exp\left\{-\frac{UA}{nwc}\right\} = 1 - e^{-q/nr} \tag{29}$$

A heat balance over the strip of width dx yields

$$-WCdT = (t_2 - t_1)wc\left(\frac{dx}{X}\right) \tag{30}$$

since the tubeside fluid is cooled with increasing x.

Eliminating $(t_2 - t_1)$,

$$\frac{dT}{T-t_1} = -K\,\frac{wc}{WC}\,\frac{dx}{X} \tag{31}$$

As for this specific case, t_1 is a constant independent of x (viz. the cold air inlet temperature), integration followed by substitution of the boundary conditions, at $x = 0$, $T = T_1$ and at $x = X$, $T = T_2$ yields

$$\frac{T_2 - t_1}{T_1 - t_1} = \exp\left\{-K\frac{wc}{WC}\right\} = e^{-KR} \tag{32}$$

since $$\frac{wc}{WC} = \frac{p}{q} = R \tag{9}$$

Rearrangement of Eqn. (32) yields the dimensionless local tubeside temperature drop

$$\frac{\Delta T_1}{T_1 - t_1} = \frac{T_1 - T_2}{T_1 - t_1} = 1 - e^{-KR} \tag{33}$$

and further rearrangement including the substitution

$$p = \frac{T_1 - T_2}{T_1 - t_1} \tag{5}$$

yields the implicit equation for the cross-flow factor, r

$$\frac{1}{1-p} = e^{KR} = \exp\left\{\frac{p}{q}\,(1 - e^{-q/r})\right\} \tag{34}$$

For this case only, r may also be expressed explicitly

$$r = \frac{-q}{\ln\left\{1 + \frac{q}{p}\ln(1-p)\right\}} \tag{35}$$

8.3 THEORETICAL EQUATIONS FOR TEMPERATURE CHANGES OF BOTH FLUIDS

The assumptions made in the derivation of the equations for M.T.D.'s and dimensionless local tubeside temperature drops are given, along with the definition of parameters, in Section 3.

8.3.1 Mean temperature differences

Implicit equations for the cross-flow factor, r, which can be solved by iteration for known p and q are given.

8.3.1.1 *Sequential air flow model*

Let $$R = \frac{p}{q} \qquad (9)$$

and $$K = 1 - e^{-q/nr} = 1 - \exp(-\ NTU_{an}) \qquad (29)$$

where n is the number of heated rows.

Single tubeside pass. Schedwill's formula[21] in terms of the nomenclature used here is

$$\frac{1}{1-p} = \frac{ne^{nKR}}{1 + \sum_{i=1}^{n-1} \sum_{j=0}^{i} \binom{i}{j} K^j e^{-(i-j)q/nr} \sum_{k=0}^{j} \frac{(nKR)^k}{k!}} \qquad (36)$$

where

$$\binom{i}{j} = \frac{i!}{(i-j)!\,j!}, \quad \text{i.e.} \qquad (37)$$

the number of combinations of i taken j at a time.

By expansion of equation (36), the following equations are obtained for the specific arrangements considered :

Rows	Passes		
1	1	$\frac{1}{1-p} = e^{KR}$	(38a)
2	1	$\frac{1}{1-p} = \frac{e^{2KR}}{1 + RK^2}$	(38b)
3	1	$\frac{1}{1-p} = \frac{e^{3KR}}{\{1 + RK^2(3-K) + \frac{3}{2}R^2K^4\}}$	(38c)
4	1	$\frac{1}{1-p} = \frac{e^{4KR}}{\{1 + RK^2(6-4K+K^2) + 4R^2K^4(2-K) + \frac{8}{3}R^3K^6\}}$	(38d)

Multipass arrangements. Solutions for the 2 row, 2 pass and 3 row, 3 pass cases are taken from Stevens, Fernandez and Woolf[20]

Rows	Passes		
2	2	$\frac{1}{1-p} = \frac{K}{2} + (1 - \frac{K}{2})e^{2KR}$	(39a)
3	3	$\frac{1}{1-p} = K\{1 - \frac{K}{4} - RK(1-\frac{K}{2})\}e^{KR} + (1-\frac{K}{2})^2 e^{3KR}$	(39b)

Multipass arrangements (cont.) : the following cases were derived in this work :

Rows	Passes		
4	2	$\frac{1}{1-p} = \{\frac{R}{2}K^3[4 - K + 2RK^2] + e^{4KR} + K[1 - \frac{K}{2} + \frac{K^2}{8}][1 - e^{4KR}]\} \div (1 + RK^2)^2$	(40a)
4	4	$\frac{1}{1-p} = \frac{K}{2}(1 - \frac{K}{2} + \frac{K^2}{4}) + K(1 - \frac{K}{2})\{1 - \frac{R}{8}K(1 - \frac{K}{2})\}e^{2KR} + (1 - \frac{K}{2})^3 e^{4KR}$	(40b)
5	5	$\frac{1}{1-p} = \{K(1 - \frac{3}{4}K + \frac{K^2}{2} - \frac{K^3}{8}) - RK^2[1 - K + \frac{3}{4}K^2 - \frac{1}{4}K^3 - \frac{R}{2}K^2(1 - \frac{K}{2})^2]\}e^{KR}$	(40c)
		$+\{K(1 - \frac{3}{4}K + \frac{1}{16}K^3) - 3RK^2(1 - \frac{K}{2})^3\}e^{3KR} + (1 - \frac{K}{2})^4 e^{5KR}$	
6	6	$\frac{1}{1-p} = \frac{K}{2}(1 - K + K^2 - \frac{1}{2}K^3 + \frac{1}{8}K^4) + K(1 - K + \frac{3}{4}K^2 - \frac{5}{16}K^3 + \frac{1}{32}K^4)e^{2KR}$	
		$- RK^2\{2 - 3K + 3K^2 - \frac{7}{4}K^3 + \frac{3}{8}K^4 - RK^2(2 - 3K + \frac{3}{2}K^2 - \frac{1}{4}K^3)\}e^{2KR}$	(40d)
		$+\{\frac{K}{2}(2 - 2K + \frac{1}{2}K^3 - \frac{1}{8}K^4) - 4RK^2(1 - \frac{K}{2})^4\}e^{4KR} + (1 - \frac{K}{2})^5 e^{6KR}$	

8.3.1.2 *Bypass air flow model*

$$\text{Let} \quad K_1 = 1 - \exp\{-\frac{2g_1}{f_B}\frac{q}{nr}\} \tag{41}$$

$$K_2 = 1 - \exp\{-\frac{g_2}{1 - f_B}\frac{q}{nr}\} \tag{42}$$

$$Z = R[\frac{f_B}{2} K_1 + (1 - f_B) K_2] \tag{43}$$

Single pass arrangements:

Rows	Passes		
1	1	$\frac{1}{1-p} = e^{Z}$	(44a)
2	1	$\frac{1}{1-p} = \frac{e^{2Z}}{\{1 + RK_2^2(1 - f_B)\}}$	(44b)
3	1	$\frac{1}{1-p} = \frac{e^{3Z}}{\{1 + RK_2^2(1 - f_B)[3 - K_2 + \frac{3}{2}RK_2^2(1 - f_B) + RK_1^2\frac{f_B}{2}\}}$	(44c)
4	1	$\frac{1}{1-p} = \frac{e^{4Z}}{\{1 + RK_2^2(1 - f_B)[6 - 4K_2 + K_2^2 + RK_1^2 f_B + 4RK_2^2(1 - f_B)(2 - K_2 + \frac{2}{3}RK_2^2)] + RK_1^2 f_B + R^2K_1^2K_2^2 f_B(1 - f_B)\}}$	(44d)

Multipass arrangements with a single row per pass:

Rows	Passes		
2	2	$\frac{1}{1-p} = \{1 - RK_2^2\frac{1 - f_B}{2Z}(1 - e^{-2Z})\}e^{2Z}$	(45a)
3	3	$\frac{1}{1-p} = \{1 - RK_2^2\frac{1 - f_B}{2Z}(1 - e^{-2Z})\}^2 e^{3Z} - R\{\{1 - K_2 + R\frac{1 - f_B}{2Z}K_2^2[1 - \frac{1}{2Z}(1 - e^{-2Z})]\}(1 - f_B)K_2^2 + \frac{f_B}{2}K_1^2\}e^{Z}$	(45b)

8.3.2 Local dimensionless tubeside temperature drops

In the following equations for the local tubeside temperature drops per row, where n is the total number of heated rows, the individual rows are numbered in *ascending* order from the *air inlet*, e.g. ΔT_1 is the temperature drop across the lowest heated row.

8.3.2.1 *Single pass arrangements*

For the *sequential air flow* model,

where $K = 1 - e^{-q/nr} = 1 - \exp(-\frac{UA}{nwc})$ (29)

$$\frac{\Delta T_1}{T_1 - t_1} = 1 - e^{-nKR} \tag{46a}$$

$$\frac{\Delta T_2}{T_1 - t_1} = 1 - (1 + nRK^2)e^{-nKR} \tag{46b}$$

$$\frac{\Delta T_3}{T_1 - t_1} = 1 - \{1 + nRK^2(2 - K) + \frac{1}{2}n^2R^2K^4\}e^{-nKR} \tag{46c}$$

$$\frac{\Delta T_4}{T_1 - t_1} = 1 - \{1 + nRK^2[3 - 3K + K^2 + \frac{n}{2}RK^2(3 - 2K) + \frac{1}{6}n^2R^2K^4]\}e^{-nKR} \tag{46d}$$

For the *bypass air flow* model, where K_1, K_2 and Z are defined in equations (41) to (43)

$$\frac{\Delta T_1}{T_1 - t_1} = 1 - e^{-nZ} \tag{47a}$$

$$\frac{\Delta T_2}{T_1 - t_1} = 1 - \{1 + nRK_2^2(1 - f_B)\}e^{-nZ} \tag{47b}$$

$$\frac{\Delta T_3}{T_1 - t_1} = 1 - \{1 + nRK_2^2(1 - f_B)[2 - K_2 + \frac{n}{2}RK_2^2(1 - f_B)] + nRK_1^2\frac{f_B}{2}\}e^{-nZ} \tag{47c}$$

$$\frac{\Delta T_4}{T_1 - t_1} = 1 - \{1 + nRK_2^2(1 - f_B)[3 - 3K_2 + K_2^2 + \frac{n}{2}RK_2^2(1 - f_B)(3 - 2K_2) + \frac{1}{6}n^2R^2(1 - f_B)^2K_2^4 + nR\frac{f_B}{2}K_1^2] + nRK_1^2\frac{f_B}{2}\}e^{-nZ} \tag{47d}$$

8.3.2.2 *Multipass arrangements with a single row per pass*

For the *sequential air flow* model, where K is defined in equation (29)

$$\psi_1 = e^{-KR} \tag{48a}$$

$$\psi_2 = \frac{\psi_1}{1 - \frac{K}{2} + \frac{K}{2}\psi_1^2} \tag{48b}$$

$$\psi_3 = \frac{\psi_1}{1 - \frac{K}{2} - [R(1 - \frac{K}{2})K^2 - \frac{K}{2}]\psi_1\psi_2} \tag{48c}$$

$$\psi_4 = \frac{\psi_1}{1 - \frac{K}{2} + \frac{\phi_1}{\phi_2}} \tag{48d}$$

where $\phi_1 = K^2\{\frac{1}{4}(1 - \frac{K}{2}) - R(1 - \frac{K}{2})^2\} + \frac{K}{2}(1 - \frac{K}{2} + \frac{K^2}{4})\psi_1^2$ (49a)

$$\phi_2 = K(1 - \frac{K}{4}) - RK^2(1 - \frac{K}{2}) + \frac{(1 - \frac{K}{2})^2}{\psi_1^2} \tag{49b}$$

For the *bypass air flow* model, with K_1, K_2 and Z as defined in equations (41) to (43),

$$\psi_1' = e^{-Z} \tag{50a}$$

$$\psi_2' = \frac{\psi_1'}{1 - RK_2{}^2 \frac{1 - f_B}{2Z}(1 - \psi_1'\psi_1')} \tag{50b}$$

$$\psi_3' = \frac{\psi_1'}{\psi_1'/\psi_2' - \phi_3 \psi_1'\psi_2'} \tag{50c}$$

where $$\phi_3 = RK_1{}^2 \frac{f_B}{2} + RK_2{}^2 (1 - f_B)\{1 - K_2 \tag{51}$$

$$+ RK_2{}^2 \frac{1 - f_B}{2Z} [1 - \frac{1}{2Z}(1 - \psi_1'\psi_1')]\}$$

Then using either equations (48 a) to (48 d) for the sequential air flow model or equations (50 a) to (50 c) for the bypass model the local tubeside temperature drops become:

$$\frac{\Delta T_1}{T_1 - t_1} = (1 - \psi_1) \prod_{i=2}^{n} \psi_i \tag{52a}$$

$$\frac{\Delta T_2}{T_1 - t_1} = (1 - \psi_2) \prod_{i=3}^{n} \psi_i \tag{52b}$$

$$\frac{\Delta T_3}{T_1 - t_1} = (1 - \psi_3) \prod_{i=4}^{n} \psi_i \tag{52c}$$

$$\frac{\Delta T_4}{T_1 - t_1} = (1 - \psi_4) \tag{52d}$$

where $$\prod_{i=j}^{n} \psi_i = \psi_j \ \psi_{j+1} \cdots \psi_n \tag{53a}$$

but $$\prod_{i=j}^{n} \psi_i = 1 \text{ for } j > n \tag{53b}$$

For the bypass model ψ_1', ψ_2', ψ_3' and ψ_i' replace ψ_1, ψ_2, ψ_3 and ψ_i respectively in equations (52a) to (52c). Equations for the 4 row, 4 pass arrangement have not been derived for the bypass model.

8.3.2.3 *The 4 row, 2 pass arrangement*

Equations are given for the *sequential air flow* model only.

$$K = 1 - e^{-q/nr} = 1 - \exp(-NTU_{an}) \tag{29}$$

$$\theta_1 = e^{-2KR} \tag{54a}$$

$$\theta_2 = \theta_1^2 \tag{54b}$$

$$\theta_3 = 1 + RK^2 \tag{54c}$$

$$\theta_4 = 1 + 2RK^2 \tag{54d}$$

$$\chi = \frac{\theta_1 \theta_3}{\{1 - K[1 - \frac{K}{2} + \frac{K^2}{8}](1 - \theta_2) + \frac{R}{2} K^3 [3 - K + \theta_4]\ \theta_2\}} \tag{55}$$

Then, $$\frac{\Delta T_1}{T_1 - t_1} = (1 - \theta_1)\ \chi \tag{56a}$$

$$\frac{\Delta T_2}{T_1 - t_1} = (1 - \theta_1 \theta_4)\ \chi \tag{56b}$$

$$\frac{\Delta T_3}{T_1 - t_1} = 1 - \{\theta_1 + \frac{K}{2}[1 + (1 - \frac{K}{2})(1 - \theta_2) - \theta_2 \theta_4]\chi\} \tag{56c}$$

$$\frac{\Delta T_4}{T_1 - t_1} = 1 - \{\theta_1 \theta_4 + [K(1 - \frac{3}{4} K + \frac{1}{4} K^2)(1 - \theta_2) - RK^3 (2 - K + \theta_4)\ \theta_2]\chi\} \tag{56d}$$

8.4 CORRECTION FACTOR FOR BYPASS FLOW MODEL WITH ISOTHERMAL TUBESIDE CONDITIONS

These equations are discussed in Section 3.3

$$K_1 = 1 - \exp\{-\frac{2g_1}{f_B}\frac{UA}{nwc}\} \tag{41}$$

$$K_2 = 1 - \exp\{-\frac{g_2}{1 - f_B}\frac{UA}{nwc}\} \tag{42}$$

Then for any *even number* of heated rows

$$F_T'' = \frac{wc}{UA}\{-\ln[f_B(1 - K_1)^{\frac{n}{2}} + (1 - f_B)(1 - K_2)^n]\} \tag{57}$$

For a *single row*

$$F_T'' = \frac{wc}{UA}\{-\ln[\frac{f_B}{2}(2 - K_1) + (1 - f_B)(1 - K_2)]\} \tag{58}$$

For *3 heated rows*

$$F_T'' = \frac{wc}{UA}\{-\ln[\frac{f_B}{2}(2 - 3K_1 + K_1^2) + (1 - f_B)(1 - K_2)^3]\} \tag{59}$$

8.5 DETERMINATION OF AIR FLOW RATE

Various potentially useful methods (equipment and techniques) for the determination of air flow rates through air-cooled fin-tube bundles are reviewed. The preliminary test rig results from several such methods are discussed and the technique and calculational procedure ultimately adopted are described.

8.5.1 Continuous scanning techniques

Vane anemometers of the integrating type have been found to be the most suitable instrument for continuous scanning of the entire flow area of the duct or plenum chamber over a measured period of time. This gives the "mean" velocity. Although Todd[42] has claimed that the air flow rate could be determined to within ± 10%, field work by the CEG[43] has shown that for *induced draught* exchangers, the air flow rate may be overestimated by up to 40%.

8.5.2 Multipoint velocity measurements

8.5.2.1 *Pitot tubes*

Stationay Pitot tubes may be used for measuring local velocities at selected points in ducts where the gas velocities are relatively high (> 10 m/s). However, at the low face velocities (3 to 4 m/s) normally encountered in air-cooled exchangers Pitot tube differential pressures are small (less than 1 mm water gauge) and hence difficult to measure accurately. In any event the measurements tend to be erratic as the Pitot calibrations may no longer apply accurately in this range. Furthermore, Pitot tube readings are affected greatly by yaw or swirl in the flow, or by the local velocity distribution existing in flow immediately downstream of a fin-tube bundle. In one case[43] where an ellipsoidal-head Pitot tube was used, the air flow rate was overestimated by 40 to 50%.

8.5.2.2 *Vane anemometers*

Direct reading vane anemometers are better suited to the measurement of low air velocities and may be used at multiple

stationary points[43;44;45;46]. These anemometers do not yield a true point velocity reading but rather a value averaged over the diameter of the instrument.

The behaviour of vane anemometers when located downstream of a fin-tube bundle situated in a wind tunnel has been extensively investigated elsewhere[47]. The anemometer readings were found to depend markedly on the distance between the anemometer and the fin-tubes, especially close to the bundle where the positioning of the instrument relative to the tube pitch pattern then determines the reading, and leads to considerable overestimation of the air flow rate.

8.5.2.3 *Thermistors and hot wire probes*

Although thermistors[48] and various hot wire probes[49] are suited to certain specific applications, the measurement of air flow through air-cooled exchangers with these devices has not been reported.

8.5.2.4 *Major limitation*

The major limitation of all the instruments mentioned so far for multipoint measurements is that none can really provide simultaneous measurements of both direction and magnitude, and thus none can give the required velocity component normal to the flow area. Because of time dependent fluctuations, e.g., wind effects on industrial exchangers, the direction of flow (using for example a yawmeter) cannot first be determined, followed by measurement of the magnitude in that direction. It may, however, be possible to devise an assembly of thermistors (or similar inexpensive probes), so arranged electronically as to give directly the required velocity component.

8.5.3 Tracer techniques

Two approaches based on injection of a tracer appear superficially suitable for measuring air flow rates through air-cooled exchangers: (i) the determination of residence times (using pulse injection), and (ii) the steady state sampling of tracer dilution.

With radioactive ^{85}Kr as the tracer both techniques have been reported[50] to yield accurate measurements of gas flow provided the tracer is well mixed with the gas. As, however, the airside residence times through air-cooled exchanger bundles are usually very short (ca. 50 millisecond), the former technique is difficult to implement in practice.

The second technique, constant-rate injection of the tracer, has been tested (again with ^{85}Kr as the tracer) or a forced draught industrial rig[46]. Over the large cross-sectional flow area of the exchanger incomplete mixing of the tracer with the main air stream was observed unless the tracer was injected and also sampled simultaneously at a very large number of points. The method thus requires further development and testing before it can be applied with confidence to air-cooled heat exchangers.

In principle any tracer gas which could be sampled and analysed, while being injected in sufficiently small quantities so as not to change the overall flow rate or heat transfer appreciably could be used.

8.5.4 Flow distribution and the measurement technique adopted

Apart from the tracer technique none of the previously discussed methods presented any marked advantages in the case of the test rig. As the last discussed technique would have required considerable effort to implement with respect to instrumentation, the measurement of multipoint velocities with a stationary probe was chosen. A 115 mm diameter electronic vane-anemometer (Airflow Developments) reading rate directly via a capacitance cell was used.

8.5.4.1 *Overall distribution : balancing of the two fans*

For equal fan blade pitch settings on both fans (more than 10^{o}), the two fans did not deliver equal flows of air. The fan delivering air to the shorter total flow path (see Figure 2) delivered ca. 15% more air than the other. Adjusting the louvres in the ducting downstream of the bundle did not correct the flow maldistribution.

Louvres would perhaps have been more effective if they had been located upstream of the bundle and relatively close to the fans, especially before the flow from the two fans had combined. By setting the blade pitches on the two fans at different angles, it was possible, however, to balance the flow reasonably well.

8.5.4.2 *Detailed investigation of local air flow distributions*

Local air velocities were measured at 30 points at distances of 80 mm, 400 mm and 1,5 m upstream of the bundle, as well as at distances 80 mm and 200 mm downstream of the bundle.

(i) *Upstream of the bundle* : At a distance 1,5 m upstream of the bundle, before the flow from the two fans had combined and upstream of the diamond mesh screen but downstream of the honeycombs, the flow was highest near the walls of the rectangular duct especially in the corners and lowest at the centre. The residual swirl imparted to the air by the fan, was however found to be small (maximum yaw 10^{o} at the walls; zero to 5^{o} at the centre), thus illustrating the relative effectiveness of the honeycomb. Results have been reported[30] showing similar low velocities, at points corresponding to the fan centres of a forced draught exchanger. In the present test rig, however, once the air from the two fans had combined and passed through the screen, the distribution at both 80 mm and 400 mm upstream of the bundle was relatively uniform provided the average flow velocity was less than 5 m/s. This corresponded to pitch settings of 25^{o} and 15^{o} on the two fans. With the fan blade pitches set at greater angles the fans developed incipient stalling, as detected by a surging at the air intake. Under incipient surging the measured velocities fluctuated with time as well as from point to point.

(ii) *Downstream of the bundle* : Air velocity measurements taken only 80 mm downstream of the bundle yielded "high" or "low" readings, depending on whether the anemometer was located directly over a gap in the last row of fin-tubes or over the centre of a fin-tube, (see Section 8.5.2.2). Measurements taken 200 mm downstream of the bundle showed however that

these velocity peaks had decayed and that the velocity profile was again relatively flat. The apparent average velocity at this location was, however, up to 8% greater than that measured 400 mm *upstream* of the bundle.

8.5.4.3 *Measurement technique adopted*

Based on the preceding results, total air flow rates for the heat transfer tests, were determined from 8 standard point velocity measurements based on the equal areas principle and taken 400 mm upstream of the bundle. In the earlier runs, for check purposes only, 8 similar measurements were also taken 200 mm downstream of the bundle.

All readings were corrected for air density based on a calibration curve. Air velocity was also measured periodically (using the same anemometer) at a reference point located at approximately the centre of the duct in the same plane as the equal area measurements. This provided a check on possible velocity fluctuations with time.

8.5.5 Analysis of multipoint measurements

The total volumetric air flow rate was determined by computer fitting and integration of the velocity profile passing through the point measurements[51]. All readings were first corrected to standard conditions of temperature and pressure (21,1°C; 1 atm.), and normalised with respect to time according to the reference point readings. The profiles so fitted were based on a first-order polynomial modification of the $\frac{1}{7}$ power law distribution for rectangular chambers[52].

This method takes velocity decay at the walls into account, and should therefore yield more realistic values of total flow than a simple weighted summation. In a recent publication[53], however, it is recommended that, in rectangular ducts, and for an ideal velocity profile (which may not have existed in the experimental duct), 16 point measurements should be taken and that these be located at representative points according to the $\frac{1}{7}$ power law distribution. As this procedure was not used, small (up to 5%) systematic positive errors may be expected.

8.6 DIFFERENTIAL TEMPERATURE MEASUREMENT

Four types of temperature sensors were considered for measuring temperature drops across individual tubes. Initially, an accuracy of 0,01°C over a temperature difference of 10°C (i.e. 0,1%) was desired. A digital voltmeter (DVM) with a resolution of 1 μV, connected to a data acquisition system, was available for recording voltages from the sensors together with their associated electronic circuitry.

The sensors had to be small enough not to disturb the flow excessively when inserted in a 25 mm i.d. rubber hose connecting the fin-tubes to the headers. This was chosen as the most convenient point for measuring the local tubeside temperature.

8.6.1 Platinum resistance thermometers

These sensors can probably measure *absolute* temperatures to within 0,005°C, yielding a linear response over a wide range. However, the cost of 80 of these sensors to measure all the local tubeside temperatures simultaneously, combined with the cost of the required precision d.c. bridge would have been prohibitive.

8.6.2 Thermistors

Owing to their large negative temperature coefficients, thermistors can measure, in principle, temperature changes to within $0,5 \times 10^{-3}$ °C. However, as resistance changes rapidly and *non-linearly* with temperature, relatively complex electronic circuitry would have been required to achieve the required temperature accuracy. More important, as no two apparently identical thermistors yield exactly the same response curves, each of 80 such thermistors would have had to be calibrated at many points within the temperature range, a prohibitively time-consuming procedure.

8.6.3 Silicon transistors

Silicon *transistors* can, in principle, be converted into highly accurate thermometers yielding a linear voltage response with temperature[57]. Such a circuit using two matched transistors for

differential temperature measurement was designed[58], built and calibrated for a maximum temperature difference of 14°C. By manual adjustment of variable resistances within the circuit the difference in base emitter voltages, after amplification, could be set numerically equal to the temperature differential where a signal of 1,00V corresponded to a temperature difference of 1,00°C.

The output signals after calibration of 20 such transistor-pair differential thermometers, varied only slightly (< 5 mV) for any given temperature difference, but when the transistors were inserted in 5 mm diameter metal wells located in the rubber hoses of the test rig, the apparently measured temperature drops for various tubes within the same tube row differed by as much as 40%. For a reasonably even flow distribution among the various tubes, discrepancies of this magnitude would *not* be expected. Hence severe maldistribution of flows was apparently being induced by the uncontrolled flow resistance of these large-diameter thermowells. As transistors of a smaller physical size, but having the required electrical rating, could not be obtained at the time, experiments with transistor thermometers were discontinued.

8.6.4 Copper/constantan differential thermocouples

Copper/constantan thermocouples (thermal e.m.f. 42,8 μV per °C in the range 40 to 60°C) were arranged in a differential temperature measuring circuit. Initially, the small diameter (30 SWG) thermocouple wires were screened and inserted into the rubber hosing through 1 mm stainless steel thermowells. The thermocouple tips were soldered to the "open" end of the thermowells so that the tips were in direct contact with the water. Owing to possible short circuit current paths between the thermocouple wires, stainless steel wells and through the mildly conductive mains water the resulting temperature difference measurements were unreliable.

Subsequently, sealed thermowells, filled with a medium grade oil, were tested but as the insulation around the thermocouple wires continually absorbed and depleted the oil eventually resulting in "dry" conditions and poor thermal contact, erroneous differential temperature readings again were obtained.

Finally, the thermocouple wires were inserted directly (without any thermowell or protective sheath) into the rubber hoses so that the tips were in direct contact with the water but at a distance from any other metal conductor. As leakage current paths through the mildly conductive water were then apparently negligible, reproducible voltage readings were then attained and the indicated temperature differences varied but little from tube to tube in a given row. This method was therefore adopted. Owing to the limited sensitivity (1 μV) of the DVM the temperature differences could only be measured to a precision equivalent to $(1/42{,}8)^{o}C$.

8.7 DETERMINATION OF THE AIRSIDE HEAT TRANSFER COEFFICIENT

8.7.1 Condensation of steam

Low pressure steam at approximately 120 kN/m^2 abs. was condensed in selected tubes of a 4 row bundle. Precautions were taken to approach isothermal condensation: e.g. the venting of non-condensables from both headers; provision of steam traps and a slight sloping of the tubes (ca. 1^o to the horizontal) to facilitate the draining of the condensate.

The condensate collected and inlet and outlet temperatures were measured. The air flow rate was determined as described in Appendix 8.5. The results are filed[26] within the CEG.

More than one tube row could not be used without substantial subcooling of the condensate, owing to the limited steam supply combined with the high condensing coefficient. Moreover, the steam may have entered the exchanger in a partly condensed or "wet" condition, or air may have been entrained, as shown by inconsistencies between the measured pressures and temperatures at the inlet.

The experimental data were therefore not expected to give particularly reliable estimates of the airside heat transfer coefficients and, indeed, preliminary simplified analysis[26] confirmed a large scatter of the calculated coefficient for any specific air flow rate. Further, as at most only one row of tubes could be used, the effects of thermal by-passing even for isothermal tubeside conditions (Section 3.3) would also have had to be taken into account.

Therefore an alternative method for establishing the airside film coefficient was adopted.

8.7.2. Cooling of water at high flow rates

Initially, to investigate possible row-to-row variations of the transfer coefficient, hot water, at relatively high flow rates (Re_t >20 000) with correspondingly small water temperature changes (p<~0,1), was cooled in separate runs through the bottom, middle

and top two rows of a six row bundle. The results, together with the calculated logarithmic mean temperature differences, the F_T correction factors (in this case for the 2 row, 1 pass arrangement), overall heat transfer coefficients and estimated airside film coefficients, calculated as described in detail in the following Section 8.7.2.1, are given in Table 1.1.1.

Subsequently to determine the airside coefficient more accurately, a similar series of runs were performed, in which the water flowed through the top 4 rows of the 6 row bundle. The results (measured and calculated) are presented in Table 1.1.2.

8.7.2.1 *Analysis*

The discrepancies in heat balances as calculated from tubeside and airside data respectively, and the calculation of the air velocities for use in correlating the airside film coefficient, have already been discussed (Section 5.1.3).

The overall heat transfer coefficient was calculated from

$$U = \frac{Q_{water}}{A\ \Delta T_m} \qquad (60)$$

where

$$\Delta T_m = F_T\ \Delta T_{l.m.} \qquad (4)$$

For a small tubeside effectiveness ($p<\sim 0,1$) and a single tubeside pass, the assumptions regarding mixing on the air side and the effect of the number of rows in parallel was not critical. F_T was therefore expected to be very close to unity. As, however, implicit equations for the M.T.D. for the 2 row and 4 row arrangements in a single pass without airside bypassing were available (Appendix 8.3.1), these were used in analysing this data.

It was subsequently considered desirable to re-analyse the data from the 4 row 1 pass arrangement, assuming a given fraction of the air had bypassed alternate tube rows without transverse mixing between the air streams. For the fin-tube bank geometry used in

this work, and based on the simplified formula (Equation (13); Section 3.2.2), a hypothetical bypass fraction of 0,3 was calculated. This hypothetical fraction was arbitrarily increased to one-third to allow for the unknown but presumably lower pressure drop friction factor for air flow in the gap between fin-tubes versus that for flow between the fins.

The theoretical formula for the M.T.D. for the 4 row, 1 pass arrangement with bypassing and with a tubeside temperature change ($p \neq 0$) had not been derived at the time of analysing this data. Therefore, the correction factor, F_T, without bypassing but with a tubeside temperature change was first applied to $\Delta T_{l.m.}$. This was followed, as an approximation to account for bypassing, by application of the correction factor, F_T'', for the case of corresponding isothermal tubeside conditions (i.e., $p = 0$ but with the same airside effectiveness q as the experimental data).

Thus $$F_T' \simeq (F_T)_{comp} = F_T \; F_T'' \qquad (23)$$

As Equation (57) (Appendix 8.4) for F_T'' requires that, to avoid iteration, U, rather than the airside effectiveness q, be known, the value of U used was that calculated using the logarithmic M.T.D. corrected only for the 4 row, 1 pass arrangement *without* bypass. Since the F_T'' correction factors from Equation (57) were in all cases between 0,99 and unity for the values of p and q involved, iteration to make U consistent with measured q was not necessary. The compounded correction factors for no-bypass multiplied by those for bypass for the case of isothermal tubeside conditions are given *in italics* in Table 1.1.2. A possible further correction to account for the "interaction" of these two correction factors versus the true correction factor for the 4 row, 1 pass arrangement would apparently be extremely close to unity.

The airside film coefficient was obtained by difference, based on the overall coefficient calculated according to Equation (60):

$$\frac{1}{h_o} = \frac{1}{U} - \frac{1}{h_{io}} - F_i - \frac{1}{h_m} \qquad (15)$$

where h_{io} and h_m are defined in Equations (16) and (17). The tubeside fouling factor, F_i, was taken in all cases to be zero as the tubes were periodically cleaned, and no scale deposit was observed during the time of the experiments. For similar reasons no fouling factor on the air side was included. The tubeside film coefficient, h_i, for all runs used to evaluate the airside film coefficient, was calculated using the well-known Dittus-Boeltar equation for fully developed turbulent flow[41]:

$$h_i = 0{,}023 \frac{k_t}{d_i} (Re_t)^{0,8} (Pr_t)^{0,33} \qquad (61)$$

8.7.2.2 *Correlation*

For a fixed fin-tube geometry, as used in this work, the airside film coefficient may be expected[36] to vary only with the Reynolds number calculated at the minimum cross-section for flow through the fin-tube bank, and to a slight extent with the airside Prandtl number. The mean airside Prandtl numbers raised to the one-third power as is usually the case in most of these correlations, varied by less than 0,5% over the range of air temperatures encountered in the work and were therefore treated as constant. As air viscosity likewise varied only slightly, the Reynolds number was replaced by the maximum air velocity (at standard temperature and pressure) at the minimum cross-section[24]. Thus the experimental data were correlated in the form

$$h_o = a(V_m)^b \qquad (62)$$

A least squares estimation program[59] was used for determining the non-linear parameters, 'a' and 'b'. In all cases, the experimental data were screened for correlation purposes and any data point which yielded a residual greater than two standard deviations from the fitted correlation was rejected. As the computer program does not linearise the proposed form of the correlation, undue weight is not placed on the inherently less accurate data at lower values of the independent variable.

Existence of a row factor - 2 row, 1 pass data - Initially the data from the *two row* runs were correlated, neglecting the effect of air bypassing. Data from the bottom two rows gave

$$h_o = 317,6\ V_m^{0,733} \qquad (63)$$

while for the middle two rows

$$h_o = 336,0\ V_m^{0,780} \qquad (64)$$

The small range of V_m examined for the top two rows did not permit correlation of these data alone, but when the data for both the middle and top two rows were combined the resulting correlation was

$$h_o = 342,7\ V_m^{0,779} \qquad (65)$$

Thus the determined film coefficient over the top 4 rows of the 6 row bundle appeared to be independent of row number, while that for the bottom 2 rows was significantly lower (ca. 12% at V_m = 3,5 m/s). As noted in Section 4.1.1 other workers[31;60] have also found this row-to-row effect in the initial two or three rows of a fin-tube bundle. Having established that a row factor therefore did exist in the first two rows of the experimental bundle, all subsequent heat transfer tests (including the main series of runs) were performed using *only* the top 4 rows of the 6 row bundle and no further detailed analysis of these preliminary 2 row, 1 pass data was attempted.

Final determination of h_o *- 4 row, 1 pass data* - Airside film coefficients for the 4 row runs both without and with air bypass taken into account were correlated against maximum air velocity. These data were obtained in two series of runs separated by a period of approximately 2 months. The data from both series of runs together with the final fitted correlations and the non-linear 95% confidence limits calculated by the program are plotted in Figures 33 and 34. These figures show that there was no significant fouling during the work and that the results were, to a first approximation when the same rows were used, reproducible. The fitted correlations were:

for no air bypass $h_o = 341,2\ V_m^{0,787}$ (66)

for $\frac{1}{3}$ air bypass $h_o' = 345,8\ V_m^{0,784}$ (67)

h_o is the apparent air film coefficient when no air bypass is considered, while h_o' is the local or "true" coefficient over the transfer area for the case where only part of the air contacts the area of any one tube row (i.e. the bypass air flow model). These two correlations show that, for the fin-tube geometry used here and for an even number of heated rows (specifically 4), the film coefficient h_o', was only marginally (1%) higher than h_o.

In all correlations (Equations (63) to (67)), the exponent on V_m (and thus on airside Reynolds number) was higher than that normally found (~0,7)[31;36] for forced convection heat transfer across fin-tubes of this type, and was in fact closer to that for turbulent flow *inside* smooth round tubes (viz. 0,8). This difference probably resulted from the relatively small range over which the air velocity was varied (two-fold) so that h_o was determined more accurately than 'a' or 'b'. A published correlation[36] yielded a value for h_o which was 10% lower (at V_m = 3,5 m/s) than that obtained with Equation (66). Nevertheless, Equations (66) and (67) were regarded as valid for this particular bundle configuration over the examined air velocity range, and were used for calculating the airside film coefficient in the main series of runs.

8.8 FIN-TUBE CHARACTERISTICS

The dimensions of an individual fin-tube and of the assembled bundle were given in Section 4.1.2 (Figs. 5 and 6).

The following equations for auxiliary fin-tube characteristics, used in the determination of heat transfer performance, were taken from previous work.[61] All the equations are for tapered circular spirally-wound L-type fins.

Fin root diameter,

$$d_r = d_o + 2(2t_f - t_f') \tag{68}$$

Ratio of total outside area to bare tube outside area,

$$\Omega = \frac{\{(d_f + d_r)\,[(d_f - d_r)^2 + 4(t_f - t_f')^2]^{\frac{1}{2}} n_f/2 + d_f n_f t_f' + d_r[1 - n_f(2t_f - t_f')]\}}{d_o} \tag{69}$$

Ratio of overall bundle face area to minimum free area for air flow through the fin-tube bundle,

$$\xi = \frac{S_t}{S_t - (d_f - d_r)t_f n_f - d_r} \tag{70}$$

The effective fin metal resistance, R_m, really depends on the fin efficiency. Although the latter varies appreciably with the airside coefficient, h_o, R_m on the other hand varies only slightly with h_o and thus could be calculated from the simplified approximation of Dusinberre[62] in the following form with respect to the bare tube outside area[61].

$$R_m = \frac{\beta}{\Omega + \gamma(\Omega + h_o\beta)} \tag{71}$$

where

$$\beta = \frac{(d_f - d_r)^2 (d_f/d_r)^{\frac{1}{2}}}{6t_f k_f} \tag{72}$$

and

$$\gamma = \frac{d_r(1 - n_f t_f)}{(d_f^2 - d_r^2) n_f/2 + d_f n_f t_f} \tag{73}$$

For fins with a high thermal conductivity (as used here), and thus with fin efficiencies close to unity, the use of the preceeding approximation has been shown to yield reasonably accurate values of R_m. A "mean" h_o of 1 100 W/(m^{2}K) was used in Equation (71) to estimate R_m (taken as a constant). Over the experimental range ($800<h_o<1\ 250$) R_m varied by only $0,5 \times 10^{-6}$ m^{2}K/W, resulting in a negligible error in the estimate of U.

The calculated values of these fin-tube characteristics for the fin-tube bundle used in this work are:

$$\left.\begin{aligned} d_r &= 0,0263 \text{ m} \\ \Omega &= 23,13 \\ \xi &= 1,832 \\ R_m &= 1,321 \times 10^{-4} \text{ m}^2\text{K/W} \\ &\quad [\text{for } h_o \simeq 1\ 100 \text{ W/(m}^2\text{K)}] \end{aligned}\right\} \qquad (74)$$

8.9 TABLES

Note:

(i) Values given in italics are for the assumption of a given fraction (specifically $\frac{1}{3}$) of the air bypassing alternate tube rows.

(ii) Local tubeside temperature drops (Table 2.2):

Rows are numbered in *ascending* order from the *air inlet*; e.g., row 1 is the first heated row contacted by cold air.

Measured temperature drops are given as the mean (of 10 values) $\pm$ the 95% confidence limits for the mean.

TABLE 1 Determination of airside heat transfer coefficient*

1.1 Measured and calculated parameters

1.1.1 Arrangement : 2 Row 1 Pass Areas : Bare tube 3,405; total outside 78,76 m^2

Run†	Tube side				Air side					Heat transfer performance						
	Flow rate	T_1	T_2	h_i	Flow rate m^3_{NTP}/s			t_1	t_2	Q_{water}	$\frac{Q_{air_A}}{Q_{water}}$	$\frac{Q_{air_B}}{Q_{water}}$	$\Delta T_{Lm.}$	F_T	U	h_o
					Measured		Corrected									
	kg/s	°C	°C	W/(m^2 K)	Above	Below		°C	°C	kW			°C		W/(m^2 K)	W/(m^2 K)
A18	4,786	90,0	84,7	4 808	3,143	2,742	2,695	18,6	51,1	106,67	1,167	1,018	51,28	0,9904	617,1	839,0
A19	4,263	81,6	74,4	4 117	4,780	4,768	5,019	18,9	40,0	128,84	1,095	1,095	48,22	0,9902	792,7	1264,3
A20	6,701	82,8	77,1	5 992	4,822	4,716	5,636	19,3	42,7	160,39	1,086	1,084	48,41	0,9915	981,6	1564,0
A21	6,748	45,0	43,0	4 518	4,864	4,891	4,504	18,2	28,5	56,44	1,080	1,086	20,37	0,9926	820,0	1290,6
A22	6,670	76,4	71,8	5 730	4,556	4,655	4,968	20,0	41,3	128,72	1,092	1,094	42,91	0,9920	888,3	1356,3
A23	6,775	61,0	58,0	5 190	4,722	4,820	4,664	20,3	35,3	85,10	1,013	1,034	31,32	0,9931	803,8	1199,3
A25	6,788	42,3	40,5	4 428	4,860	5,026	4,385	18,4	28,0	51,09	1,109	1,147	17,92	0,9920	844,4	1361,9
A26	6,811	59,7	56,7	5 158	4,615	4,642	4,521	19,5	35,1	85,55	1,021	1,027	30,48	0,9925	830,7	1262,5
A27	6,663	76,8	72,4	5 746	4,787	4,679	4,445	19,8	42,6	123,05	1,077	1,053	42,74	0,9918	852,7	1274,1
A28	4,678	77,0	71,3	5 315	4,588	4,741	4,554	19,7	39,8	111,85	1,007	1,041	44,01	0,9912	753,3	1148,9
A29	6,788	76,8	72,5	5 834	4,603	4,768	4,723	20,5	41,7	112,46	0,975	1,010	43,00	0,9926	842,9	1247,5
A31	6,663	76,8	72,7	5 751	4,433	4,712	4,833	21,7	41,2	114,61	0,917	0,975	42,84	0,9934	791,1	1141,1
A32	4,640	77,0	71,5	4 290	4,569	4,742	4,808	22,5	40,8	107,05	0,950	0,986	42,78	0,9915	750,2	1143,8
A33	6,743	60,5	57,8	5 156	4,566	4,800	4,647	22,5	36,0	76,26	0,982	1,033	29,57	0,9937	762,0	1110,5
A34	6,710	60,5	57,8	5 136	4,710	5,051	4,664	22,3	35,7	75,85	1,011	1,084	29,83	0,9939	751,5	1089,5
A35	6,764	44,0	42,5	4 494	4,539	4,933	4,538	22,2	29,9	42,43	1,001	1,088	17,01	0,9940	737,1	1098,0

* h_o and h_o' based on bare tube outside area

† A18 - A23 middle 2 rows; A25 - A29 top 2 rows; A31 - A35 bottom 2 rows

TABLE 1.1 (Cont.)

1.1.2 Arrangement : 4 Row 1 Pass Areas : bare tube 6,810; total outside 157,52 m^2

Run	Tube side				Air side					Heat transfer performance						
	Flow rate kg/s	T_1 °C	T_2 °C	h_i W/(m² K)	Flow rate m^3_{NTP}/s Measured Above	Measured Below	Corrected	t_1 °C	t_2 °C	Q_{water} kW	Q_{air_A}/Q_{water}	Q_{air_B}/Q_{water}	$\Delta T_{Lm.}$ °C	F_T / F_T'	U / U' W/(m² K)	h_o / h_o' W/(m² K)
1	8,250	49,8	48,4	3 194	3,031	2,625	2,501	26,9	42,7	48,31	1,210	1,048	12,98	0,9835 *0,9747*	556,1 *561,1*	804,2 *814,7*
2	8,194	68,2	65,4	3 676	3,125	2,647	2,822	27,8	55,8	96,15	1,108	0,938	22,73	0,9810 *0,9722*	633,3 *639,0*	931,3 *943,8*
3	9,037	49,7	48,4	3 434	3,008	2,691	2,535	26,8	42,7	49,15	1,185	1,060	12,95	0,9845 *0,9757*	566,2 *571,3*	807,8 *818,3*
4	8,974	69,0	66,4	3 980	3,256	2,661	2,814	28,3	56,8	97,78	1,156	0,944	22,75	0,9821 *0,9732*	642,3 *648,7*	929,9 *942,4*
5	8,250	49,7	48,1	3 188	3,746	3,506	3,135	26,8	41,2	55,22	1,195	1,119	13,94	0,9846 *0,9771*	590,7 *595,3*	879,1 *889,2*
6	8,203	68,9	65,3	3 688	3,984	3,819	3,726	25,8	52,9	123,76	1,070	1,025	26,00	0,9813 *0,9738*	712,6 *718,1*	1112,4 *1125,9*
7	9,037	49,8	48,3	3 434	3,810	3,553	3,202	26,9	41,4	56,70	1,190	1,110	13,92	0,9854 *0,9779*	607,4 *612,1*	894,5 *904,7*
8	8,977	67,9	64,4	3 935	4,070	3,767	3,904	24,7	52,1	131,66	1,043	0,964	25,93	0,9816 *0,9739*	759,7 *765,9*	1201,4 *1216,4*
9	8,249	50,1	47,9	3 190	4,043	3,818	4,461	26,9	40,8	75,91	0,906	0,856	14,33	0,9805 *0,9735*	793,6 *799,4*	1418,5 *1436,9*
10	8,195	67,9	64,1	3 654	4,030	3,999	4,073	24,8	50,9	130,49	0,990	0,982	26,56	0,9816 *0,9745*	735,1 *740,5*	1172,4 *1186,2*
11	9,036	50,1	48,5	3 441	4,098	3,842	3,625	27,4	41,0	60,48	1,130	1,060	14,22	0,9857 *0,9788*	633,8 *638,3*	952,2 *962,4*
12	8,989	64,5	61,0	3 836	4,214	4,035	4,166	22,5	48,3	131,77	1,013	0,969	25,73	0,9813 *0,9749*	765,8 *771,6*	1222,4 *1243,2*
13	8,248	50,2	47,70	3 189	4,870	4,364	4,301	22,2	38,6	86,26	1,132	1,015	17,63	0,9826 *0,9758*	731,4 *736,4*	1231,4 *1245,8*
14	8,237	64,8	61,2	3 584	4,571	4,353	4,191	23,8	47,9	124,21	1,090	1,038	25,80	0,9828 *0,9760*	719,4 *724,4*	1141,2 *1153,9*
15	9,037	49,8	47,6	3 423	4,804	4,463	4,216	22,6	38,7	83,17	1,139	1,059	17,11	0,9840 *0,9771*	725,7 *730,8*	1178,7 *1192,2*
16	9,037	64,8	61,5	3 865	4,576	4,448	4,098	23,2	48,0	124,92	1,117	1,085	26,08	0,9841 *0,9772*	715,0 *720,1*	1100,0 *1112,0*
17	8,252	49,1	47,2	3 167	4,480	4,252	4,039	26,9	40,1	65,58	1,109	1,053	13,88	0,9828 *0,9759*	706,2 *711,2*	1165,2 *1178,9*
18	8,193	68,7	64,8	3 674	4,606	4,965	4,352	26,8	51,9	133,89	1,058	1,140	25,98	0,9810 *0,9740*	771,7 *777,2*	1265,4 *1280,4*
19	9,038	49,4	47,7	3 419	4,430	4,333	4,014	27,8	40,8	64,27	1,103	1,079	13,47	0,9839 *0,9769*	712,2 *717,3*	1143,9 *1157,1*
20	8,975	68,6	65,0	3 954	4,710	4,399	4,343	26,6	52,0	135,40	1,085	1,013	25,96	0,9822 *0,9751*	780,0 *785,7*	1250,7 *1266,3*

TABLE 1.1.2 (Cont.)

Run	Tube side			Air side					Heat transfer performance						
	Flow rate kg/s	T_1 °C	T_2 °C	h_i W/(m² K)	Flow rate m^3_{NTP}/s Measured Above	Measured Below	Corrected	t_1 °C	t_2 °C	Q_{water} kW	$\frac{Q_{air_A}}{Q_{water}}$	$\frac{Q_{air_B}}{Q_{water}}$	$\Delta T_{l.m.}$ °C	F_T / F_T'	U / U' W/(m² K)	h_o / h_o' W/(m² K)
21	8,268	43,8	42,8	3 033	3,040	2,987	2,341	26,5	38,6	34,57	1,299	1,276	9,75	0,9841 *0,9752*	529,1 *533,9*	760,2 *770,2*
22	8,194	68,2	65,1	3 672	3,151	3,200	2,966	24,4	53,9	106,45	1,062	1,078	25,21	0,9818 *0,9733*	631,7 *637,2*	928,3 *940,2*
23	9,058	43,4	42,5	3 252	3,096	3,023	2,324	26,5	38,5	34,09	1,330	1,299	9,40	0,9848 *0,9756*	540,7 *545,8*	768,5 *778,7*
24	8,976	68,3	65,4	3 956	3,198	3,222	2,983	24,5	54,6	109,08	1,072	1,080	24,86	0,9822 *0,9735*	656,1 *662,0*	959,9 *972,5*
25	8,260	46,5	45,3	3 105	3,750	3,510	2,881	28,3	40,1	41,454	1,303	1,220	10,83	0,9844 *0,9765*	571,0 *575,6*	843,2 *853,4*
26	8,204	65,0	61,9	3 586	4,033	3,856	3,371	24,4	50,3	106,53	1,195	1,143	24,34	0,9825 *0,9749*	654,3 *659,5*	985,6 *997,4*
27	9,060	42,9	42,0	3 237	3,768	3,518	2,569	26,5	37,3	34,10	1,466	1,369	9,70	0,9866 *0,9785*	523,6 *527,9*	735,1 *743,7*
28	8,995	62,6	60,4	3 800	3,638	3,588	2,805	26,6	50,7	82,87	1,296	1,278	20,97	0,9846 *0,9763*	589,6 *594,7*	832,5 *842,5*
29	8,990	67,0	64,0	3 920	4,104	3,806	3,355	24,1	51,8	113,00	1,225	1,138	25,54	0,9836 *0,9752*	660,7 *666,0*	972,3 *983,8*
30	8,266	44,4	43,0	3 044	3,938	4,114	3,338	25,4	37,3	48,39	1,181	1,234	11,72	0,9837 *0,9763*	626,3 *631,1*	977,0 *988,7*
31	8,201	65,9	62,5	3 606	4,076	4,029	3,557	23,0	50,0	116,81	1,146	1,132	25,96	0,9824 *0,9748*	672,8 *678,0*	1026,1 *1038,3*
32	9,080	44,3	43,0	3 280	4,202	4,045	3,312	24,8	37,0	49,36	1,270	1,222	11,94	0,9855 *0,9781*	616,5 *621,1*	928,2 *938,9*
33	8,984	66,0	63,0	3 887	3,921	4,030	3,507	23,9	50,4	112,90	1,117	1,148	25,57	0,9842 *0,9767*	658,8 *663,9*	970,8 *981,8*

TABLE 2 Investigation of different row and pass arrangements

2.1 Measured and calculated parameters

2.1.1 Arrangement: 1 Row 1 Pass Areas: Bare tube 1,702; total outside 39,38 m^2

Run (Row)*	Tube side						Air side				Heat transfer performance				
	Flow rate	Reynolds Number	T_1	T_2	ΔT_{diff}	$\frac{\Delta T_{abs}}{\Delta T_{diff}}$	Flow rate Measured	Flow rate Corrected	t_1	t_2	Q_{water}	$\frac{Q_{air}}{Q_{water}}$	$\Delta T_{l.m.}$	Mean $(F_T)_{exp}$ / $(F_T)'_{exp}$	$\frac{U}{U'}$
	kg/s		°C	°C	°C		m^3_{NTP}/s	m^3_{NTP}/s	°C	°C	kW		°C		W/(m² °K)
b (3)	0,744	7 454	47,4	42,4	4,99	1,002	3,171	2,907	21,2	25,6	15,56	1,091	21,499	0,8817 *0,8871*	482,4 *484,9*
g (3)	0,746	9 054	60,2	52,6	7,54	1,008	3,176	3,049	22,0	28,4	23,74	1,042	31,196	0,8816 *0,8770*	507,2 *509,9*
h (3)	1,138	11 372	46,6	42,9	3,76	0,984	3,209	2,954	21,1	26,0	17,62	1,086	21,194	0,8958 *0,8906*	545,1 *548,3*
i (3)	1,500	17 940	57,8	53,2	4,56	1,009	3,199	3,123	21,4	29,0	28,88	1,024	30,275	0,9221 *0,9165*	607,8 *611,5*
b (4)	0,734	7 330	47,7	41,8	5,82	1,014	3,173	2,981	19,8	24,8	18,10	1,064	22,447	0,9766 *0,9717*	485,2 *487,7*
b (4)	0,759	7 857	49,7	43,8	5,88	1,003	3,169	3,020	21,3	26,4	18,74	1,049	22,898	0,9702 *0,9652*	495,6 *498,2*
f (4)	0,368	3 639	48,1	40,2	8,42	0,938	3,174	2,935	20,9	24,3	12,17	1,081	21,472	0,8858 *0,8822*	375,8 *377,3*
h (4)	1,178	11 503	45,4	41,6	3,82	0,995	3,126	2,907	20,3	25,6	18,71	1,075	20,541	0,9841 *0,9783*	543,9 *547,1*
i (4)	0,754	9 212	61,1	52,7	8,41	0,999	3,181	2,903	21,4	28,9	26,50	1,096	31,749	0,9834 *0,9781*	498,6 *501,3*
b (5)	0,754	7 695	48,6	43,3	5,11	1,037	3,167	2,987	23,2	27,8	16,72	1,060	20,448	0,9778 *0,9728*	491,3 *493,8*
e (5)	0,759	9 189	60,1	52,4	7,65	1,007	3,172	3,001	23,3	30,0	24,47	1,057	29,597	0,9597 *0,9546*	506,2 *508,9*
h (5)	1,499	18 426	59,7	54,8	4,91	0,998	3,157	3,008	22,6	31,0	30,75	1,050	30,416	0,9932 *0,9870*	598,0 *601,7*
a (6)	0,774	9 253	59,4	52,0	7,18	1,031	3,204	2,951	23,3	30,0	23,97	1,086	29,050	0,9608 *0,9556*	504,6 *507,3*
b (6)	0,771	7 736	47,4	42,6	4,68	1,026	3,160	2,896	23,2	27,6	15,48	1,091	19,600	0,9529 *0,9479*	486,9 *489,4*
h (6)	1,513	18 186	58,2	53,4	4,75	1,011	3,204	3,022	21,7	30,0	30,41	1,060	29,916	0,9967 *0,9905*	599,1 *602,9*

* Indicates row (from bottom of 6 row bundle) in which heat transfer run was performed.

TABLE 2.1 (Cont.)

2.1.2 Arrangement: 2 Row 1 Pass Areas: Bare tube 3,405; total outside 78,76 m^2

Run	Tube side						Air side				Heat transfer performance				
	Flow rate	Reynolds Number	T_1	T_2	ΔT_{diff}	$\frac{\Delta T_{abs}}{\Delta T_{diff}}$	Flow rate Measured	Flow rate Corrected	t_1	t_2	Q_{water}	$\frac{Q_{air}}{Q_{water}}$	$\Delta T_{l.m.}$	Mean $(F_T)_{exp}$ / $(F_T)'_{exp}$	$\frac{U}{U'}$
	kg/s		°C	°C	°C		m^3_{NTP}/s	m^3_{NTP}/s	°C	°C	kW		°C		$W/(m^2\ °K)$
a	1,512	9 165	60,3	52,4	7,87	1,004	3,184	2,894	19,2	33,4	50,01	1,100	29,940	0,9857 *0,9804*	497,8 *500,5*
b	1,522	8 046	50,7	45,3	5,41	0,998	3,156	3,111	22,4	31,5	34,38	1,015	20,996	0,9548 *0,9500*	503,8 *506,5*
c	3,008	18 748	60,6	55,7	4,94	1,992	3,213	3,001	19,8	36,7	61,71	1,071	29,494	1,0270 *1,0206*	598,5 *602,3*
d	3,020	16 033	49,9	46,6	3,28	1,006	3,142	3,092	22,2	33,3	41,69	1,016	20,250	1,0112 *1,0051*	598,1 *601,7*
e	0,754	4 485	60,9	49,5	11,36	1,004	3,176	2,925	20,4	30,5	35,95	1,086	29,745	0,9017 *0,8979*	393,8 *395,5*
f	0,759	3 980	51,7	43,4	8,12	1,022	3,147	2,926	20,6	28,0	26,34	1,076	23,247	0,8651 *0,8615*	384,8 *386,4*
g	2,256	13 962	60,8	54,6	6,20	1,000	3,184	3,026	19,8	35,5	58,56	1,052	29,888	0,8651 *1,0131*	564,8 *566,1*
h	2,265	11 900	50,0	45,3	4,67	1,006	3,201	3,128	19,2	30,9	44,53	1,023	22,418	1,0191 *1,0312*	562,7 *565,9*

2.1.3 Arrangement: 3 Rows 1 Pass Areas: Bare tube 5,106; total outside 118,14 m^2

a	2,246	8 772	57,7	50,7	6,78	1,032	3,237	3,132	19,0	36,3	65,80	1,034	26,214	0,9624 *0,9575*	510,8 *513,4*
b	2,264	7 959	50,5	45,2	5,27	1,006	3,190	3,039	19,8	33,4	50,20	1,050	20,977	0,9421 *0,9372*	497,5 *500,1*
c	4,556	18 064	57,1	53,2	3,76	1,037	3,271	3,040	19,5	39,6	74,37	1,076	24,722	0,9806 *0,9745*	600,8 *604,5*
d	4,518	16 017	50,0	46,7	3,05	1,082	3,256	3,183	20,0	36,1	62,37	1,023	19,609	1,0270 *1,0209*	606,5 *610,2*
e	5,621	22 251	56,7	53,4	3,21	1,028	3,274	3,149	19,9	40,2	77,64	1,040	24,005	0,9955 *0,9893*	636,2 *640,3*
f	5,683	20 301	50,1	47,5	2,56	1,016	3,254	3,011	19,7	36,6	61,81	1,081	19,797	0,9911 *0,9847*	616,9 *620,9*
g	3,385	13 387	57,7	52,3	5,24	1,031	3,236	3,203	18,1	37,8	76,49	1,010	26,408	0,9829 *0,9774*	577,1 *580,4*
h	3,394	11 991	50,1	46,2	3,99	0,977	3,225	3,039	19,8	34,8	55,37	1,061	20,348	0,9591 *0,9536*	555,7 *558,9*

TABLE 2.1 (Cont.)

2.1.4 Arrangement: 4 Row 1 Pass Areas: Bare tube 6,810; total outside 157,52 m^2

Run	Tube side						Air side				Heat transfer performance				
	Flow rate	Reynolds Number	T_1	T_2	ΔT_{diff}	$\frac{\Delta T_{abs}}{\Delta T_{diff}}$	Flow rate Measured	Flow rate Corrected	t_1	t_2	Q_{water}	$\frac{Q_{air}}{Q_{water}}$	$\Delta T_{l.m.}$	Mean $(F_T)_{exp}$ / $(F_T)'_{exp}$	U / U'
	kg/s		°C	°C	°C		m^3_{NTP}/s	m^3_{NTP}/s	°C	°C	kW		°C		W/(m² °K)
a	2,244	6 451	57,0	49,1	7,80	1,013	3,245	3,138	17,3	36,8	74,18	1,034	25,563	0,9173 *0,9131*	464,6 *466,8*
b	2,250	5 779	49,6	43,1	6,35	1,027	3,229	3,095	16,4	32,7	61,17	1,043	21,428	0,9246 *0,9204*	453,5 *455,6*
c	6,048	17 728	56,1	52,4	3,51	1,054	3,231	3,077	17,0	42,1	93,65	1,050	23,069	0,9887 *0,9827*	603,1 *606,8*
d	6,028	15 646	48,3	45,6	2,71	0,996	3,222	2,894	18,9	38,3	68,07	1,113	17,005	1,0191 *1,0127*	577,0 *580,6*
e	7,527	21 975	55,5	52,5	3,04	0,987	3,231	2,930	15,9	42,5	94,50	1,103	22,800	0,9945 *0,9880*	612,2 *616,2*
f	7,516	19 677	48,6	46,3	2,33	0,987	3,260	3,012	19,1	38,9	72,30	1,082	16,972	1,0177 *1,0112*	614,8 *618,8*
g	4,456	13 145	57,0	52,3	4,50	1,044	3,139	3,050	18,1	41,8	87,65	1,029	23,430	0,9777 *0,9721*	562,0 *565,2*
h	4,520	11 733	48,7	45,2	3,45	1,014	3,225	2,983	18,9	37,2	66,17	1,081	17,891	0,9891 *0,9834*	549,2 *552,4*

2.1.5 Arrangement: 2 Row 2 Pass Areas: Bare tube 3,405; total outside 78,76 m^2

a	0,732	8 299	60,0	44,3	15,43	1,017	3,142	3,149	18,0	30,6	48,11	0,998	27,821	1,0039 *0,9988*	506,0 *508,6*
b	0,749	7 437	50,1	38,7	11,22	1,016	3,036	3,134	18,8	28,2	35,71	0,969	20,884	1,0088 *1,0038*	498,0 *500,4*
c	1,439	16 992	59,5	49,9	9,73	0,987	3,102	2,961	17,1	33,2	57,81	1,047	29,430	0,9845 *0,9784*	586,1 *589,7*
d	1,518	15 689	50,5	42,9	7,60	1,000	3,111	3,158	16,9	29,5	48,24	0,985	23,411	1,0035 *0,9975*	603,3 *606,9*
e	1,878	22 480	59,6	51,5	8,29	0,977	3,180	3,036	17,1	34,4	63,67	1,048	29,562	1,0126 *1,0060*	624,9 *628,9*
f	1,867	19 262	49,9	43,3	6,46	1,022	3,205	3,125	16,2	29,8	51,53	1,026	23,426	1,0337 *1,0273*	625,7 *629,0*
g	1,118	12 974	59,6	47,6	12,08	0,993	3,189	3,067	17,0	32,1	56,15	1,040	29,022	1,0099 *1,0041*	562,8 *566,1*
h	1,137	11 504	49,7	41,3	8,58	0,979	3,165	2,967	18,6	29,7	39,93	1,067	21,322	1,0058 *1,0000*	546,9 *550,1*

TABLE 2.1 (Cont.)

2.1.6 Arrangement: 3 Row 3 Pass Areas: Bare tube 5,106; total outside 118,14 m^2

Run	Tube side						Air side				Heat transfer performance				
	Flow rate	Reynolds Number	T_1	T_2	ΔT_{diff}	$\frac{\Delta T_{abs}}{\Delta T_{diff}}$	Flow rate Measured	Flow rate Corrected	t_1	t_2	Q_{water}	$\frac{Q_{air}}{Q_{water}}$	$\Delta T_{l.m.}$	Mean $(F_T)_{exp}$ / $(F_T)'_{exp}$	U / U'
	kg/s		°C	°C	°C		m^3_{NTP}/s	m^3_{NTP}/s	°C	°C	kW		°C		W/(m^2 °K)
a	0,756	8 206	58,6	40,5	17,54	1,032	3,091	3,100	19,7	34,9	57,24	0,997	22,218	1,0007 *0,9956*	504,2 *506,8*
b	0,759	7 265	49,0	35,8	13,21	0,999	3,054	3,057	19,6	30,9	41,88	0,999	17,133	0,9730 *0,9981*	492,0 *494,5*
c	1,496	16 515	56,4	44,7	11,92	0,982	3,192	3,051	16,2	36,0	73,25	1,046	24,225	0,9945 *0,9984*	595,5 *599,1*
d	1,511	14 582	47,1	38,6	8,39	1,013	3,125	3,157	18,3	32,3	53,69	0,990	17,405	1,0101 *1,0042*	598,1 *601,6*
e	1,906	21 438	56,2	47,2	8,76	1,027	3,028	3,110	19,6	38,6	71,76	0,974	22,226	1,0023 *0,9959*	630,9 *634,9*
f	1,912	18 647	46,7	40,1	6,77	0,975	3,159	3,060	19,3	33,5	52,78	1,032	16,713	1,0012 *0,9949*	617,8 *621,7*
g	1,121	12 305	57,1	43,4	13,27	1,032	3,147	3,129	19,6	36,5	64,22	1,006	22,161	1,0055 *0,9998*	564,4 *567,6*
h	1,115	10 854	48,7	37,9	10,40	1,038	3,156	3,171	19,2	32,3	50,37	0,995	17,525	1,0078 *1,0022*	558,5 *561,6*
i	0,191	1 638	47,5	25,8	18,43	1,177	3,137	3,171	19,4	23,9	17,30	0,989	13,181	0,9470 *0,9445*	271,5 *272,2*
j	0,354	3 305	50,1	31,8	17,99	1,017	3,138	3,023	19,6	27,0	27,12	1,038	17,074	0,8439 *0,8407*	368,7 *370,1*

2.1.7 Arrangement: 4 Row 2 Pass Areas: Bare tube 6,810; total outside 157,52 m^2

a	1,455	7 995	56,0	44,6	11,33	1,006	3,124	3,028	20,2	39,1	69,39	1,032	20,421	1,0094 *1,0042*	494,4 *497,0*
b	1,496	7 328	47,9	39,4	8,73	0,974	3,147	3,005	19,8	34,4	53,19	1,047	16,361	0,9781 *0,9731*	488,2 *490,7*
c	3,007	17 078	56,0	48,6	7,36	1,005	3,151	3,114	16,7	41,4	93,09	1,012	22,135	1,0228 *1,0166*	604,0 *607,7*
d	3,027	15 319	48,1	42,9	5,20	1,000	3,088	3,000	18,9	37,0	65,82	1,029	16,729	0,9856 *0,9796*	586,4 *590,0*
e	3,605	21 117	57,1	51,3	5,66	1,025	3,132	3,020	20,4	44,3	87,50	1,037	20,538	1,0135 *1,0070*	617,4 *621,4*
f	3,743	18 562	46,3	42,4	3,85	1,013	3,126	3,015	20,4	37,1	61,04	1,037	14,682	0,9986 *0,9923*	611,6 *615,5*
g	2,245	12 677	56,1	47,8	8,30	1,000	3,077	3,019	20,6	41,9	77,95	1,019	20,001	1,0274 *1,0214*	557,2 *560,4*
h	2,251	11 215	47,9	41,3	6,67	0,990	3,165	3,106	19,1	35,6	62,14	1,019	16,766	0,9787 *0,9732*	556,3 *559,4*

TABLE 2.1 (Cont.)

2.1.8 Arrangement: 4 Row 4 Pass Areas: Bare tube 6,810; total outside 157,52 m^2

Run	Tube side						Air side				Heat transfer performance				
	Flow rate	Reynolds Number	T_1	T_2	ΔT_{diff}	$\frac{\Delta T_{abs}}{\Delta T_{diff}}$	Flow rate Measured	Flow rate Corrected	t_1	t_2	Q_{water}	$\frac{Q_{air}}{Q_{water}}$	$\Delta T_{l.m.}$	Mean $(F_T)_{exp}$ / $(F_T)'_{exp}$	$\frac{U}{U'}$
	kg/s		°C	°C	°C		m^3_{NTP}/s	m^3_{NTP}/s	°C	°C	kW		°C		W/(m^2 °K)
a	0,738	7 600	58,6	34,3	23,16	1,049	3,217	3,229	15,0	34,1	75,05	0,996	21,797	1,0019 *0,9971*	504,8 *507,2*
b	0,755	6 970	47,8	33,0	14,51	1,020	3,286	3,036	19,9	32,6	46,74	1,082	14,124	0,9980 *0,9930*	487,0 *489,5*
c	1,501	16 212	55,7	42,8	17,58	1,025	3,224	3,117	18,9	40,3	81,01	1,034	19,340	1,0241 *1,0179*	600,8 *604,4*
d	1,524	14 527	47,2	37,1	9,95	1,015	3,249	3,117	17,7	34,7	64,37	1,042	15,698	1,0129 *1,0068*	594,6 *598,2*
e	1,874	20 493	55,3	44,7	10,58	1,002	3,223	3,068	19,2	41,5	83,10	1,051	19,055	1,0284 *1,0217*	622,9 *626,9*
f	1,876	18 059	47,3	38,1	9,26	0,994	3,239	3,127	16,1	35,1	72,16	1,036	16,621	1,0258 *1,0195*	621,6 *625,5*
g	1,120	11 732	56,0	38,9	16,49	1,037	3,232	3,181	16,7	37,4	80,13	1,016	20,347	1,0232 *1,0175*	565,3 *568,5*
h	1,123	10 459	46,8	35,0	11,47	1,029	3,270	3,152	19,3	33,8	55,40	1,038	14,308	1,0254 *1,0198*	554,7 *557,7*
i	0,385	3 897	60,5	30,5	28,38	1,057	3,241	3,150	18,1	30,7	48,30	1,029	19,845	0,9081 *0,9046*	393,7 *395,2*
j	0,197	1 913	61,8	24,6	34,01	1,094	3,211	3,185	18,7	26,6	30,62	1,008	16,405	0,9595 *0,9568*	285,8 *286,6*

TABLE 2 (Cont.)

2.2 Measured and predicted overall mean and local tubeside temperature differences

2.2.1 Arrangement : 1 Row 1 Pass

Run (Row)*	p	q	K	K_1	K_2	Mean temperature differences (°C)							Local tubeside temperature drops (°C)			
						Experimental		$\Delta T_{Lm.}$	∞ rows	Finite rows			Row	Measured	Predicted	
						Lower limit	Upper limit		1 pass	No bypass	⅓ bypass	No bypass x F_T			No bypass	⅓ bypass
b(3)	0,1908	0,1679	0,2072	-	-	18,657	19,335	21,499	21,336	21,336			1	4,99 ±0,12	5,50	5,22
	do.	do.	-	*0,3471*	*0,2394*	*18,493*	*19,238*	do.	do.		*19,974*	*19,892*				
g(3)	0,1990	0,1675	0,2076	-	-	27,061	28,061	31,196	30,953	30,949			1	7,54 ±0,18	8,35	7,93
	do.	do.	-	*0,3478*	*0,2400*	*26,821*	*27,921*	do.	do.		*28,967*	*28,849*				
h(3)	0,1451	0,1922	0,2275	-	-	18,652	19,410	21,194	21,056	21,057			1	3,76 ±0,13	4,02	3,80
	do.	do.	-	*0,3777*	*0,2625*	*18,469*	*19,303*	do.	do.		*19,523*	*19,470*				
i(3)	0,1264	0,2088	0,2383	-	-	27,392	28,587	30,275	30,089	30,089			1	4,56 ±0,08	4,89	4,59
	do.	do.	-	*0,3937*	*0,2748*	*27,106*	*28,421*	do.	do.		*27,689*	*27,694*				
b(4)	0,2115	0,1792	0,2039	-	-	21,581	22,356	22,447	22,244	22,240			1	5,82 ±0,08	5,97	5,67
	do.	do.	-	*0,3422*	*0,2358*	*21,394*	*22,246*	do.	do.		*20,679*	*20,761*				
b(4)	0,2078	0,1796	0,2051	-	-	21,865	22,659	22,898	22,695	22,690			1	5,88 ±0,15	6,00	5,70
	do.	do.	-	*0,3440*	*0,2371*	*21,673*	*22,547*	do.	do.		*21,099*	*21,172*				
f(4)	0,2904	0,1250	0,1637	-	-	18,787	19,313	21,472	21,279	21,279			1	8,42 ±0,16	8,61	8,29
	do.	do.	-	*0,2796*	*0,1899*	*18,659*	*19,238*	do.	do.		*20,246*	*20,175*				
h(4)	0.1514	0,2112	0,2306	-	-	19,856	20,671	20,541	20,384	20,383			1	3,82 ±0,07	3,82	3,60
	do.	do.	-	*0,3824*	*0,2661*	*19,658*	*20,554*	do.	do.		*18,705*	*18,822*				
i(4)	0,2116	0,1889	0,2135	-	-	30,713	31,868	31,749	31,445	31,435			1	8,41 ±0,17	8,45	8,00
	do.	do.	-	*0,3568*	*0,2467*	*30,433*	*31,703*	do.	do.		*29,081*	*29,232*				
b(5)	0,2087	0,1811	0,2055	-	-	19,679	20,394	20,448	20,264	20,260			1	5,11 ±0,09	5,36	5,09
	do.	do.	-	*0,3446*	*0,2376*	*19,507*	*20,293*	do.	do.		*18,823*	*18,901*				
e(5)	0,2092	0,1821	0,2101	-	-	27,945	28,987	29,597	29,329	29,322			1	7,65 ±0,13	7,90	7,49
	do.	do.	-	*0,3516*	*0,2428*	*27,694*	*28,840*	do.	do.		*27,228*	*27,305*				
h(5)	0,1321	0,2264	0,2428	-	-	29,634	30,941	30,416	30,196	30,198			1	4,91 ±0,10	4,90	4,60
	do.	do.	-	*0,4002*	*0,2798*	*29,319*	*30,757*	do.	do.		*27,516*	*27,742*				
a(6)	0,2050	0,1856	0,2134	-	-	27,454	28,487	29,050	28,788	28,779			1	7,18 ±0,18	7,58	7,19
	do.	do.	-	*0,3566*	*0,2466*	*27,205*	*28,341*	do.	do.		*26,681*	*26,763*				
b(6)	0,1984	0,1818	0,2099	-	-	18,380	19,056	19,600	19,434	19,429			1	4,68 ±0,13	4,95	4,70
	do.	do.	-	*0,3512*	*0,2426*	*18,216*	*18,959*	do.	do.		*18,055*	*18,094*				
h(6)	0,1315	0,2274	0,2430	-	-	29,250	30,538	29,916	29,699	29,701			1	4,75 ±0,11	4,78	4,49
	do.	do.	-	*0,4005*	*0,2800*	*28,940*	*30,357*	do.	do.		*27,049*	*27,283*				

* Indicates row (from bottom of 6 row bundle) in which heat transfer run was performed.

TABLE 2.2 (Cont.)

2.2.2 Arrangement : 2 Row 1 Pass

Run	p	q	K	K_1	K_2	Mean temperature differences (°C)							Local tubeside temperature drops (°C)			
						Experimental		$\Delta T_{Lm.}$	∞ rows	Finite rows			Row	Measured	Predicted	
						Lower limit	Upper limit		1 Pass	No bypass	$\frac{1}{3}$ bypass	No bypass x F_T			No bypass	$\frac{1}{3}$ bypass
a	0,1922	0,3455	0,2138	-	-	29,030	30,123	29,940	29,395	29,395			1	8,29 ± 0,15	8,70	8,25
	do.	do.	-	*0,3572*	*0,2470*	*28,765*	*29,966*	do.	do.		*29,245*	*29,292*	2	7,45 ± 0,13	7,05	7,51
b	0,1908	0,3216	0,2031	-	-	19,732	20,446	20,996	20,654	20,654			1	5,69 ± 0,11	6,06	5,76
	do.	do.	-	*0,3408*	*0,2348*	*19,561*	*20,346*	do.	do.		*20,560*	*20,584*	2	5,14 ± 0,13	4,97	5,27
c	0,1201	0,4142	0,2434	-	-	29,712	31,026	29,494	29,085	29,085			1	5,22 ± 0,12	5,37	5,04
	do.	do.	-	*0,4012*	*0,2806*	*29,396*	*30,841*	do.	do.		*28,918*	*28,964*	2	4,66 ± 0,13	4,15	4,59
d	0,1191	0,4007	0,23741	-	-	20,095	20,964	20,250	19,990	19,985			1	3,50 ± 0,08	3,65	3,43
	do.	do.	-	*0,3924*	*0,2737*	*19,887*	*20,842*	do.	do.		*19,878*	*19,905*	2	3,06 ± 0,12	2,84	3,07
e	0,2815	0,2494	0,17162	-	-	26,478	27,257	29,745	29,183	29,187			1	11,77 ± 0,29	13,01	12,51
	do.	do.	-	*0,2921*	*0,1989*	*26,289*	*27,146*	do.	do.		*29,079*	*29,106*	2	10,95 ± 0,30	11,18	11,68
f	0,2669	0,2379	0,1681	-	-	19,859	20,430	23,247	22,855	22,863			1	8,46 ± 0,17	9,77	9,40
	do.	do.	-	*0,2865*	*0.1948*	*19,720*	*20,349*	do.	do.		*22,787*	*22,800*	2	7,78 ± 0,23	8,42	8,78
g	0,1505	0,3859	0,2297	-	-	29,912	31,151	29,888	29,407	29,408			1	6,51 ± 0,14	6,76	6,37
	do.	do.	-	*0,3810*	*0,2651*	*29,614*	*30,977*	do.	do.		*29,245*	*29,294*	2	5,88 ± 0,14	5,34	5,73
h	0,15260	0,37987	0,2225	-	-	22,842	23,763	22,418	22,058	22,061			1	4,90 ± 0,10	5,04	4,76
	do.	do.	-	*0,3702*	*0,2568*	*22,622*	*23,635*	do.	do.		*21,941*	*21,979*	2	4,40 ± 0,10	4,02	4,30

TABLE 2.2 (Cont.)

2.2.3 Arrangement : 3 Row 1 Pass

Run	p	q	K	K_1	K_2	Mean temperature differences (^oC)							Local tubeside temperature drops (^oC)			
						Experimental		$\Delta T_{l.m.}$	∞ rows 1 pass	Finite rows			Row	Measured	Predicted	
						Lower limit	Upper limit			No bypass	¼ bypass	No bypass x F_T			No bypass	¼ bypass
	0,1809	0,4470	0,2043	-	-	24,830	25,74	26,214	25,571	25,579			1	7,47 ±0,13	8,50	8,08
a	do.	do.	-	*0,3428*	*0,2362*	*24,613*	*25,610*	do.	do.		*24,860*	*24,876*	2	7,28 ±0,14	6,97	7,39
													3	5,58 ±0,13	5,71	5,40
	0,1726	0,4430	0,2050	-	-	19,450	20,156	20,977	20,494	20,503			1	5,91 ±0,10	6,54	6,22
b	do.	do.	-	*0,3438*	*0,2370*	*19,281*	*20,057*	do.	do.		*19,939*	*19,937*	2	5,61 ±0,11	5,36	5,68
													3	4,29 ±0,13	4,38	4,14
	0,1037	0,5346	0,2415	-	-	23,781	24,827	24,722	24,277	24,289			1	4,28 ±0,10	4,93	4,63
c	do.	do.	-	*0,3384*	*0,2784*	*23,530*	*24,680*	do.	do.		*23,444*	*23,475*	2	4,05 ±0,10	3,82	4,13
													3	2,99 ±0,11	2,96	2,75
	0,1100	0,5367	0,2339	-	-	19,765	20,614	19,609	19,230	19,240			1	3,45 ±0,08	4,02	3,78
d	do.	do.	-	*0,3872*	*0,2698*	*19,563*	*20,497*	do.	do.		*18,562*	*18,620*	2	3,30 ±0,09	3,15	3,39
													3	2,41 ±0,13	2,46	2,29
	0,0897	0,5516	0,2466	-	-	23,429	24,494	24,005	23,607	23,625			1	3,67 ±0,08	4,17	3,90
e	do.	do.	-	*0,4058*	*0,2841*	*23,175*	*24,347*	do.	do.		*22,770*	*22,814*	2	3,45 ±0,10	3,20	3,47
													3	2,50 ±0,14	2,46	2,28
	0,0855	0,5559	0,2496	-	-	19,235	20,110	19,797	19,479	19,494			1	2,91 ±0,09	3,31	3,09
f	do.	do.	-	*0,4102*	*0,2875*	*19,024*	*19,987*	do.	do.		*18,782*	*18,815*	2	2,77 ±0,07	2,53	2,75
													3	2,01 ±0,13	1,93	1,79
	0,1364	0,4975	0,2235	-	-	25,501	26,538	26,408	25,864	25,856			1	5,93 ±0,10	6,65	6,28
g	do.	do.	-	*0,3717*	*0,2580*	*25,255*	*26,395*	do.	do.		*25,032*	*25,067*	2	5,65 ±0,09	5,29	5,67
													3	4,14 ±0,12	4,22	3,95
	0,1287	0,4951	0,2260	-	-	19,172	19,951	20,348	19,956	19,953			1	4,56 ±0,10	4,90	4,62
h	do.	do.	-	*0,3755*	*0,2609*	*18,985*	*19,841*	do.	do.		*19,326*	*19,335*	2	4,27 ±0,06	3,89	4,17
													3	3,15 ±0,10	3,08	2,89

TABLE 2.2 (Cont.)

2.2.4 Arrangement : 4 Row 1 Pass

Run	p	q	K	K_1	K_2	Mean temperature differences (°C)							Local tubeside temperature drops (°C)			
						Experimental		$\Delta T_{Lm.}$	∞ rows	Finite rows			Row	Measured	Predicted	
						Lower limit	Upper limit		1 pass	No bypass	½ bypass	No bypass x F_T			No bypass	½ bypass
a	0,1990	0,4912	0,1877	-	-	23,112	23,877	25,563	24,782	24,768			1	9,10 ±0,18	10,41	9,96
	do.	do.	-	*0,3172*	*0,2173*	*22,929*	*23,771*	do.	do.		*24,599*	*24,617*	2	8,92 ±0,21	8,74	9,20
													3	7,27 ±0,18	7,33	6,98
													4	5,93 ±0,21	6,15	6,46
b	0,1958	0,4910	0,1859	-	-	19,532	20,169	21,428	20,784	20,775			1	7,43 ±0,15	8,52	8,15
	do.	do.	-	*0,3144*	*0,2152*	*19,379*	*20,080*	do.	do.		*20,634*	*20,649*	2	7,23 ±0,17	7,16	7,53
													3	5,89 ±0,15	6,04	5,72
													4	4,78 ±0,16	5,05	5,30
c	0,0946	0,6419	0,2405	-	-	22,378	23,357	23,069	22,526	22,554			1	4,36 ±0,12	5,17	4,85
	do.	do.	-	*0,3969*	*0,2773*	*22,143*	*23,220*	do.	do.		*22,346*	*22,373*	2	4,20 ±0,17	4,01	4,34
													3	3,13 ±0,19	3,11	2,90
													4	2,36 ±0,12	2,42	2,61
d	0,0918	0,6599	0,2441	-	-	17,002	17,745	17,005	16,594	16,615			1	3,44 ±0,08	3,74	3,50
	do.	do.	-	*0,4022*	*0,2813*	*16,822*	*17,639*	do.	do.		*16,454*	*16,480*	2	3,31 ±0,13	2,88	3,12
													3	2,43 ±0,13	2,23	2,07
													4	1,67 ±0,08	1,72	1,86
e	0,0758	0,6717	0,2542	-	-	22,223	23,246	22,800	22,329	22,356			1	3,84 ±0,11	4,29	4,01
	do.	do.	-	*0,4169*	*0,2927*	*21,976*	*23,101*	do.	do.		*22,140*	*22,166*	2	3,63 ±0,14	3,26	3,55
													3	2,68 ±0,16	2,48	2,29
													4	2,02 ±0,09	1,88	2,05
f	0,0780	0,6712	0,2492	-	-	16,937	17,703	16,972	16,612	16,633			1	3,01 ±0,09	2,23	3,02
	do.	do.	-	*0,4096*	*0,2870*	*16,750*	*17,595*	do.	do.		*16,471*	*16,495*	2	2,86 ±0,10	2,47	2,68
													3	2,06 ±0,13	1,89	1,75
													4	1,39 ±0,08	1,44	1,56
g	0,1208	0,6093	0,2279	-	-	22,502	23,424	23,430	22,814	22,818			1	5,49 ±0,16	6,43	6,07
	do.	do.	-	*0,3783*	*0,2630*	*22,280*	*23,295*	do.	do.		*22,618*	*22,646*	2	5,31 ±0,20	5,10	5,47
													3	4,05 ±0,19	4,04	3,78
													4	3,15 ±0,14	3,20	3,42
h	0,1175	0,6141	0,2278	-	-	17,385	18,092	17,891	17,424	17,431			1	4,29 ±0,10	4,75	4,49
	do.	do.	-	*0,3782*	*0,2629*	*17,214*	*17,992*	do.	do.		*17,277*	*17,300*	2	4,15 ±0,14	3,77	4,05
													3	3,15 ±0,13	2,99	2,79
													4	2,24 ±0,08	2,36	2,53

TABLE 2.2 (Cont.)

2.2.5 Arrangement: 2 Row 2 Pass

Run	p	q	K	K_1	K_2	Mean temperature differences (°C)							Local tubeside temperature drops (°C)			
						Experimental		$\Delta T_{Lm.}$	∞ rows	Finite rows			Row	Measured	Predicted	
						Lower limit	Upper limit		1 pass	No bypass	⅓ bypass	No bypass x F_T"			No bypass	⅓ bypass
a	0,3738	0,3000	0,2019	-	-	27,493	28,483	27,821		27,526			1	6,92 ±0,29	7,57	7,14
	do.	do.	-	*0,3391*	*0,2335*	*27,257*	*28,346*	do.			*27,006*	*27,434*	2	8,51 ±0,19	7,99	8,28
b	0,3642	0,3003	0,2000	-	-	20,743	21,480	20,884		20,671			1	5,07 ±0,20	5,50	5,19
	do.	do.	-	*0,3361*	*0,2313*	*20,567*	*21,378*	do.			*20,292*	*20,602*	2	6,15 ±0,15	5,76	5,98
c	0,2264	0,3797	0,2426	-	-	28,428	29,670	29,430		29,211			1	4,79 ±0,24	5,10	4,75
	do.	do.	-	*0,3999*	*0,2796*	*28,128*	*29,494*	do.			*28,751*	*29,090*	2	4,93 ±0,15	4,56	4,85
d	0,2261	0,3750	0,2352	-	-	23,057	24,047	23,411		23,240			1	3,74 ±0,19	3,92	3,71
	do.	do.	-	*0,3891*	*0,2713*	*22,820*	*23,910*	do.			*22,881*	*23,148*	2	3,86 ±0,11	3,57	3,79
e	0,1906	0,4071	0,2510	-	-	29,341	30,685	29,562		29,363			1	4,19 ±0,23	4,30	4,00
	do.	do.	-	*0,4122*	*0,2891*	*29,018*	*30,497*	do.			*28,921*	*29,237*	2	4,10 ±3,96	3,69	3,95
f	0,1959	0,4036	0,2448	-	-	23,747	24,813	23,426		23,265			1	3,25 ±0,17	3,44	3,20
	do.	do.	-	*0,4032*	*0,2821*	*23,492*	*24,665*	do.			*22,912*	*23,168*	2	3,21 ±0,10	2,98	3,18
g	0,2817	0,3545	0,2271	-	-	28,792	29,969	29,022		28,761			1	5,73 ±0,26	6,08	5,69
	do.	do.	-	*0,3770*	*0,2621*	*28,510*	*29,805*	do.			*28,256*	*28,652*	2	6,35 ±0,15	5,77	6,07
h	0,2701	0,3569	0,2280	-	-	21,069	21,926	21,322		21,139			1	4,11 ±0,18	4,29	4,01
	do.	do.	-	*0,3785*	*0,2631*	*20,862*	*21,804*	do.			*20,779*	*21,058*	2	4,47 ±0,11	4,03	4,25

TABLE 2 (Cont.)

2.2.6 Arrangement: 3 Row 3 Pass

Run	p	q	K	K_1	K_2	Mean temperature differences (°C)							Local tubeside temperature drops (°C)			
						Experimental		$\Delta T_{l.m.}$	∞ rows 1 pass	Finite rows			Row	Measured	Predicted	
						Lower limit	Upper limit			No bypass	⅓ bypass	No bypass x F_T''			No bypass	⅓ bypass
a	0,4653	0,3908	0,2038	-	-	21,885	22,678	22,218		21,992			1	4,86 ±0,17	5,74	5,45
	do.	do.	-	*0,3419*	*0,2356*	*21,694*	*22,568*	do.			*21,354*	*21,389*	2	6,15 ±0,22	5,99	6,26
													3	6,54 ±0,09	6,26	6.05
b	0,4490	0,3834	0,2023	-	-	16,411	16,998	17,133		16,973			1	3,60 ±0,07	4,28	4,06
	do.	do.	-	*0,3396*	*0,2339*	*16,270*	*16,916*	do.			*16,502*	*16,512*	2	4,48 ±0,19	4,44	4,64
													3	4,77 ±0,09	4,61	4,56
c	0,2910	0,4925	0,2396	-	-	23,638	24,665	24,225		24,048			1	3,89 ±0,07	4,34	4,06
	do.	do.	-	*0,3957*	*0,2763*	*23,391*	*24,521*	do.			*23,228*	*23,250*	2	4,32 ±0,18	3,88	4,14
													3	3,71 ±0,07	3,47	3,30
d	0,2951	0,4861	0,2331	-	-	17,258	17,993	17,405		17,279			1	2,72 ±0,07	3,10	2,91
	do.	do.		*0,3860*	*0,2689*	*17,083*	*17,892*	do.			*16,700*	*16,724*	2	3,05 ±0,14	2,79	2,98
													3	2,62 ±0,05	2,52	2,40
e	0,2459	0,5191	0,2475	-	-	21,840	22,833	22,226		22,084			1	2,91 ±0,10	3,44	3,21
	do.	do.	-	*0,4071*	*0,2851*	*21,602*	*22,695*	do.			*21,296*	*21,322*	2	3,22 ±0,14	2,96	3,18
													3	2,63 ±0,06	2,55	2,41
f	0,2409	0,5183	0,2464	-	-	16,407	17,146	16,713		16,609			1	2,25 ±0,07	2,53	2,36
	do.	do.	-	*0,4055*	*o,2839*	*16,230*	*17,043*	do.			*16,021*	*16,039*	2	2,51 ±0,13	2,17	2,34
													3	2,01 ±0,04	1,87	1,77
g	0,3653	0,4507	0,2234	-	-	21,893	22,778	22,161		21,969			1	4,01 ±0,07	4,75	4,47
	do.	do.	-	*0,3712*	*0,2579*	*21,682*	*22,655*	do.			*21,267*	*21,299*	2	4,76 ±0,20	4,52	4,78
													3	4,50 ±0,08	4,32	4,13
h	0,3661	0,4441	0,2191	-	-	17,358	18,045	17,525		17,376			1	3,20 ±0,08	3,72	3,51
	do.	do.	-	*0,3651*	*0,2530*	*17,194*	*17,951*	do.			*16,833*	*16,858*	2	3,66 ±0,20	3,56	3,76
													3	3,54 ±0,08	3,41	3,27
i	0,7722	0,1601	0,1132	-	-	12,378	12,614	13,181		13,049			1	2,99 ±0,47	4,37	4,28
	do.	do.	-	*0,1976*	*0,1318*	*12,322*	*12,581*	do.			*12,847*	*12,864*	2	6,35 ±0,44	6,87	6,97
													3	9,09 ±1,00	10,84	10,72
j	0,6000	0,2426	0,1573	-	-	14,240	14,623	17,074		16,930			1	4,28 ±0,37	5.06	4,88
	do.	do.	-	*0,2695*	*0,1826*	*14,148*	*14,570*	do.			*16,619*	*16,585*	2	5,90 ±0,21	6,48	6,65
													3	7,81 ±0,13	8,32	8,16

TABLE 2.2 (Cont.)

2.2.7 Arrangement: 4 Row 2 Pass

Run	p	q	K	K_1	K_2	Mean temperature differences (°C)							Local tubeside temperature drops (°C)			
						Experimental		$\Delta T_{lm.}$	∞ rows	Finite rows			Row	Measured	Predicted	
						Lower limit	Upper limit		1 pass	No bypass	⅓ bypass	No bypass x F_T"			No bypass	⅓ bypass
a	0,3184	0,5279	0,2049	-	-	20,289	21,023	20,421		20,015			1	6,14 ±0,23	6,72	-
	do.	do.	-	*0,3436*	*0,2368*	*20,112*	*20,920*	do.			-		2	5,87 ±0,13	5,51	-
												19,881	3	5,86 ±0,14	5,61	-
													4	4,81 ±0,18	4,60	-
b	0,3025	0,5196	0,2039	-	-	15,754	16,319	16,361		16,068			1	4,72 ±0,13	5,12	-
	do.	do.	-	*0,3422*	*0,2358*	*15,617*	*16,240*	do.			-		2	4,56 ±0,14	4,20	-
												15,961	3	4,51 ±0,10	4,24	-
													4	3,67 ±0,13	3,48	-
c	0,1883	0,6285	0,2387	-	-	22,213	23,179	22,135		21,820			1	4,37 ±0,17	4,85	-
	do.	do.	-	*0,3943*	*0,2752*	*21,983*	*23,044*	do.			-		2	4,24 ±0,17	3,77	-
												21,647	3	3,38 ±0,11	3,32	-
													4	2,74 ±0,14	2,53	-
d	0,1781	0,6199	0,2400	-	-	16,180	16,881	16,729		16,514			1	3,10 ±0,11	3,49	-
	do.	do.	-	*0,3962*	*0,2767*	*16,011*	*16,782*	do.			-		2	3,28 ±0,13	2,71	-
												16,382	3	2,47 ±0,08	2,37	-
													4	1,84 ±0,10	1,84	-
e	0,1580	0,6512	0,2495	-	-	20,407	21,334	20,538		20,282			1	3,46 ±0,17	3,93	-
	do.	do.	-	*0,4101*	*0,2874*	*20,184*	*21,204*	do.			-		2	3,43 ±0,18	3,01	-
												20,113	3	2,48 ±0,10	2,55	-
													4	1,95 ±0,14	1,96	-
f	0,1506	0,6448	0,2478	-	-	14,376	15,023	14,682		14,513			1	2,31 ±0,11	2,66	-
	do.	do.	-	*0,4076*	*0,2855*	*14,220*	*14,932*	do.			-		2	2,32 ±0,12	2,04	-
												14,393	3	1,72 ±0,07	1,73	-
													4	1,34 ±0,09	1,33	-
g	0,2338	0,6000	0,2283	-	-	20,184	21,010	20,001		19,663			1	4,77 ±0,18	5,23	-
	do.	do.	-	*0,3789*	*0,2634*	*19,985*	*20,894*	do.			-		2	4,62 ±0,20	4,14	-
												19,514	3	4,01 ±0,10	3,82	-
													4	3,21 ±0,14	3,03	-
h	0,2292	0,5730	0,2223	-	-	16,124	16,769	16,766		16,516			1	3,82 ±0,14	4,23	-
	do.	do.	-	*0,3699*	*0,2566*	*15,969*	*16,679*	do.			-		2	3,84 ±0,16	3,37	-
												16,395	3	3,18 ±0,08	3,14	-
													4	2,50 ±0,12	2,50	-

8.10 FIGURES

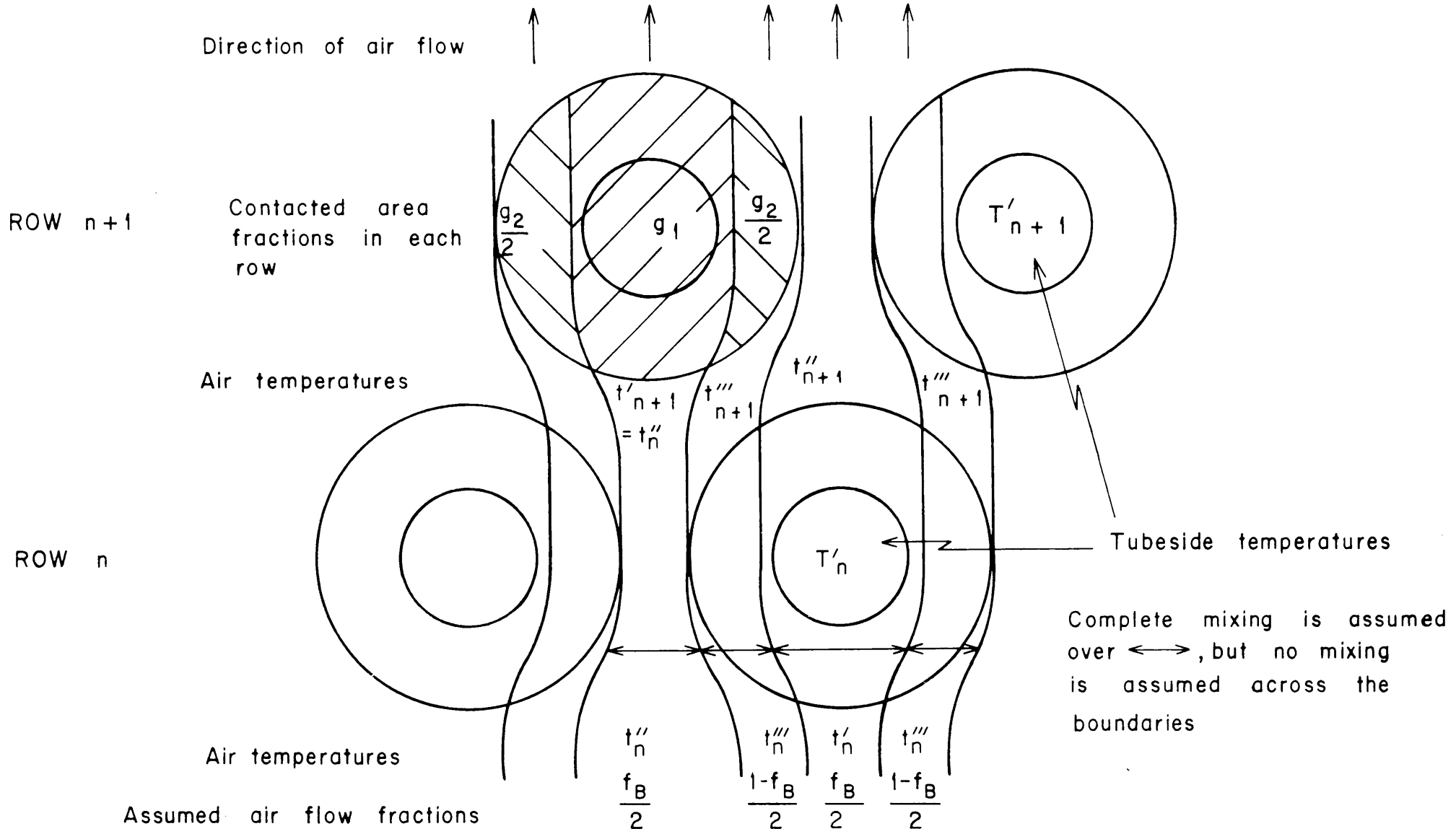

FIG. 1 AIR FLOW PATTERN THROUGH A SECTION OF FIN-TUBE BUNDLE FOR THE BYPASS MODEL WITHOUT TRANSVERSE MIXING

TABLE 2.2 (Cont.)

2.2.8 Arrangement: 4 Row 4 Pass

Run	p	q	K	K_1	K_2	Mean temperature differences (°C)							Local tubeside temperature drops (°C)			
						Experimental		$\Delta T_{l.m.}$	∞ rows 1 pass	Finite rows			Row	Measured	Predicted	
						Lower limit	Upper limit			No bypass	⅓ bypass	No bypass x F_T''			No bypass	⅓ bypass
a	0,5573	0,4381	0,1964	-	-	21,505	22,264	21,797		21,575			1	4,62 ±0,08	5,52	-
	do.	do.	-	*0,3306*	*0,2272*	*21,325*	*22,160*	do.			-		2	5,69 ±0,21	5,85	-
												21,437	3	6,32 ±0,19	6,21	-
													4	6,53 ±0,14	6,58	-
b	0,5305	0,4552	0,2017	-	-	13,879	14,373	14,124		13,985			1	3,15 ±0,09	3,49	-
	do.	do.	-	*0,3387*	*0,2332*	*13,760*	*14,303*	do.			-		2	3,54 ±0,11	3,61	-
												13,893	3	3,88 ±0,11	3,75	-
													4	3,94 ±0,11	3,89	-
c	0,3505	0,5815	0,2367	-	-	19,436	20,275	19,340		19,190			1	3,35 ±0,06	3,70	-
	do.	do.	-	*0,3913*	*0,2730*	*19,235*	*20,159*	do.			-		2	3,40 ±0,11	3,32	-
												19,039	3	3,19 ±0,09	2,99	-
													4	2,64 ±0,07	2,69	-
d	0,3424	0,5763	0,2346	-	-	15,606	16,273	15,698		15,583			1	2,64 ±0,05	2,92	-
	do.	do.	-	*0,3882*	*0,2705*	*15,447*	*16,181*	do.			-		2	2,70 ±0,09	2,62	-
												15,462	3	2,55 ±0,07	2,35	-
													4	2,06 ±0,05	2,11	-
e	0,2936	0,6177	0,2476	-	-	19,210	20,080	19,055		18,925			1	2,97 ±0,06	3,21	-
	do.	do.	-	*0,4074*	*0,2853*	*19,001*	*19,959*	do.			-		2	2,90 ±0,10	2,77	-
												18,786	3	2,63 ±0,08	2,39	-
													4	2,08 ±0,06	2,05	-
f	0,2949	0,6090	0,2431	-	-	16,722	17,468	16,621		16,511			1	2,59 ±0,04	2,77	-
	do.	do.	-	*0,4008*	*0,2802*	*16,544*	*17,365*	do.			-		2	2,56 ±0,08	2,40	-
												16,377	3	2,32 ±0,07	2,08	-
													4	1,79 ±0,05	1,80	-
g	0,4351	0,5267	0,2201	-	-	20,459	21,277	20,347		20,165			1	4,01 ±0,08	4,48	-
	do.	do.	-	*0,3666*	*0,2541*	*20,264*	*21,164*	do.			-		2	4,36 ±0,15	4,29	-
												20,019	3	4,19 ±0,13	4,11	-
													4	3,94 ±0,10	3,94	-
h	0,4291	0,5273	0,2189	-	-	14,420	14,990	14,308		14,183			1	2,86 ±0,08	3,10	-
	do.	do.	-	*0,3649*	*0,2528*	*14,284*	*14,911*	do.			-		2	3,00 ±0,09	2,96	-
												14,080	3	3,01 ±0,11	2,83	-
													4	2,60 ±0,09	2,70	-
i	0,7076	0,2972	0,1604	-	-	17,803	18,300	19,845		19,648			1	4,25 ±0,16	5,25	-
	do.	do.	-	*0,2743*	*0,1860*	*17,684*	*18,231*	do.			-		2	5,85 ±0,21	6,66	-
												19,547	3	8,15 ±0,15	8,46	-
													4	10,13 ±0,26	10,73	-
j	0,8631	0,1833	0,1179	-	-	15,603	15,915	16,405		16,223			1	3,73 ±0,44	4,14	-
	do.	do.	-	*0,2054*	*0,1372*	*15,528*	*15,872*	do.			-		2	5,90 ±0,38	6,55	-
												16,163	3	9,04 ±1,03	10,39	-
													4	15,70 ±0,61	16,44	-

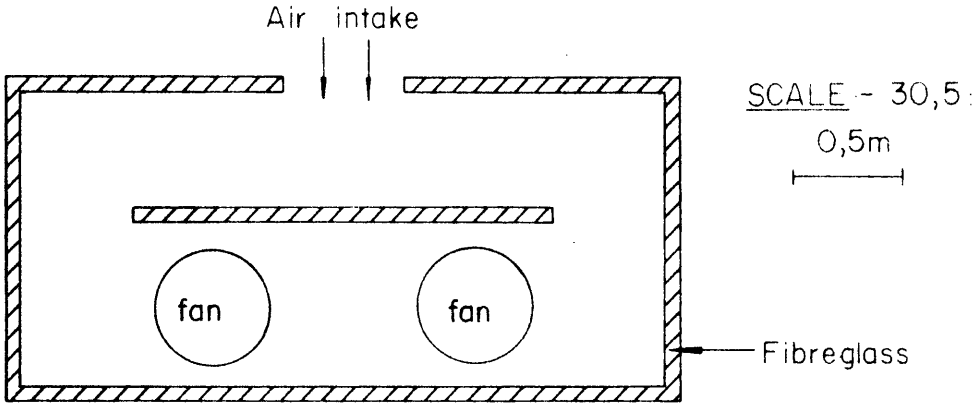

FIG. 3 FAN INTAKE SOUND PROOFING ENCLOSURE (PLAN)

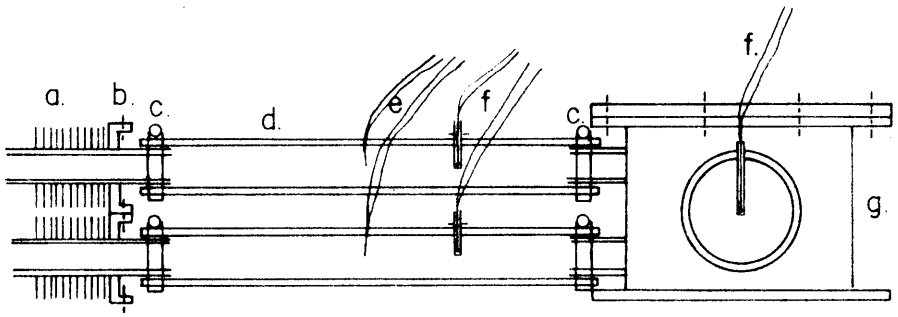

SCALE :- 5,1 : 1

50 mm

KEY :

a. fin-tubes
b. tube support
c. hose clips
d. rubber hosing
e. screened Cu/Constantan differential thermocouples
f. Fe/Constantan thermocouples (absolute); thermowells
g. header

FIG. 4 HEADER TO FIN-TUBE CONNECTIONS AND THERMOCOUPLE LOCATIONS

C4 – 2534/3

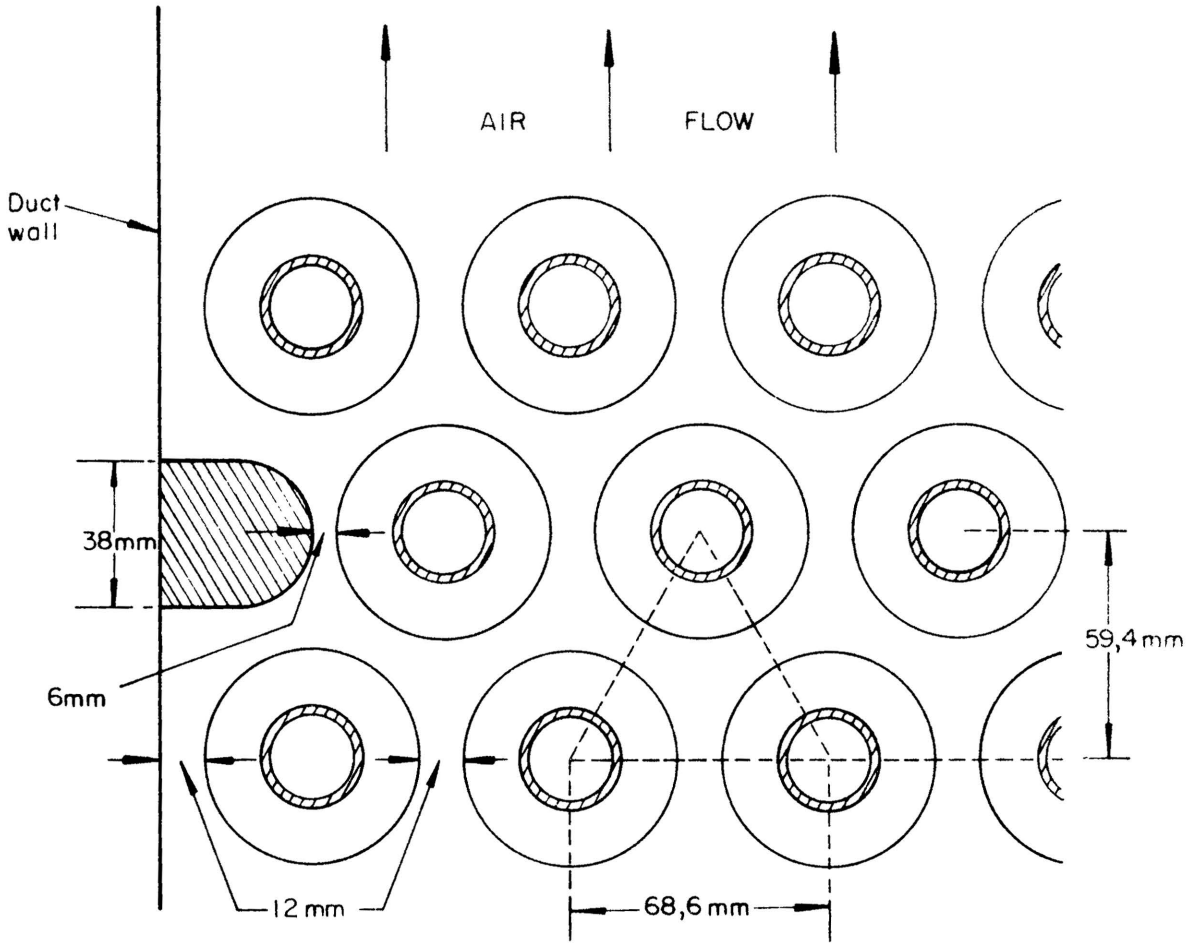

FIG. 5 SECTION OF FIN TUBE BUNDLE SHOWING WOODEN SECTION ON DUCT WALL

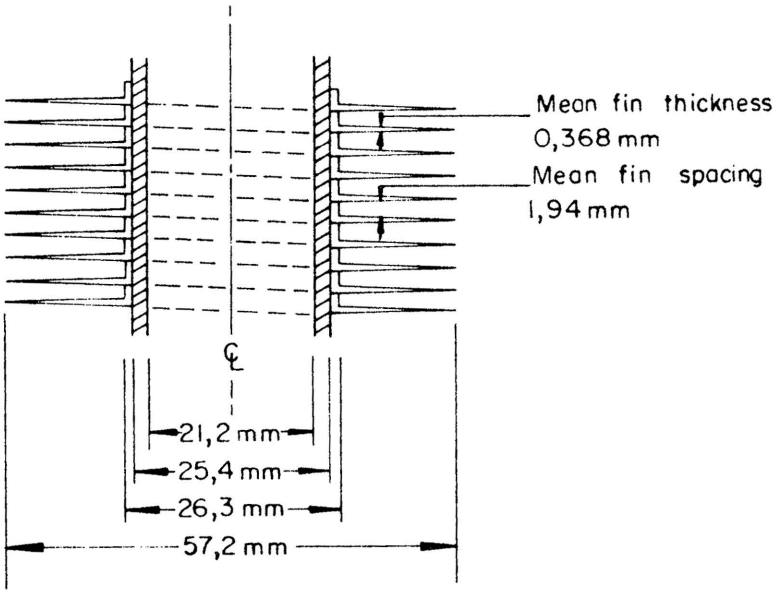

FIG. 6 CROSS-SECTION OF FIN-TUBE (SCHEMATIC)

C4—2534,4

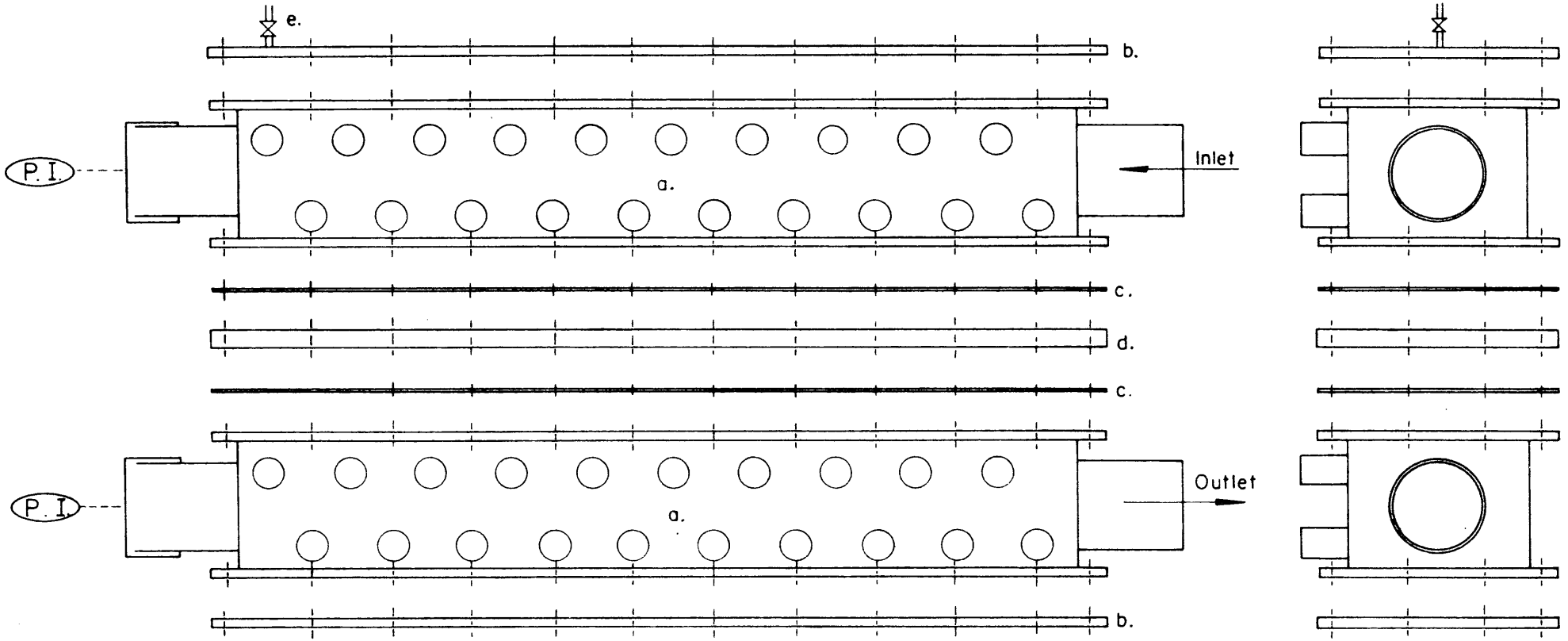

SIDE ELEVATION

ELEVATION

KEY:

a. header tank with two tube rows inlet/outlet and pressure indicator connections
b. blind flanges
c. rubber gasket
d. PVC/styrofoam pass partition
e. air bleed valve

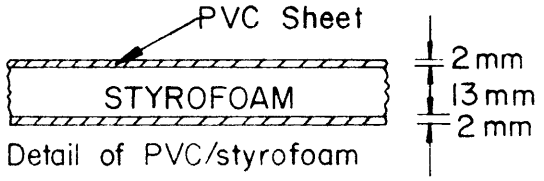

Detail of PVC/styrofoam pass partition

SCALE:- 5,1 : 1
50 mm

FIG. 7 TYPICAL HEADER ASSEMBLY (4 ROW, 2 PASS ARRANGEMENT)

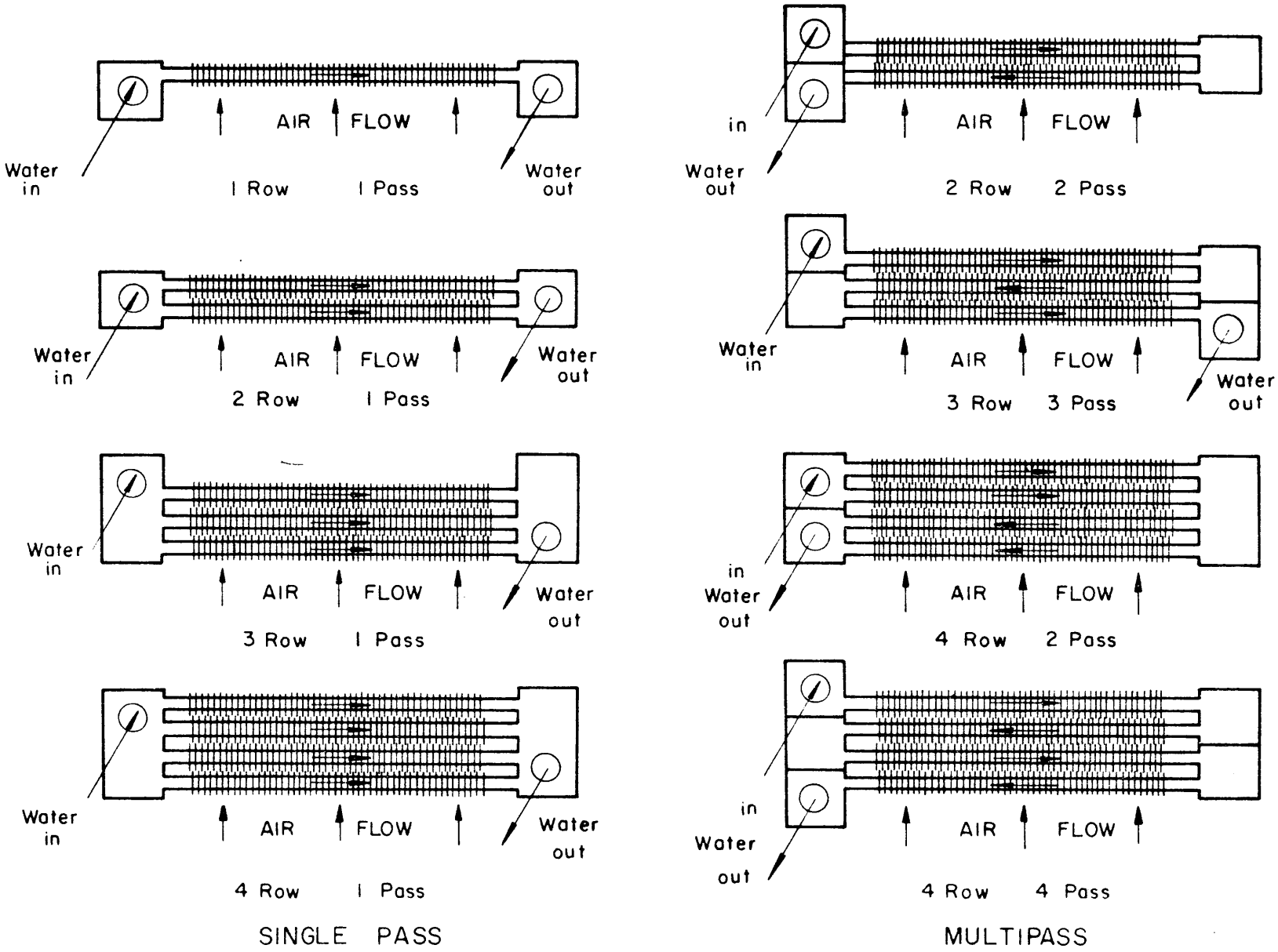

FIG. 8 TUBE ROW AND PASS ARRANGEMENTS STUDIED

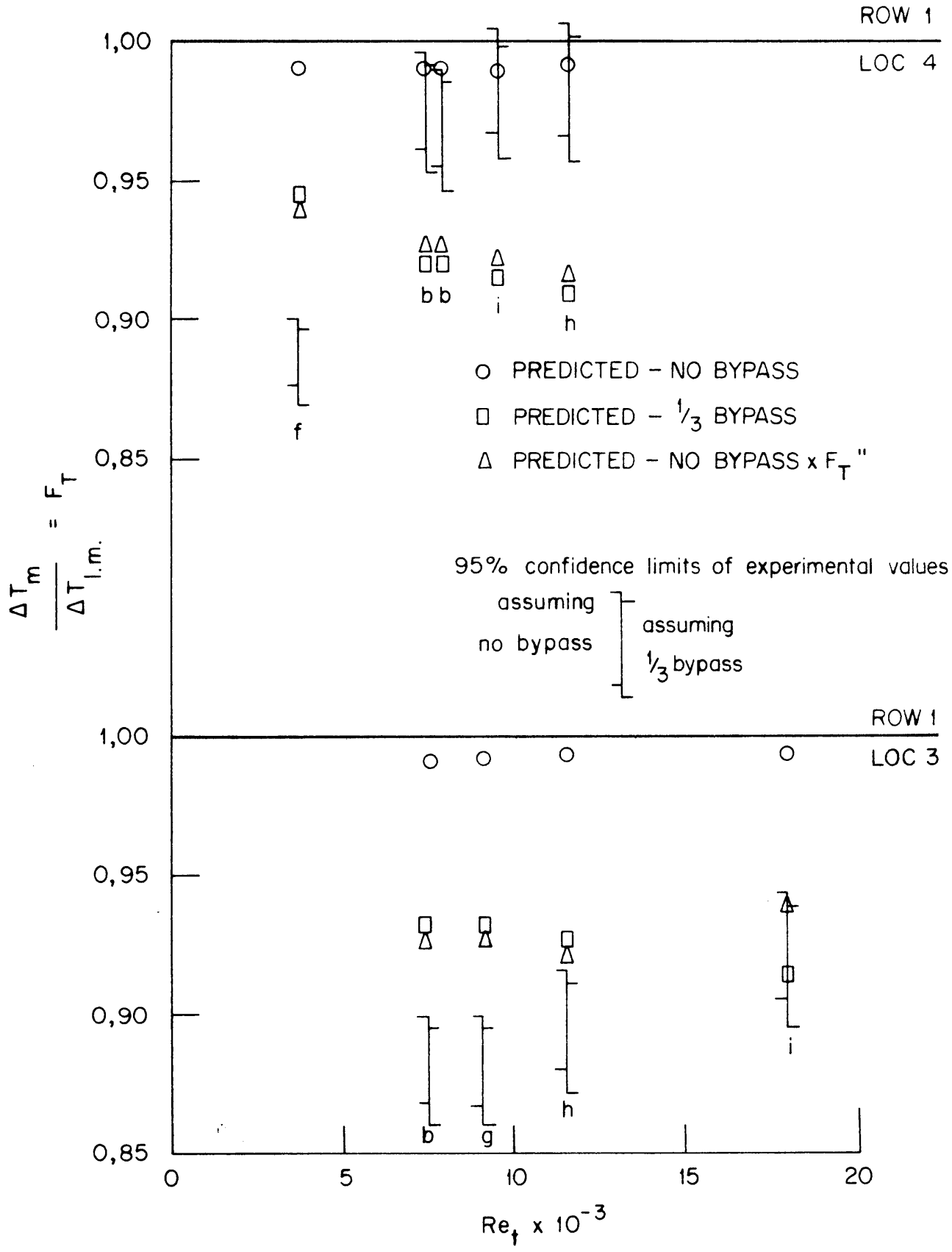

C4-2561/10

FIG.9 MEAN TEMPERATURE DIFFERENCES 1 ROW 1 PASS

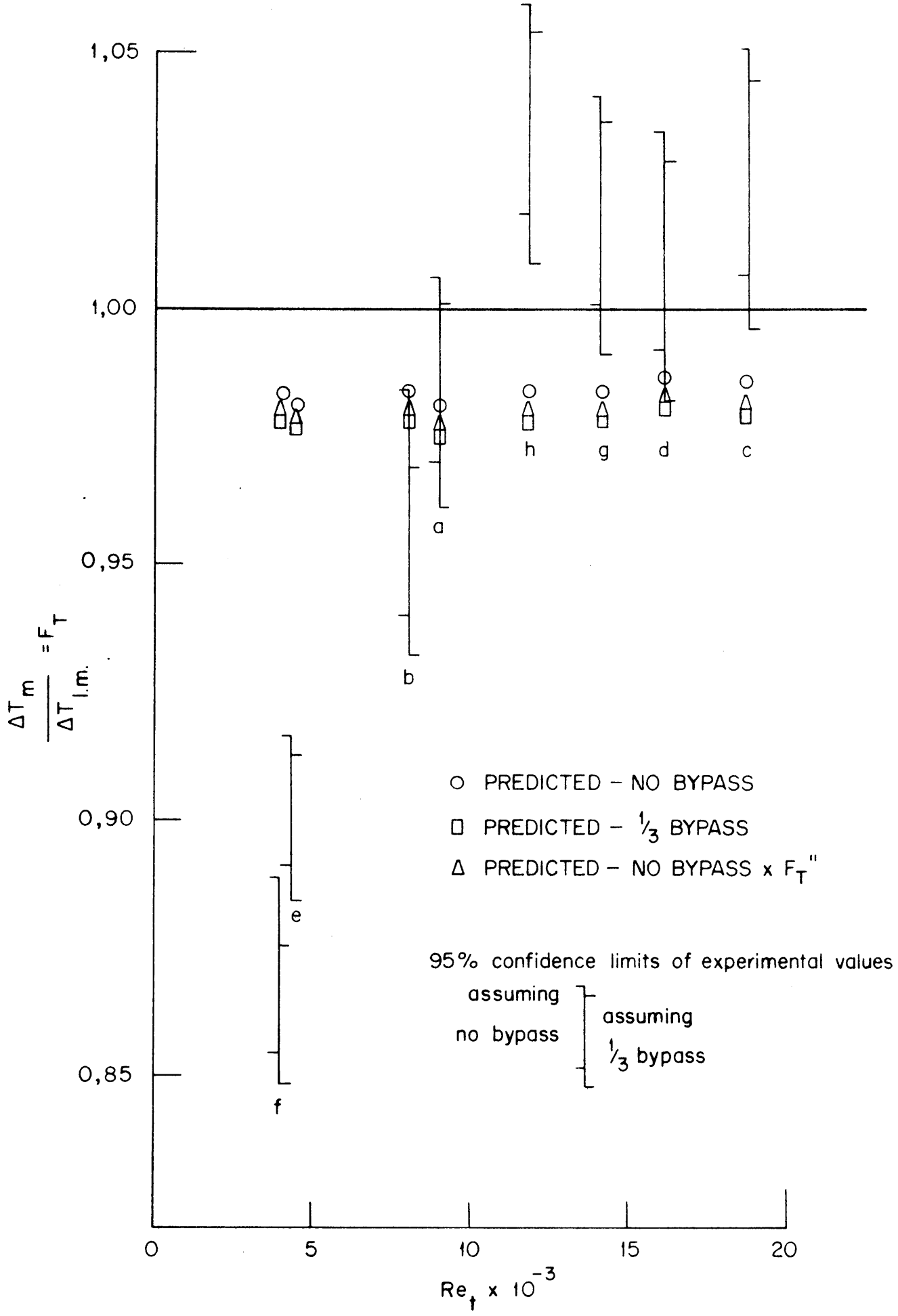

C4-2561/9

FIG 10 MEAN TEMPERATURE DIFFERENCES 2 ROW 1 PASS

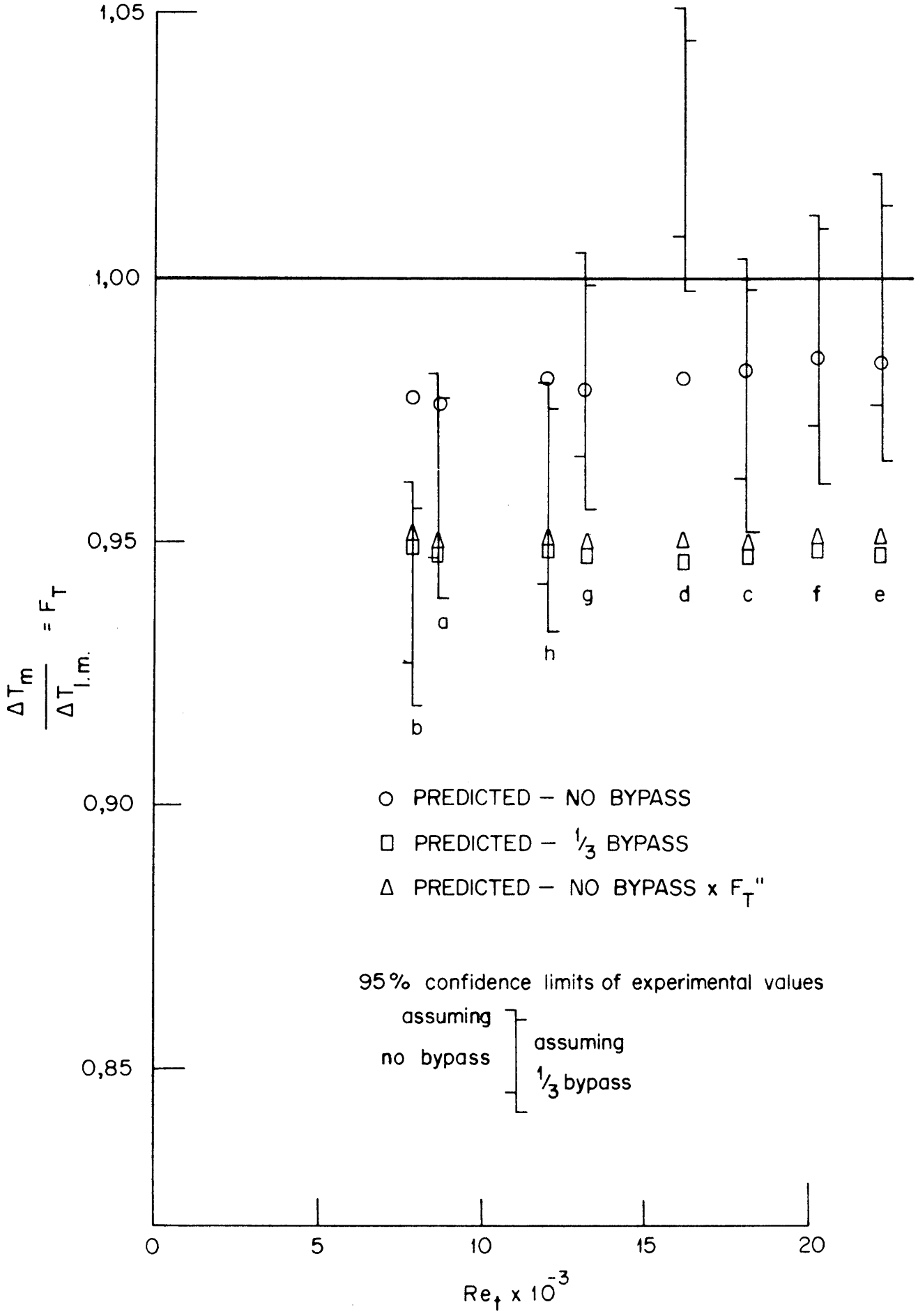

C4-2561/7

FIG 11 MEAN TEMPERATURE DIFFERENCES 3 ROW 1 PASS

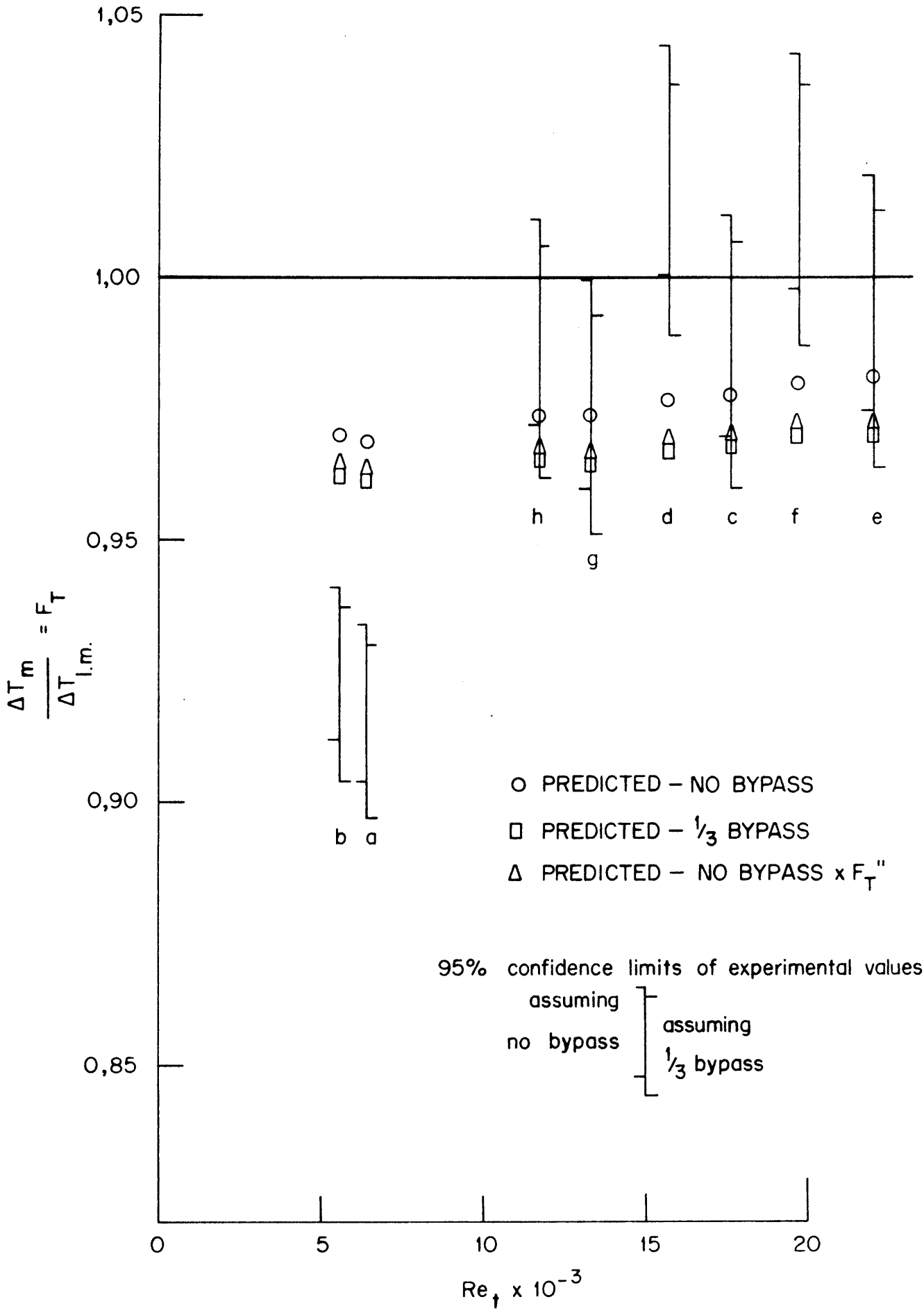

C4-2561/8

FIG 12 MEAN TEMPERATURE DIFFERENCES 4 ROW 1 PASS

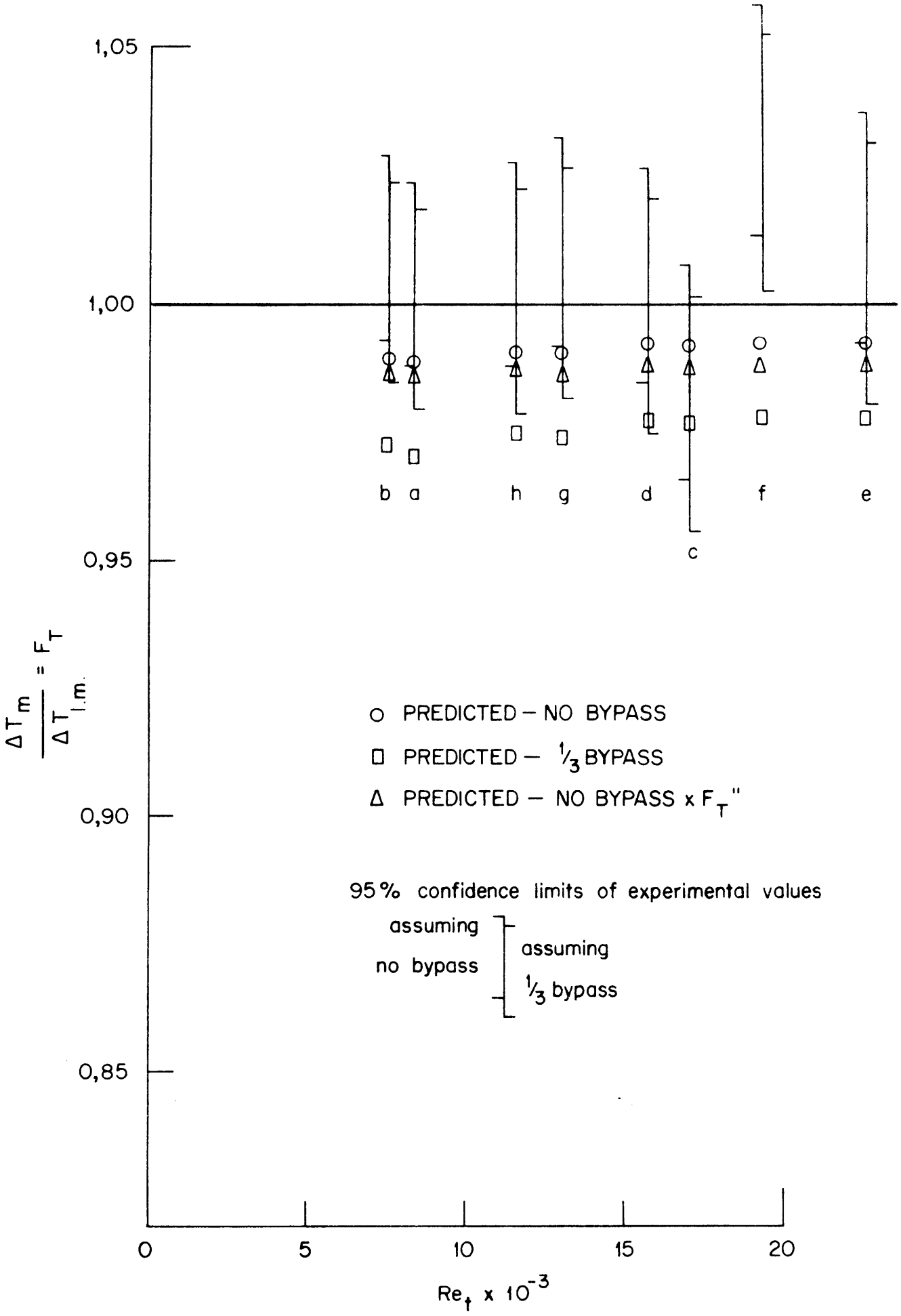

C4-2561/3

FIG 13 MEAN TEMPERATURE DIFFERENCES 2 ROW 2 PASS

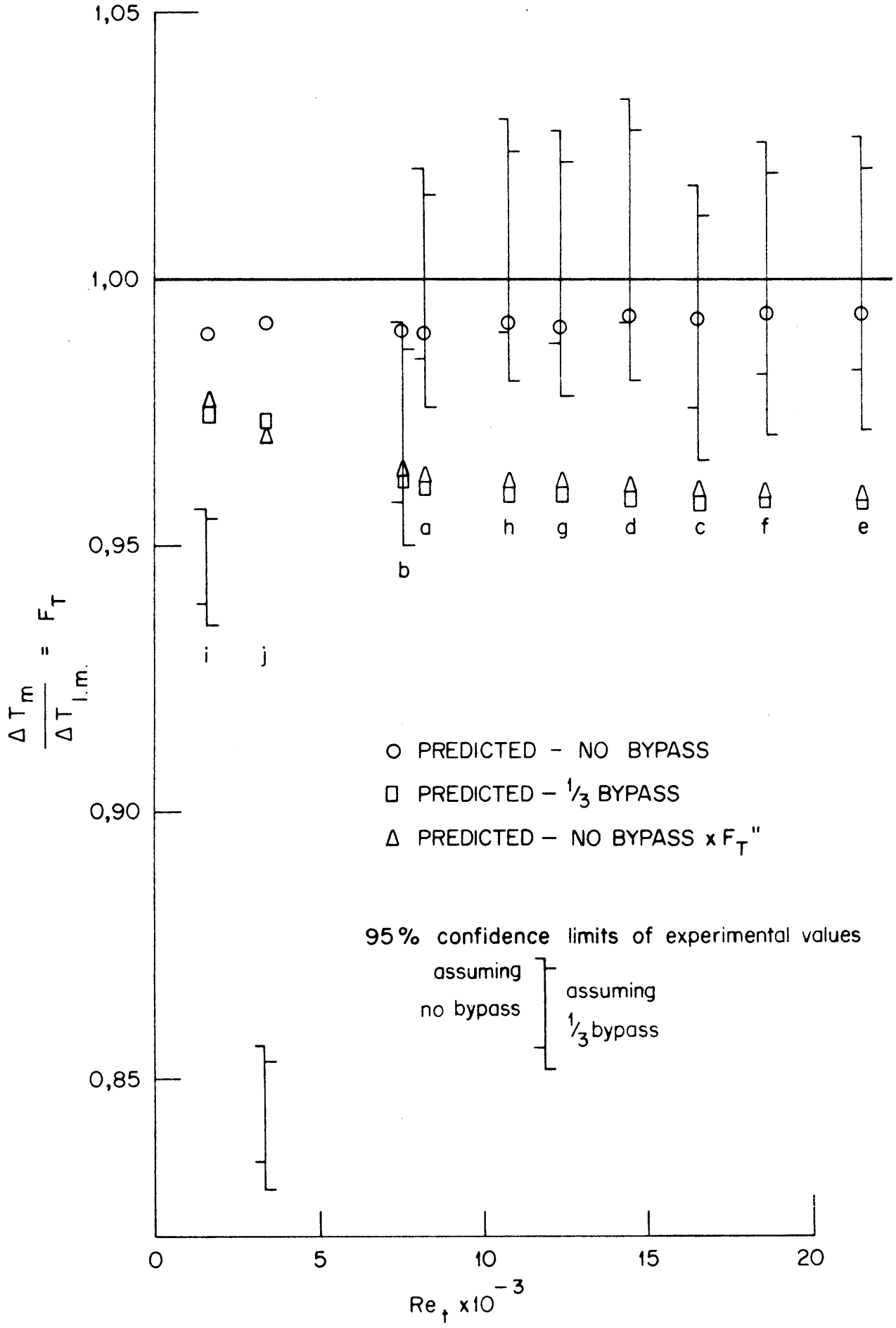

C4-2561/6

FIG 14 MEAN TEMPERATURE DIFFERENCES 3 ROW 3 PASS

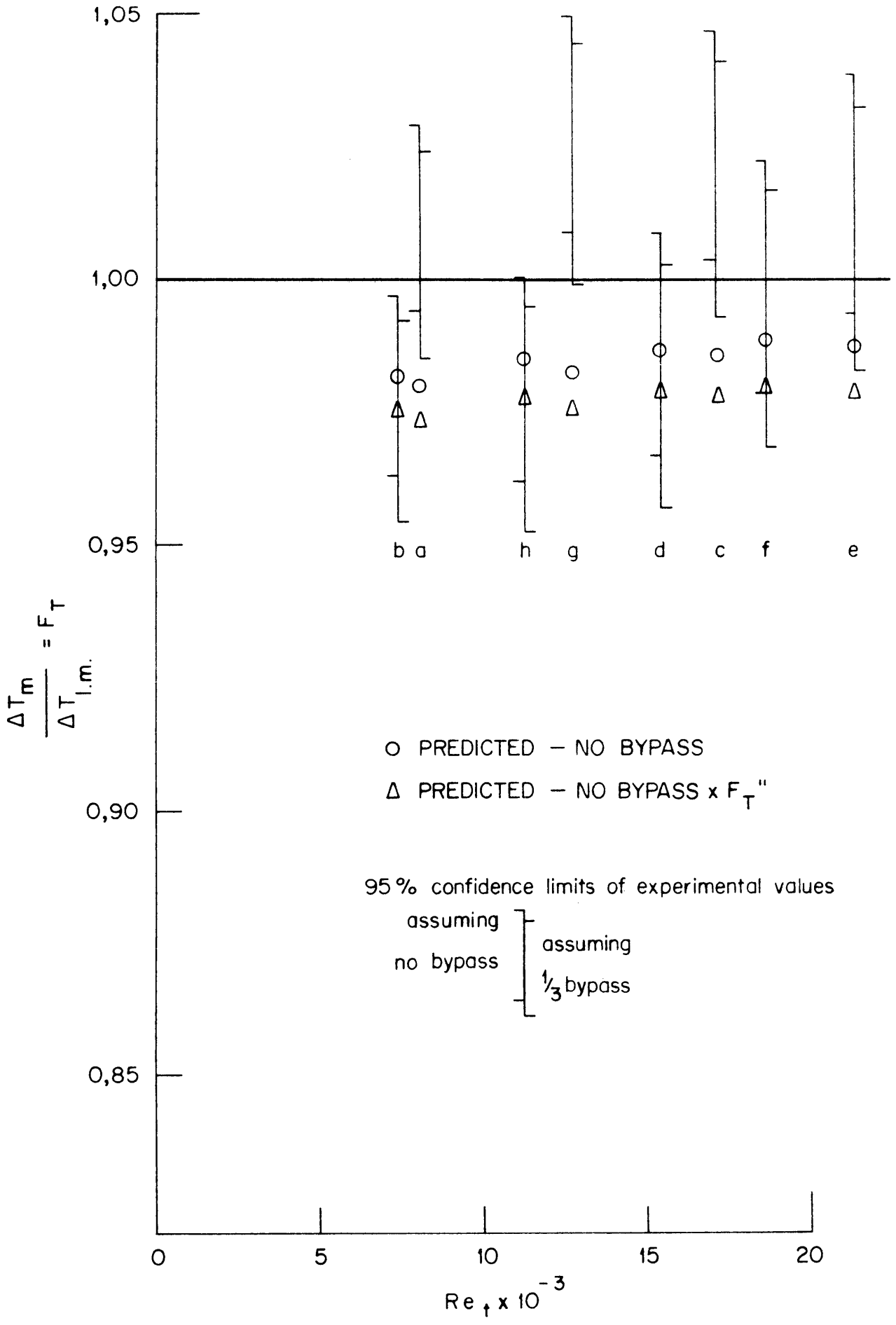

C4-2561/4

FIG 15 MEAN TEMPERATURE DIFFERENCES 4 ROW 2 PASS

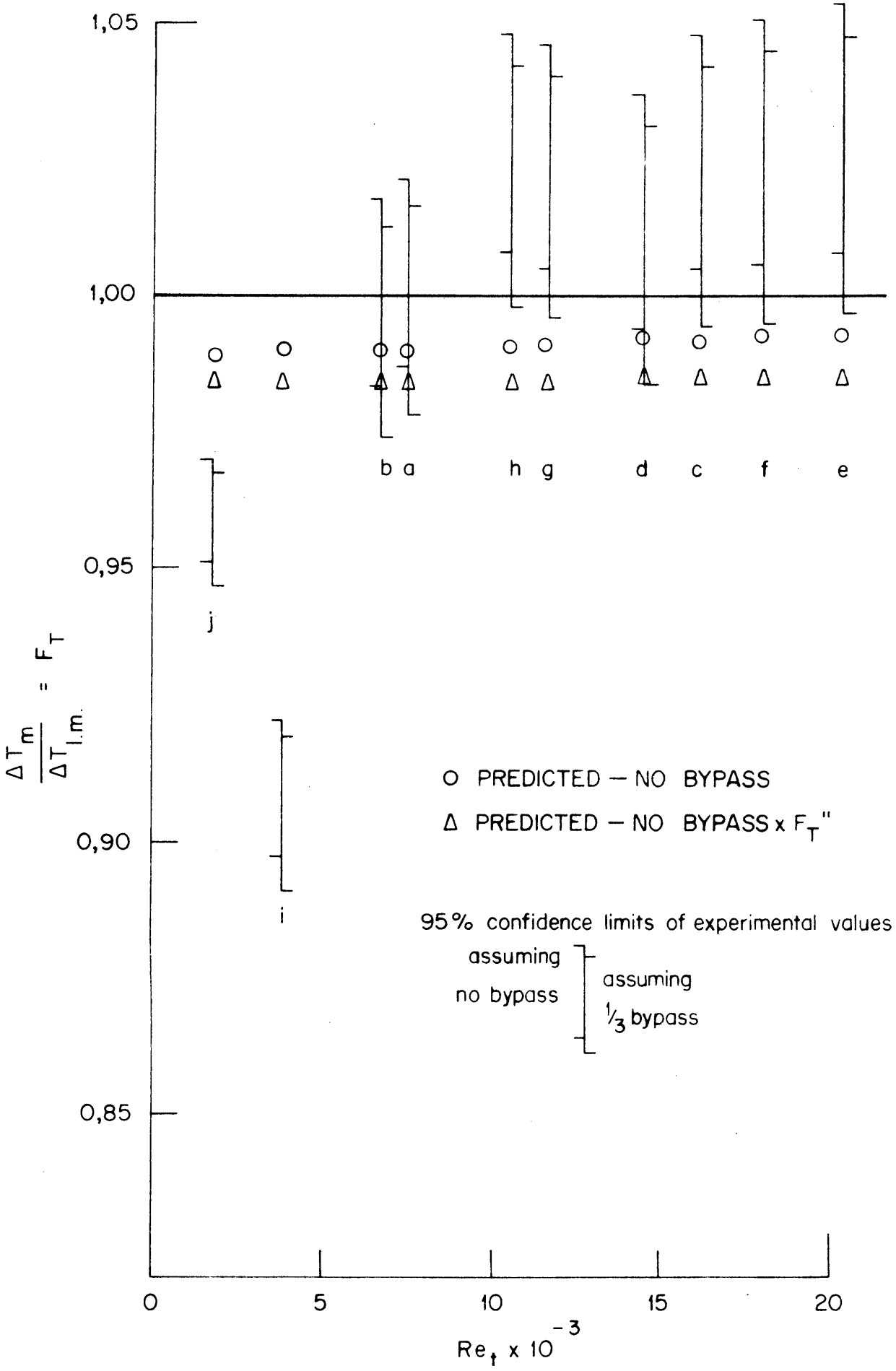

C4-2561/5

FIG 16 MEAN TEMPERATURE DIFFERENCES 4 ROW 4 PASS

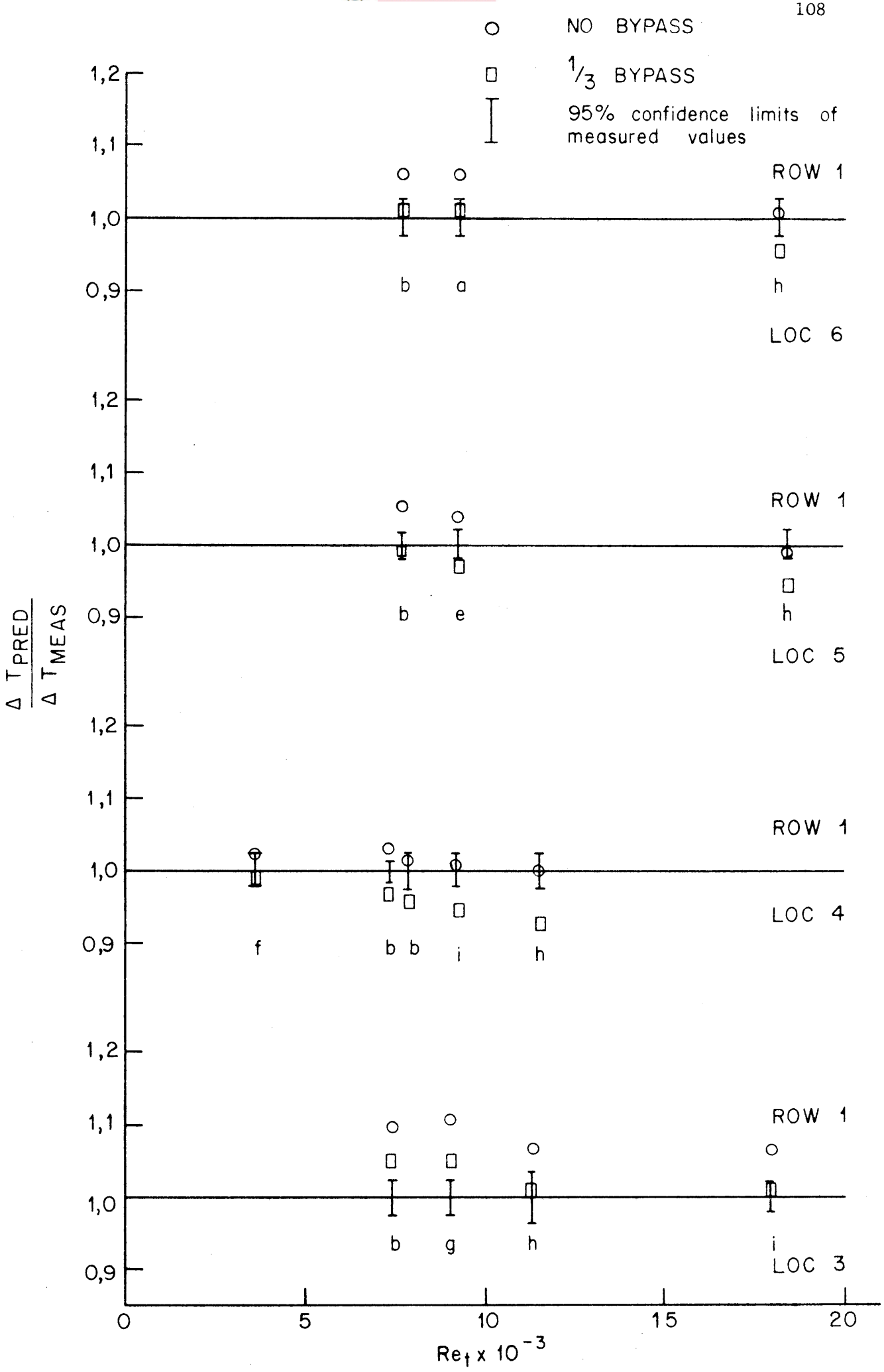

FIG 17 LOCAL TEMPERATURE DIFFERENCES 1 ROW 1PASS

C4-2561/11

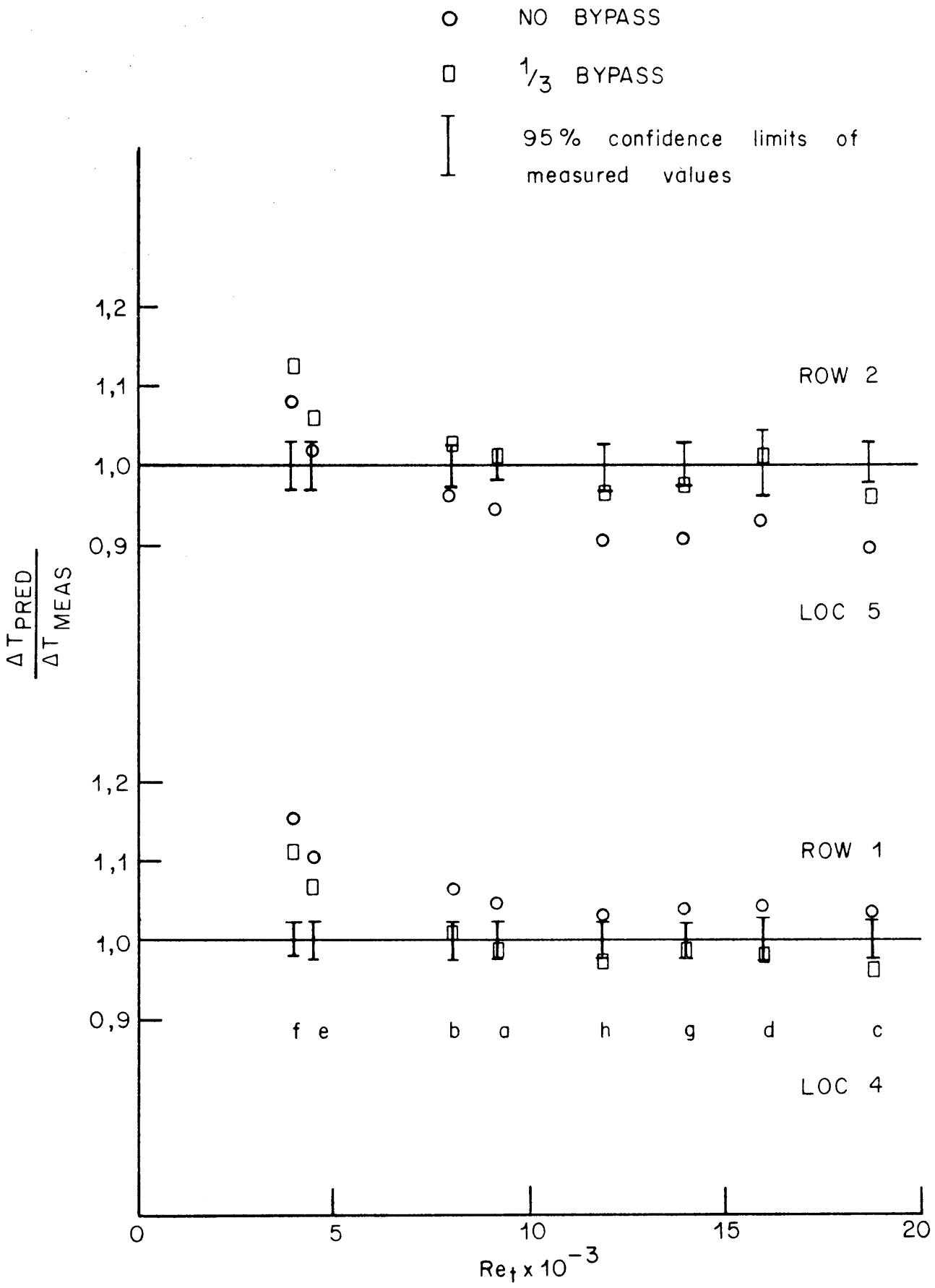

FIG 18 LOCAL TEMPERATURE DIFFERENCES 2ROW 1 PASS

C4-2561/13

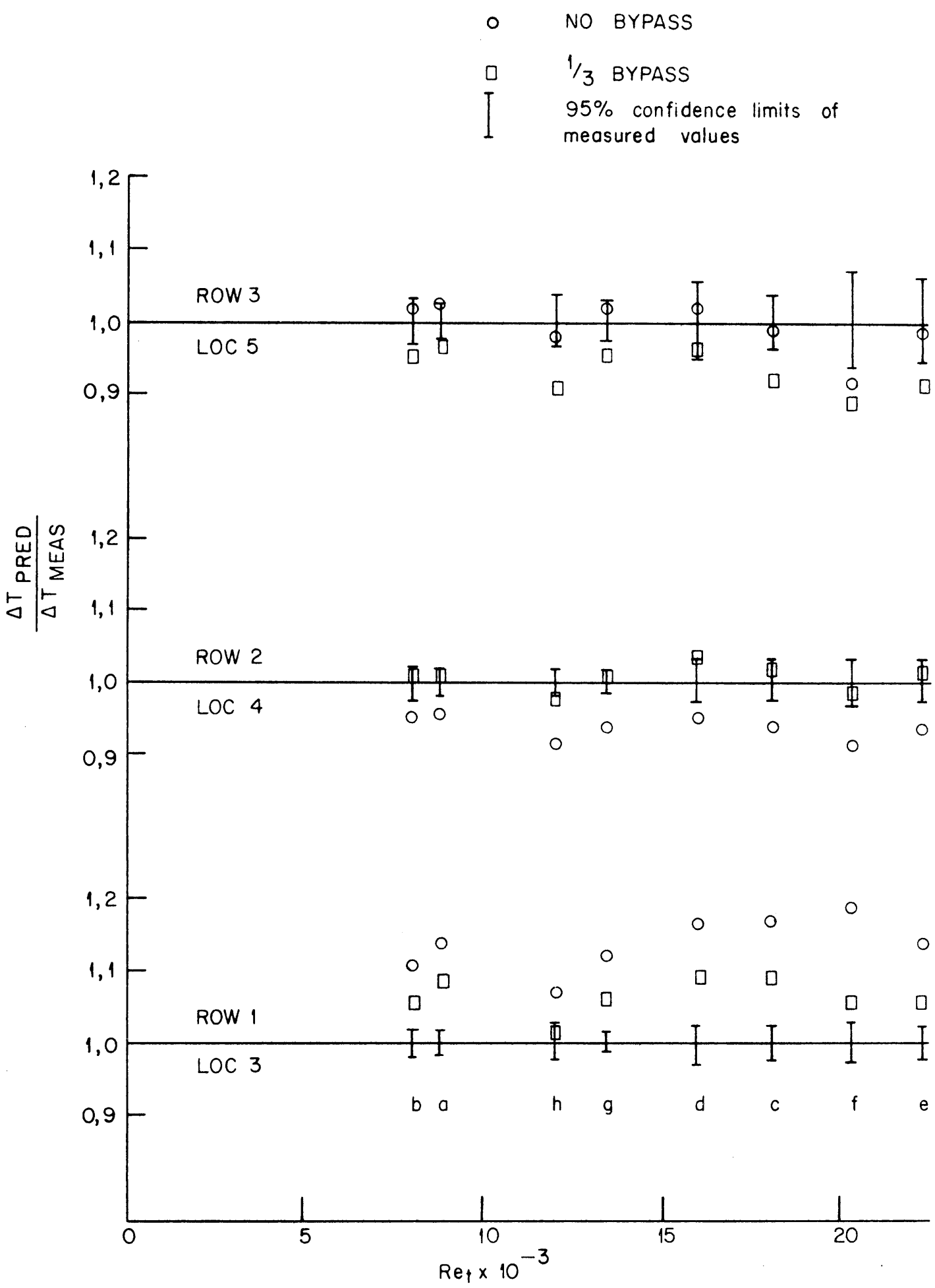

FIG. 19 LOCAL TEMPERATURE DIFFERENCES 3 ROW 1 PASS

C4-2561/16

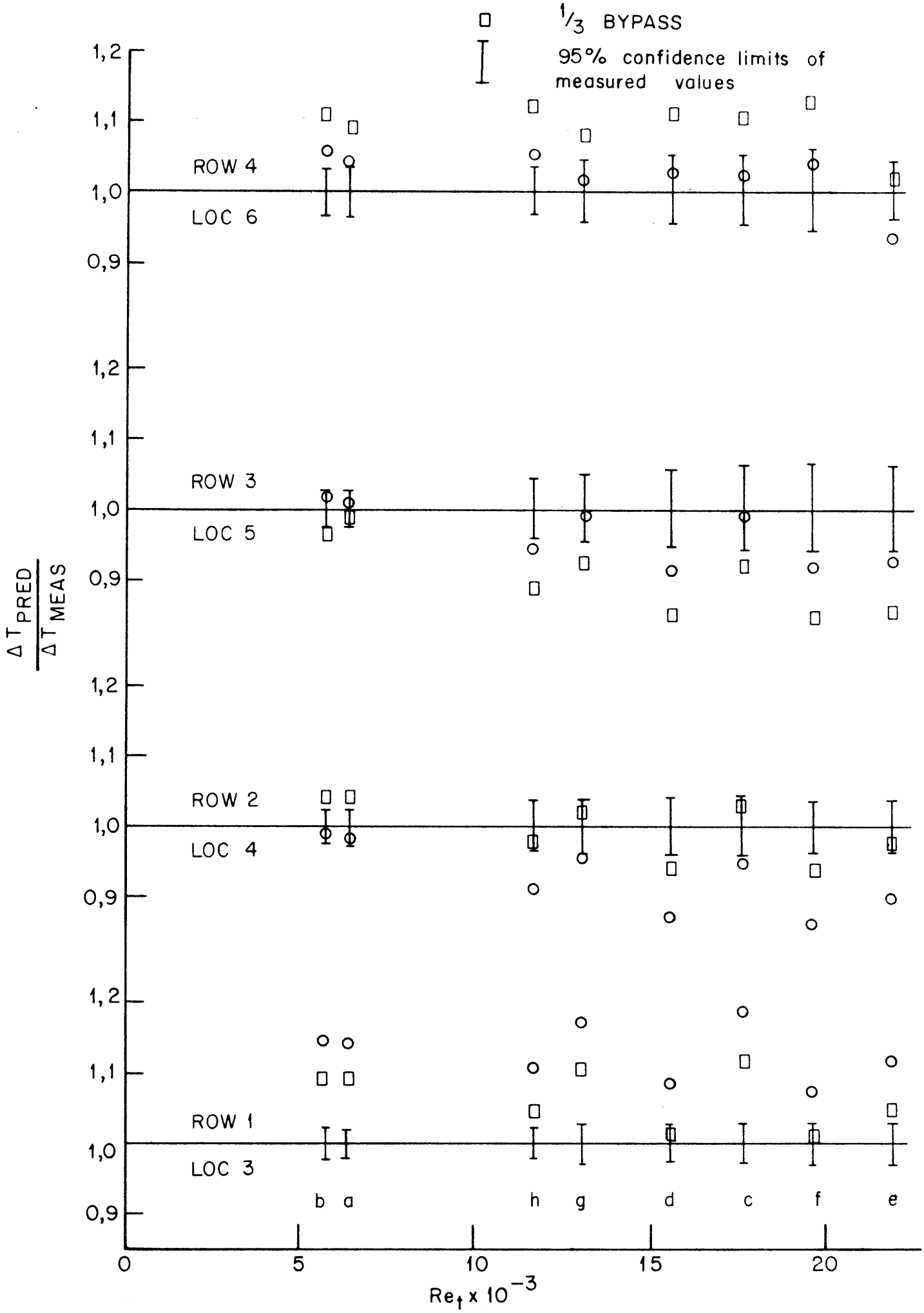

C4 - 2561/14

FIG 20 LOCAL TEMPERATURE DIFFERENCES 4 ROW 1 PASS

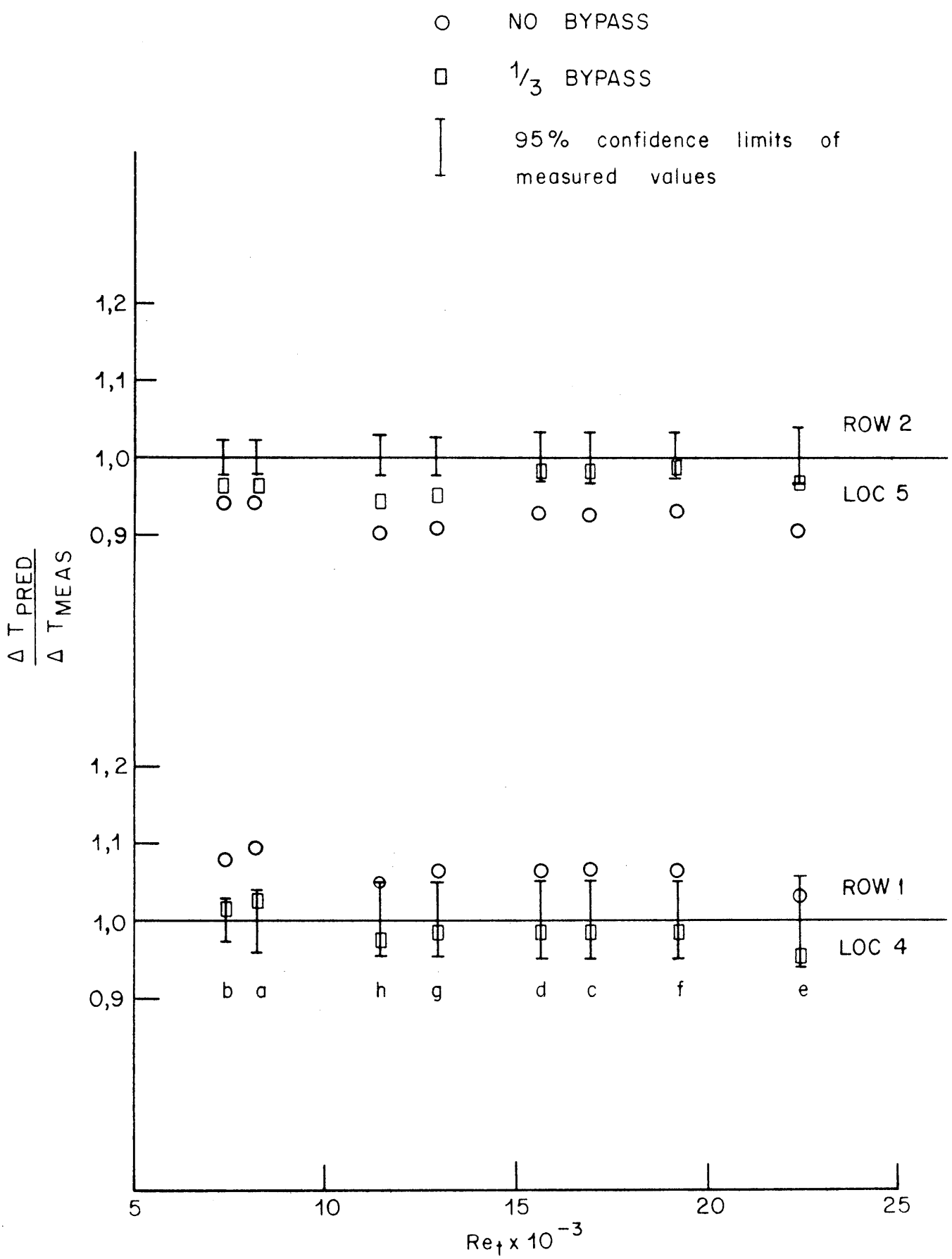

FIG21 LOCAL TEMPERATURE DIFFERENCES 2 ROW 2 PASS

C4-2561/12

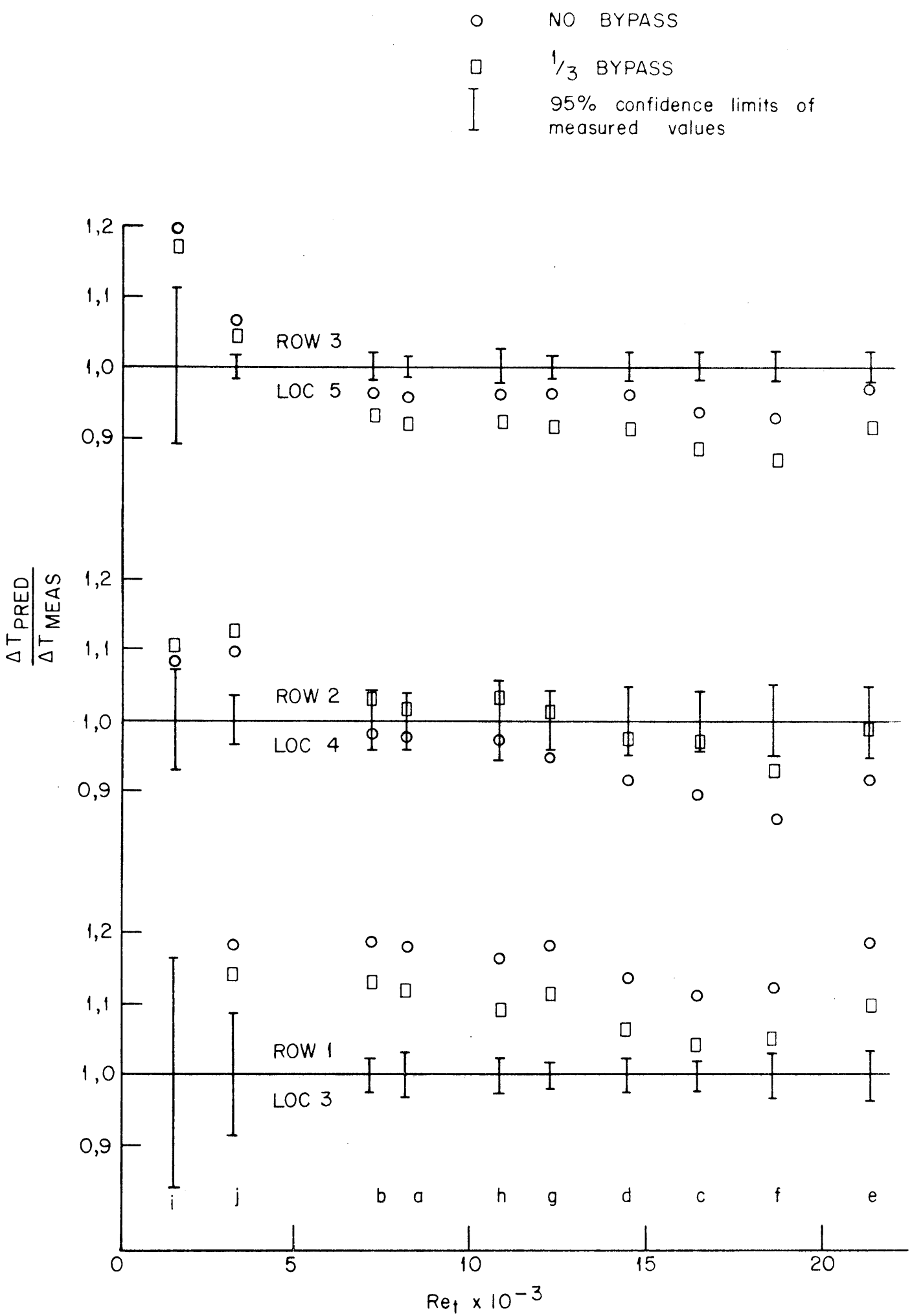

C4-2561/15

FIG. 22 LOCAL TEMPERATURE DIFFERENCES 3 ROW 3 PASS

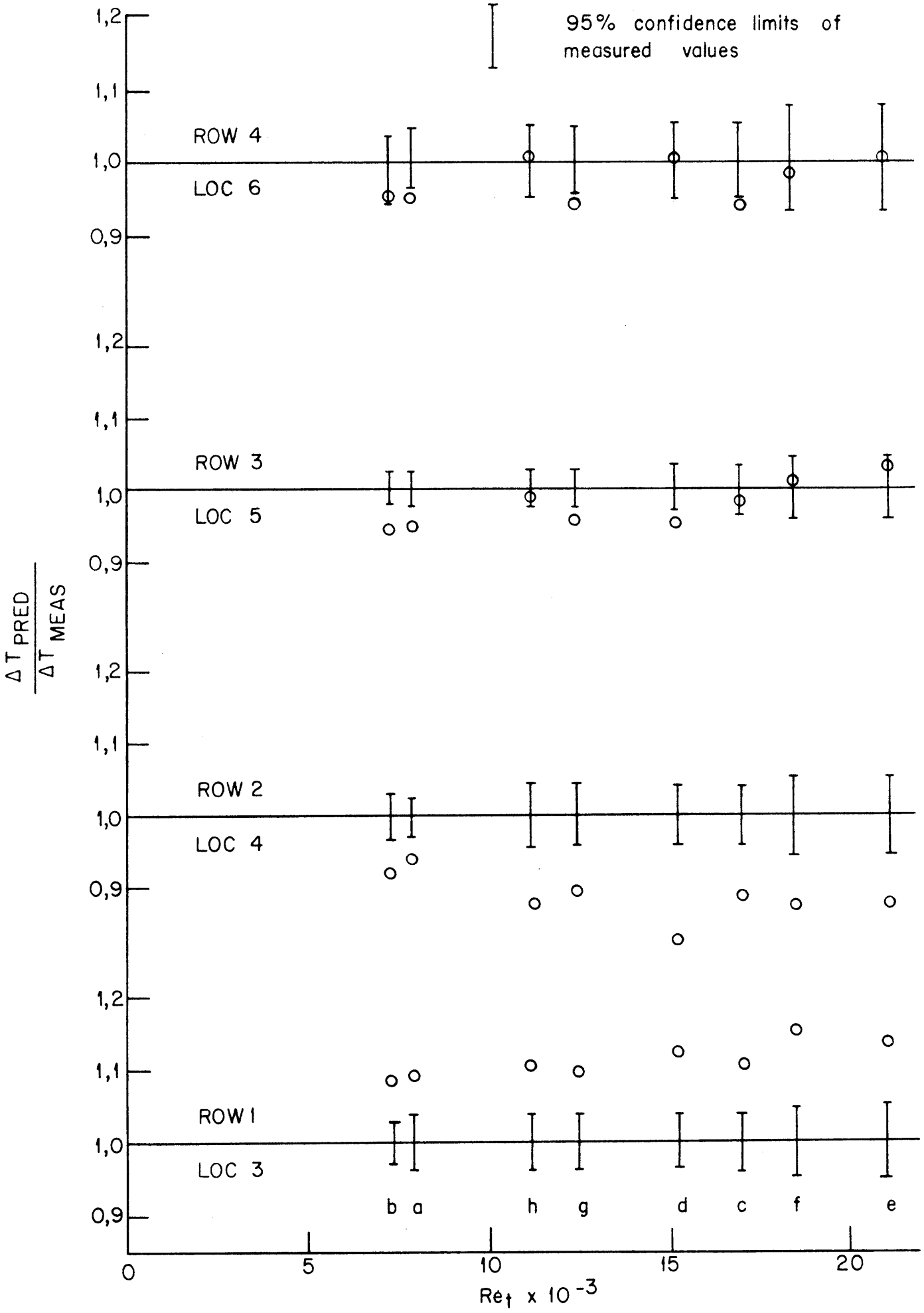

FIG. 23 LOCAL TEMPERATURE DIFFERENCES 4 ROW 2 PASS

C4-2561/18

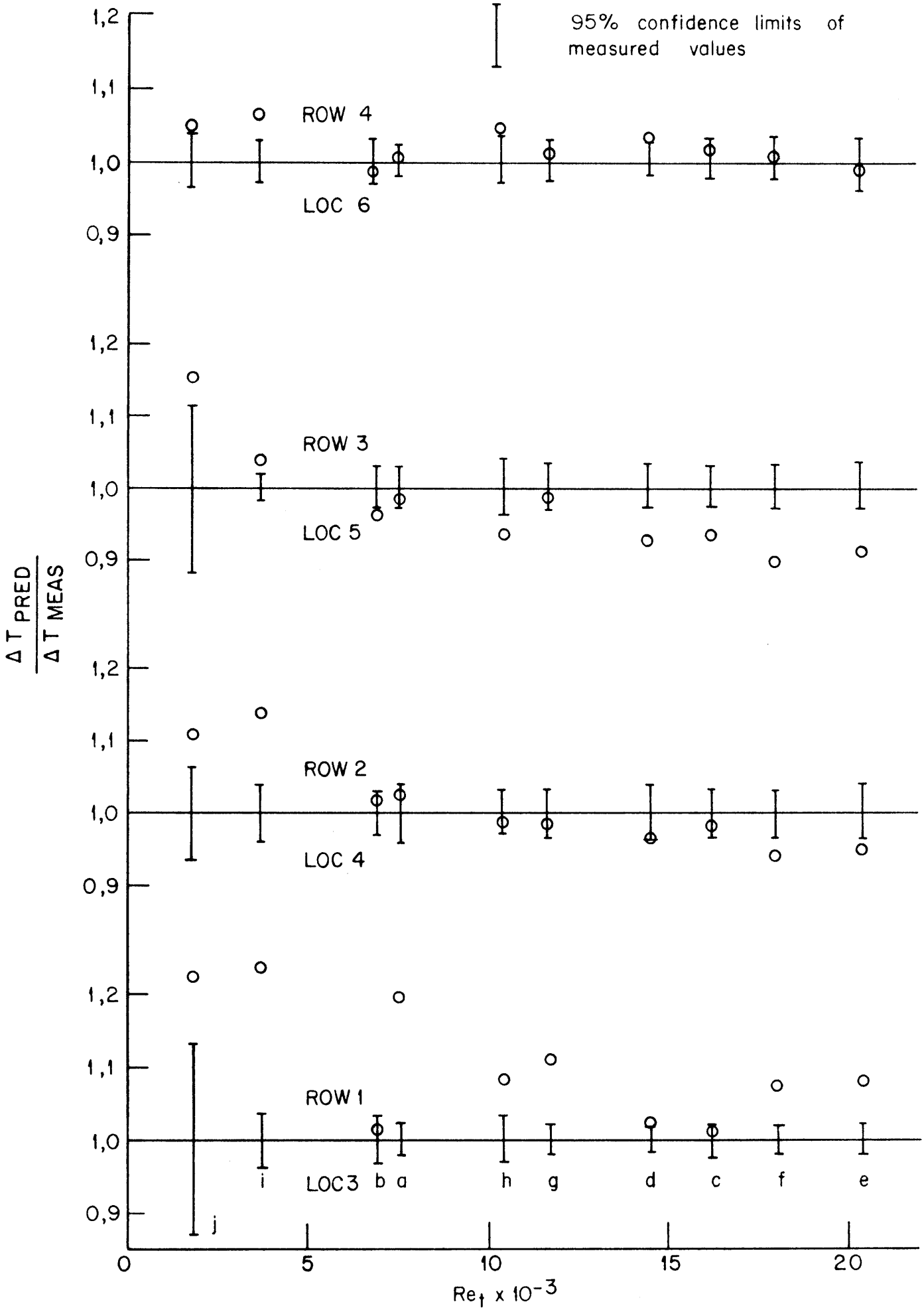

FIG. 24 LOCAL TEMPERATURE DIFFERENCES 4 ROW 4 PASS

C4 2561/17

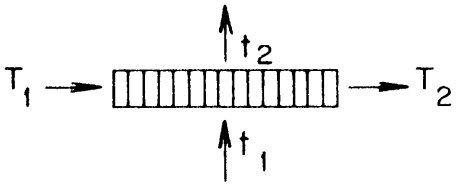

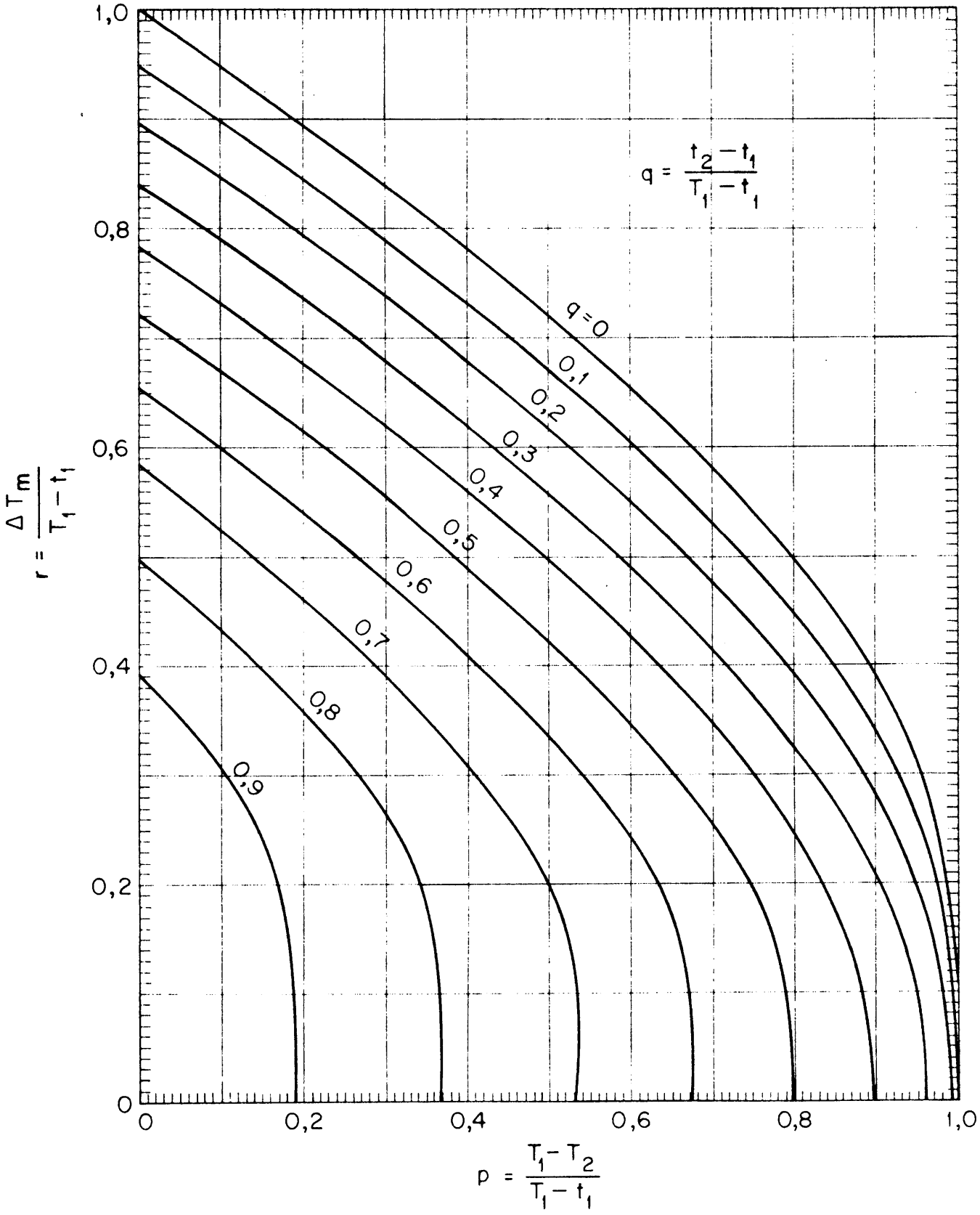

FIG 25 CROSS - FLOW FACTOR 1 ROW 1 PASS

C4-2561/26

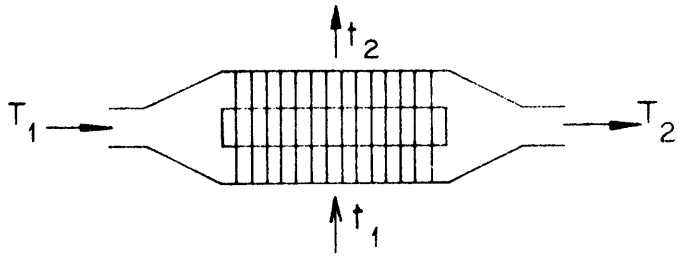

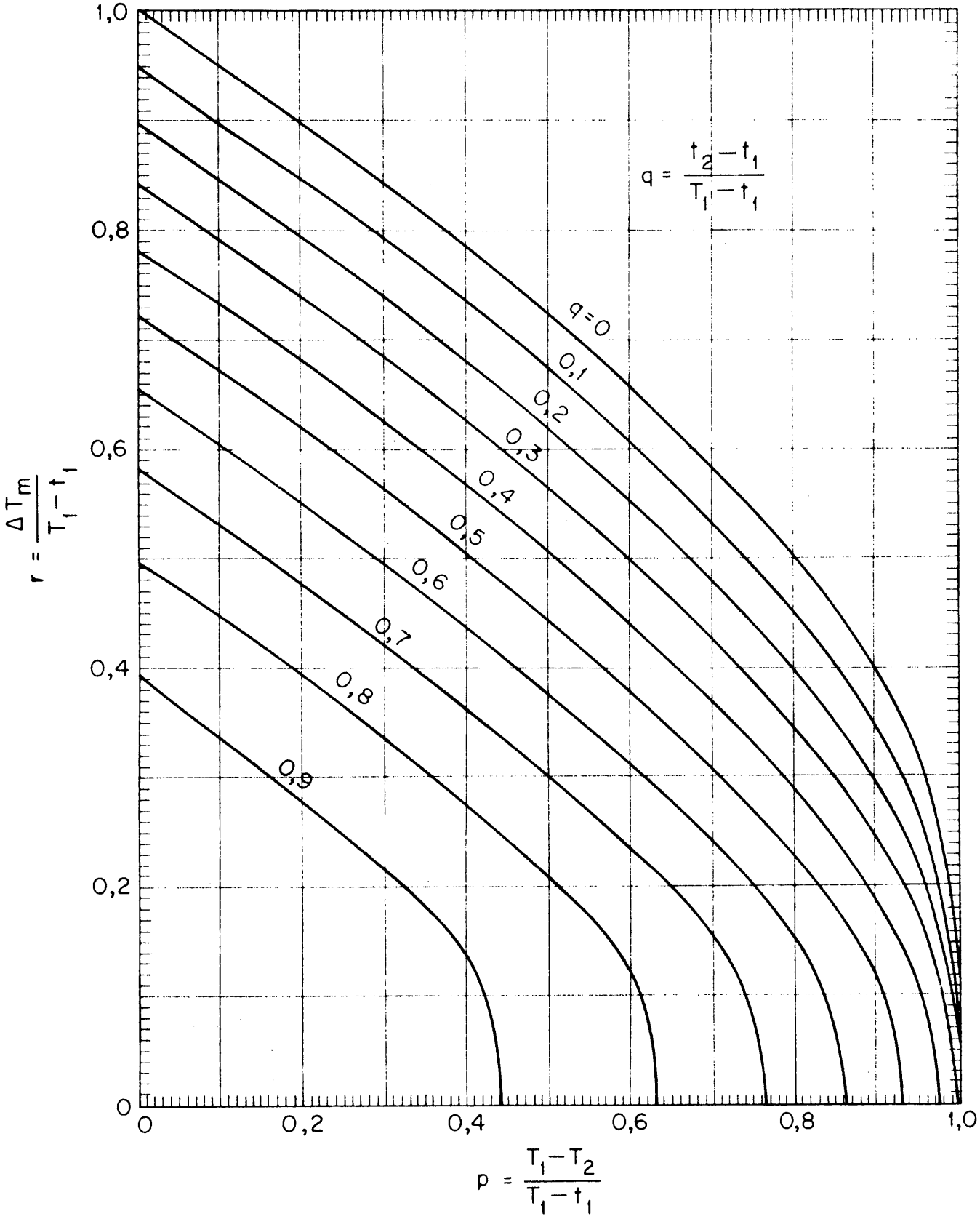

FIG 26 CROSS - FLOW FACTOR 2 ROW 1 PASS

C4-2561/20

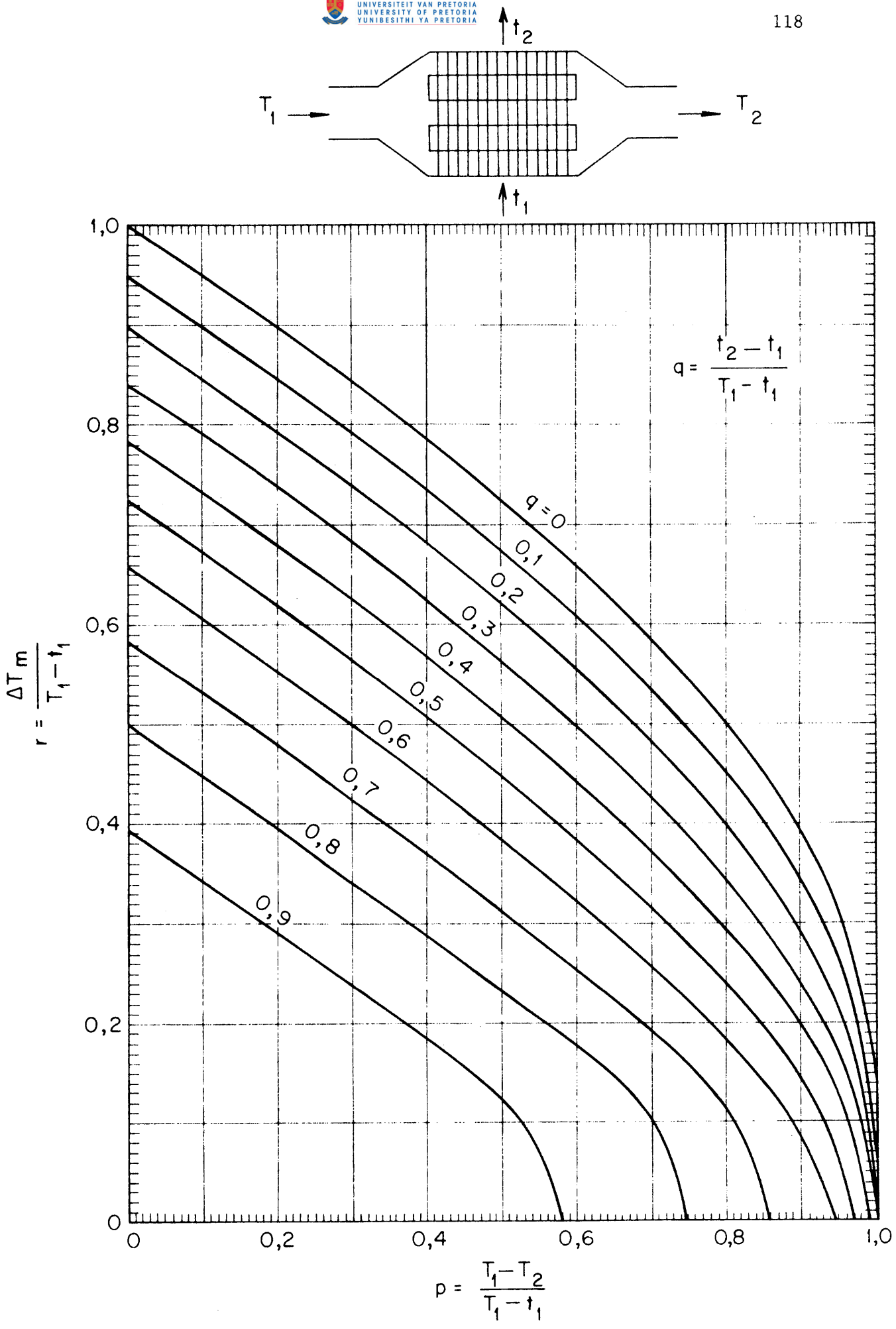

FIG 27 CROSS – FLOW FACTOR 3 ROW 1 PASS

C4-2561/21

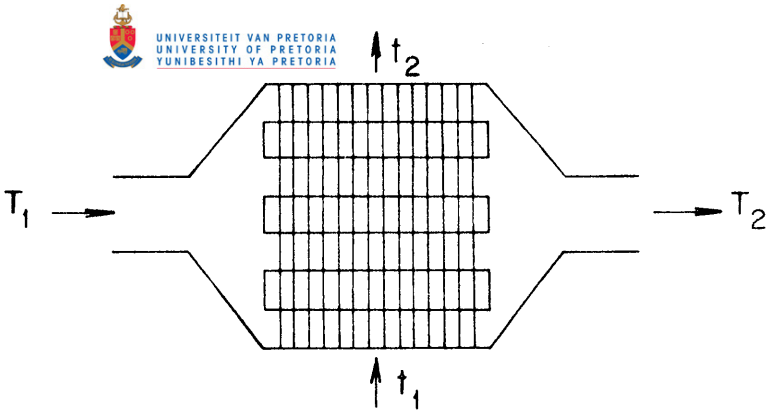

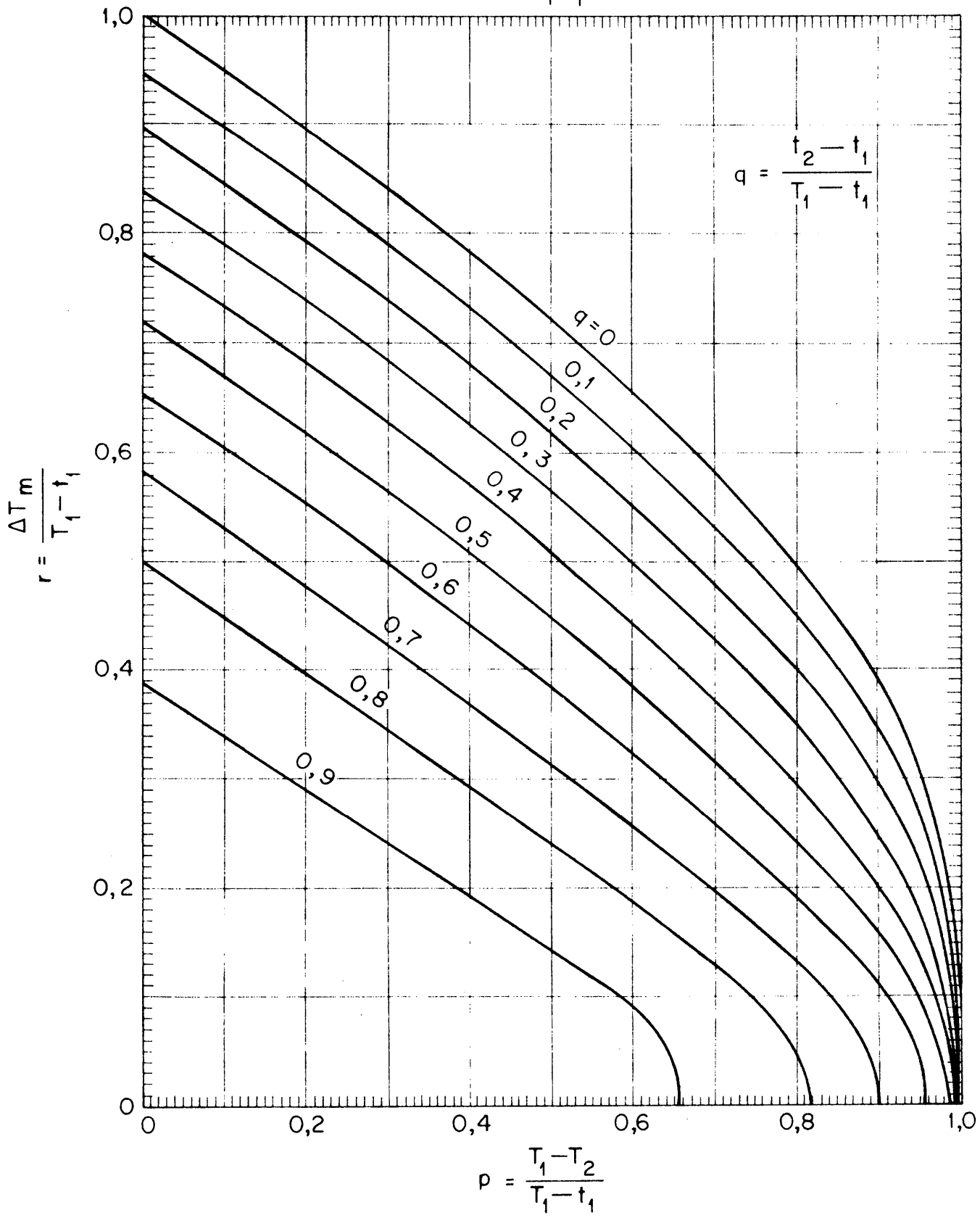

FIG 28 CROSS-FLOW FACTOR 4 ROW 1 PASS

C4-2561/22

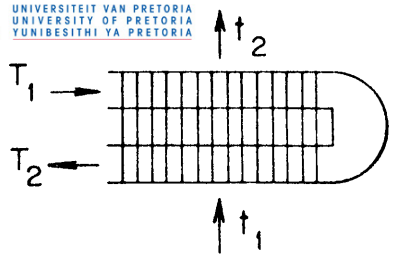

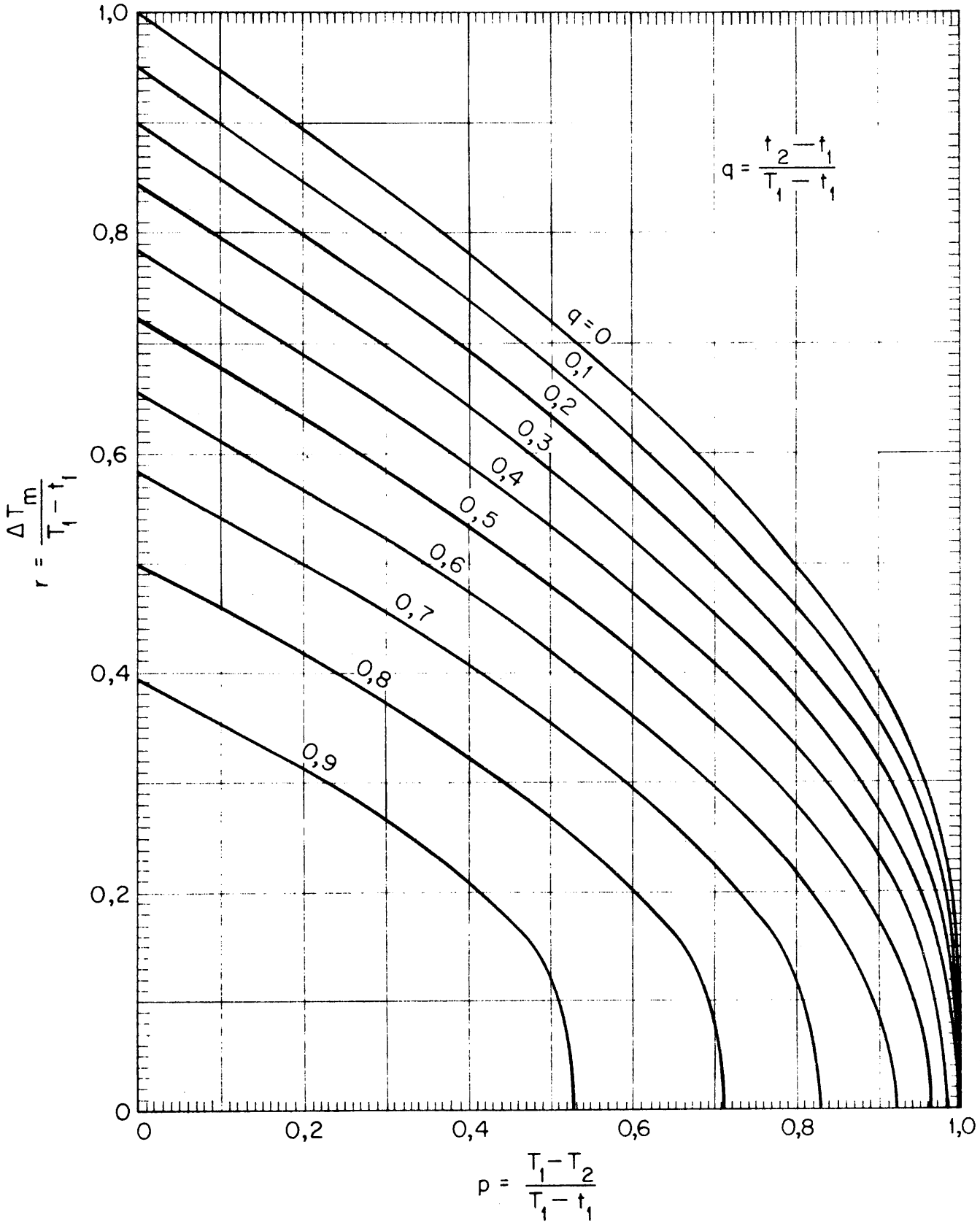

FIG 29 CROSS - FLOW FACTOR 2 ROW 2 PASS

C4-2561/23

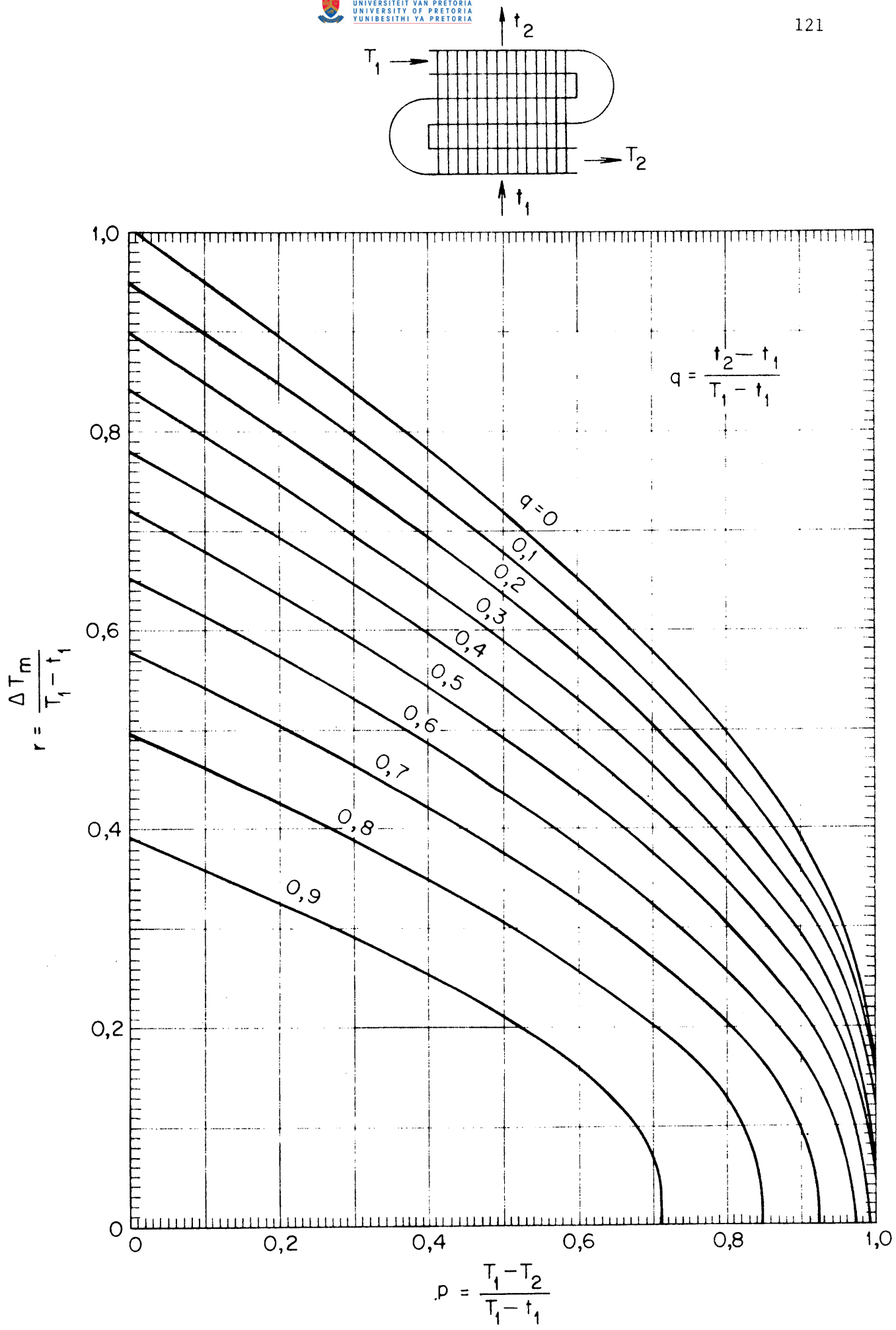

FIG 30 CROSS-FLOW FACTOR 3 ROW 3 PASS

C4-2561/24

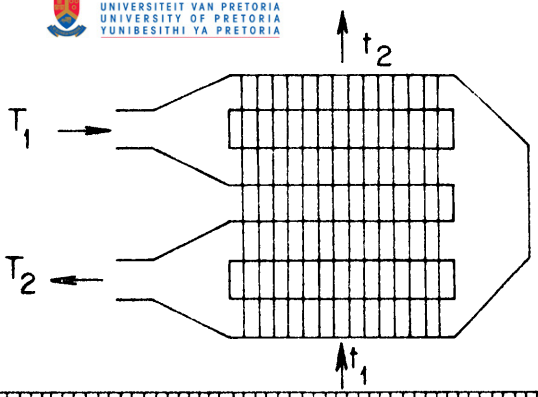

$$q = \frac{t_2 - t_1}{T_1 - t_1}$$

$$r = \frac{\Delta T_m}{T_1 - t_1}$$

$$p = \frac{T_1 - T_2}{T_1 - t_1}$$

q=0 0,1 0,2 0,3 0,4 0,5 0,6 0,7 0,8 0,9

0 0,2 0,4 0,6 0,8 1,0

0 0,2 0,4 0,6 0,8 1,0

FIG 31 CROSS-FLOW FACTOR 4 ROW 2 PASS

C4-2561/25

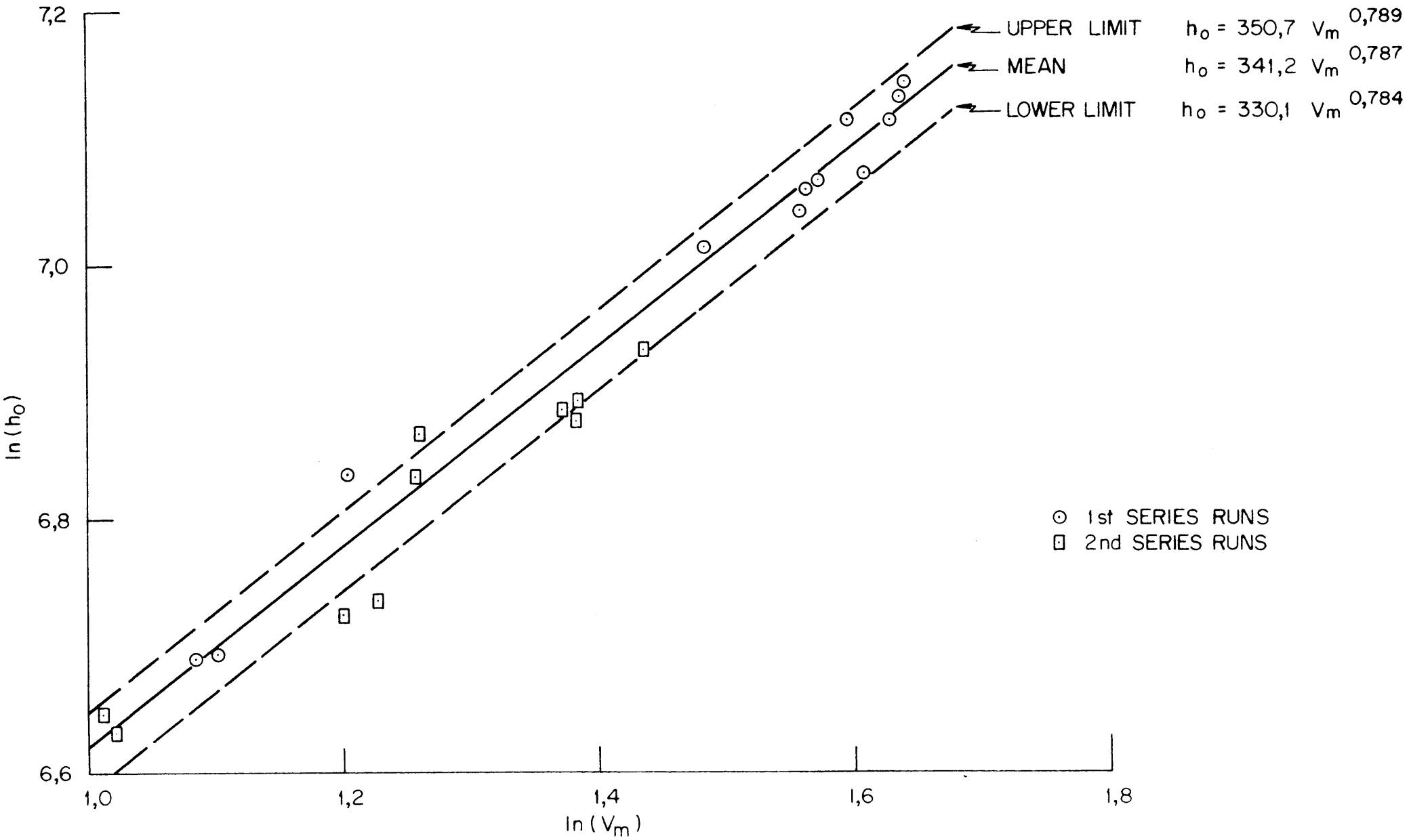

FIG 33 AIRSIDE FILM HEAT TRANSFER COEFFICIENT — NO AIR BYPASS

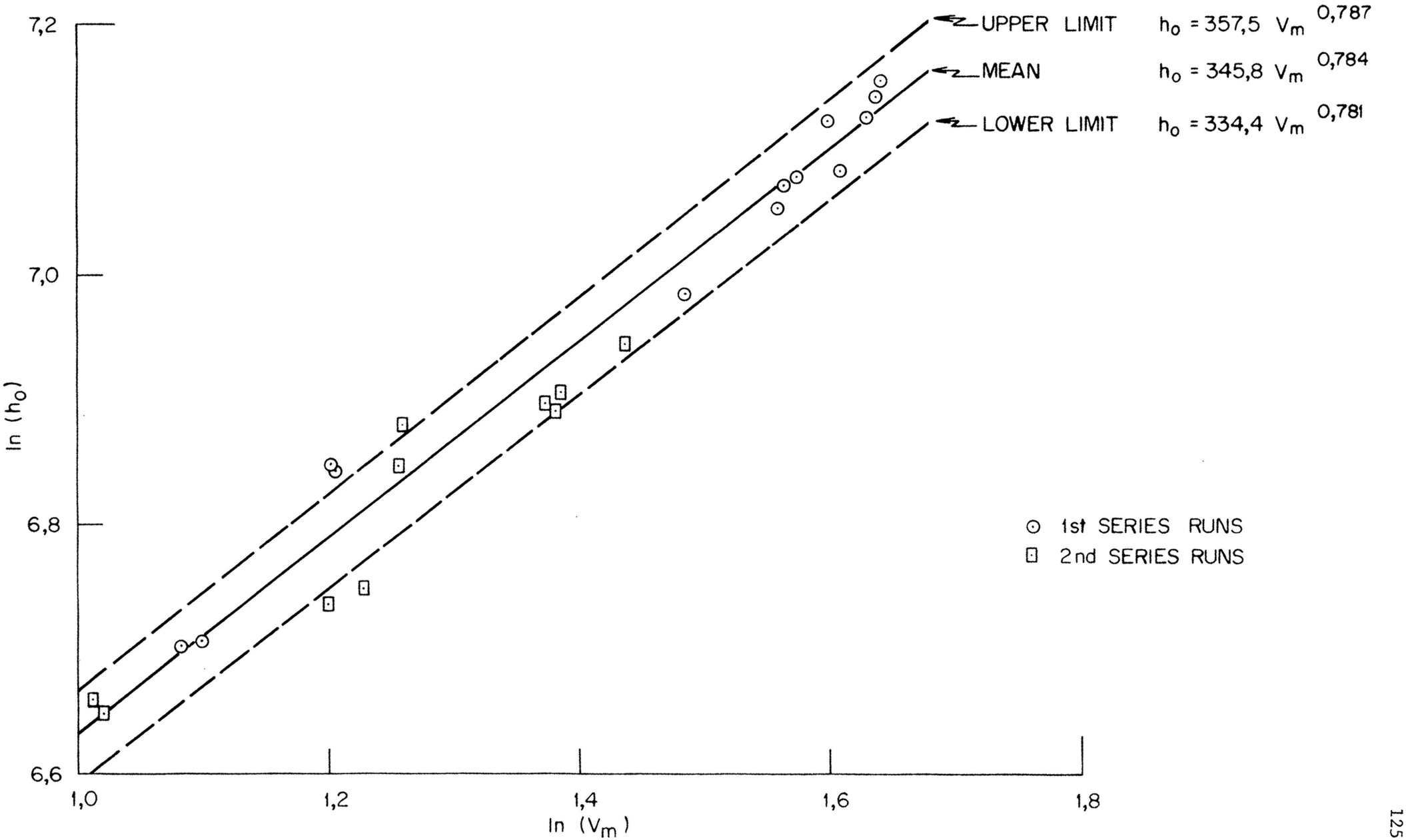

FIG 34 AIRSIDE FILM HEAT TRANSFER COEFFICIENT — 1/3 AIR BYPASS

8.11 NOMENCLATURE

Symbol	Definition	Unit
A	Total outside (bare tube) heat transfer area	m^2
a, b	Parameters used in Equation (62)	-
C	Specific heat capacity of tubeside fluid (water)	J/(kg K)
c	Specific heat capacity of air	J/(kg K)
d_f	Outside diameter of fin	m
d_i	Inside diameter of base tube	m
d_o	Outside diameter of base tube	m
d_r	Root diameter of fin	m
F_i	Tubeside fouling factor	m^2 K/W
F_T	Logarithmic mean temperature difference (LMTD) correction factor for cross-flow (assuming no air bypass)	-
F''_T	LMTD correction factor for bypass air flow model with isothermal tubeside conditions (Appendix 8.4)	-
f_B	Twice the fraction of the total air flow which bypasses alternate tube rows	-
g_1	Fractional area of fin-tube contacted by the air flow fraction, $\frac{f_B}{2}$	-
g_2	(= 1 - g_1); Fractional area of fin-tube contacted by the air flow fraction, 1 - f_B	-
h_i	Tubeside film coefficient for heat transfer	W/(m^2 K)
h_{io}	h_i corrected to outside (bare tube) area	W/(m^2 K)
h_m	Total metal (fins plus tube wall) heat transfer conductance	W/(m^2 K)
h_o	Apparent airside film coefficient for heat transfer (assuming all the air contacts all the fin-tube area) (bare tube outside area basis)	W/(m^2 K)
h_w	Tube wall (metal) heat transfer conductance	W/(m^2 K)
i, j, k	Summation counters used in Equation (36)	-
K	Parameter defined in Equation (29)	-
K_1	Parameter defined in Equation (41)	-
K_2	Parameter defined in Equation (42)	-
k_f	Thermal conductivity of fin metal	W/(m K)
k_t	Thermal conductivity of tubeside fluid (water)	W/(m K)
k_w	Thermal conductivity of tube wall metal	W/(m K)
LOC	Location of row (from bottom of 6 row bundle) in which heat transfer took place	-
NTU	Number of transfer units (Equations (10) and (11))	-
NTU_{an}	Number of transfer units on the air side on a per row basis (Equation (12))	-
n	Number of tube rows for heat transfer	-
n_f	Number of fins per unit length	m^{-1}
Pr_t	Tubeside Prandtl number at mean water temperature	-
p	Effectiveness of tubeside fluid (Equation (5))	-
Q	Heat duty	W
q	Effectiveness of air (Equation (5))	-
R	Thermal capacity ratio (Equation (9))	-
Re_t	Tubeside Reynolds number at mean water temperature	-
R_m	Fin metal resistance	m^2 K/W
r	Cross-flow factor	-
r_{count}	Counterflow factor	-
$r_{n;m}$	Cross-flow factor for n tube rows and m tubeside passes	-
S_t	Transverse fin tube pitch (between adjacent tubes in the same row)	m
St	(= h_i/CW'); Tubeside Stanton number at mean water temperature	-
T	Tubeside temperature	°C
T'	Local tubeside temperature (Figure 1)	°C
t	Airside temperature	°C
t', t'', t'''	Local airside temperatures (Figure 1)	°C
t_f	Mean fin thickness	m
t'_f	Fin thickness at tip	m
U	Overall heat transfer coefficient (assuming no air bypass) (bare tube outside area basis)	W/(m^2 K)
V_m	Maximum air velocity (standard) within bundle	m/s
W	Mass flow rate of tubeside fluid (water)	kg/s
W'	Mass flow rate of tubeside fluid per unit area	kg/(s m^2)
w	Mass flow rate of air	kg/s
X	Distances used in Appendix 8.2	m
Y	Distances used in Appendix 8.2	m
y	Parameter defined in Equation (14)	-
Z	Parameter defined in Equation (43)	-

Symbol	Definition	Unit
Greek letters		
β	Parameter defined in Equation (72)	W/(m^2 K)
γ	Parameter defined in Equation (73)	-
ΔT_{abs}	Overall tubeside temperature change from absolute measurements of inlet and exit temperature	°C
ΔT_{diff}	Overall tubeside temperature change from local differential temperature measurements per row	°C
$\Delta T_{l.m.}$	Logarithmic mean temperature difference for counterflow	°C
ΔT_m	Effective (true) mean temperature difference for cross-flow	°C
ΔT_n	Local tubeside temperature difference across row n	°C
θ_1 to θ_4	Parameters defined in Equation (54)	-
ξ	Ratio of overall bundle face area to minimum free area for air flow through the fin-tube bundle	-
ϕ_1 ; ϕ_2	Parameters defined in Equation (49)	-
ϕ_3	Parameter defined in Equation (51)	-
χ	Parameter defined in Equation (55)	-
ψ_1 to ψ_4	Parameters defined in Equation (48)	-
ψ'_1 to ψ'_3	Parameters defined in Equation (50)	-
Ω	Ratio of total outside area to bare tube outside area	-

Subscripts (except where otherwise previously defined)

A	Airside conditions downstream of (after) the bundle
a	Airside (total heat transfer area basis)
B	Airside conditions upstream of (before) the bundle
comp	Compounded value (Equations (22) and (23))
exp	Calculated from experimental measurements
n	Heated row number from inlet air
p	Process or tube side
pred	Theoretically predicted value
1	Inlet conditions
2	Exit conditions

Superscript (except where otherwise previously defined)

'	Value assuming a fraction of the air bypasses alternate tube rows

968:66

N I C O L E , Francis John Lorraine
Mean temperature difference in cross-flow heat exchange, applied to multipass air cooled fin-tube units with a finite number of rows. Pretoria, 1972.
441 681 125p. 30cm. illus. Verhandeling (M.Sc.) - Pretoria.